Nonlinear Aeroelastic Analysis, Flight Dynamics, and Control of a Complete Aircraft

A THESIS

Presented to

The Academic Faculty

by

Mayuresh J. Patil

In Partial Fulfillment

of the Requirements for the Degree

Doctor of Philosophy in Aerospace Engineering

Georgia Institute of Technology

May, 1999

Nonlinear Aeroelastic Analysis, Flight Dynamics, and Control of a Complete Aircraft

Approved:

Dewey H. Hodges, Chairman

Olivier A. Bauchau

Anthony J. Calise

Marilyn J. Smith

Date Approved by Chairman _____

Acknowledgments

I would like to acknowledge the complete support and advice given by Prof. Dewey Hodges, my thesis advisor, throughout the course of my PhD. He has been a great source of inspiration and knowledge to me. He always had an answer or a path towards it, be it a technical question or just any other problems that may have arisen. But even though he advised me when I needed it he never forced his advice on me. He always put his students first and kept an open door policy. In his way of treating his students he set an example that I would love to follow.

I would also like to acknowledge the help and support of Prof. Carlos Cesnik from MIT. Carlos was a post-doctoral student at Georgia Tech when I first arrived. He was part of the group when we first conceived of the Aeroelasticity project which finally lead to my PhD thesis. I will always appreciate his high standards and eye for details which I am sure helped make the papers we wrote and finally my thesis a lot better.

I would like to take this opportunity to thank my thesis committee, Profs. Olivier Bauchau, Anthony Calise and Marilyn Smith for the suggestions which helped improve my thesis. I especially appreciate the discussion during my thesis defense which helped me get a more practical perspective on the work I had done and for all the ideas for future work. I would also like to thank Profs. Bauchau, Haddad, Hanagud, Hodges and Kamat for the courses offered by them and for teaching them with passion. These courses did form the basis for my advanced research.

I would like to thank the help from other students and post-docs in the school

of aerospace engineering who have constantly helped and supported me. Specifically Dr. Vitali Volovoi and Maxime Bayon De Noyer. Vitali being the senior PhD student and later postdoc was always given the responsibility of taking care of the lab. Which basically meant that he had to give up his precious time from his really busy schedule to help make the computers right so that we the junior students could continue our work. I would also like to thank him for giving me the theoretical perspective, talking of beam theories and asymptotic analysis. I am in debt to Max for his experimental and control perspective. Being the Nobleman that he is he helped me through my fight to put control into my thesis! I am also grateful to Joe Corrado for providing me with control routines which helped in designing control. I would like to acknowledge the time that he spent to make the routines applicable to my problem.

Finally there are innumerable friends and roommates that have made Atlanta my home away from home. Even when they graduated and moved on they still managed to make me feel at home. Here I would like to mention a few with whom I spent most of my non-academic time relaxing, enjoying, arguing, discussing, cooking and doing just about everything that makes up our lives. I still remember the one month vacation from house work that was given to me just cause I was giving my PhD qualifiers. Tina, Ananjan, Jasjit, Athanu, Subhashri, Anurag, Prameela, Nithya, Aman and Priyen where my only family for the first half of my stay here. I got married in my third year as a graduate student. So for the past two years my wife Pradnya had to deal with staying with a Doctoral student. Limited finances is just the beginning of student life, it goes along with deadlines and latenight, besides never having a settled feeling. Pradnya not only manage to survive but also supported me, especially for the past six months by taking the complete responsibility of the house. She was one of the primary motivators who changed me from a living-for-today kind of student to a responsible professional. Finally, my parent are responsible for making

me the kind of person that I am. I will always cherish their constant encouragement during my graduate studies and in life.

The last but not the least, my stay at Georgia Tech was possible due to financial support via graduate assistantships. The first three years were funded by the school (first year was a graduate research assistantship followed by two years of graduate teaching assistantship) and the last two years were funded by United States Air Force Office of Scientific Research. I am grateful to the funding agencies.

Contents

List of Tables

List of Figures

Summary

Aeroelastic instabilities have long constrained the flight envelope of many types of aircraft and thus are considered important during the design process. As designers strive to reduce weight and raise performance levels using directional material, thus leading to an increasingly flexible aircraft, there is a need for reliable (less conservative yet accurate) analysis tools, which model all the important characteristics of the fluid-structure interaction problem. Such a model would be used in preliminary design and control synthesis. Traditionally, the most accurate aeroelasticity results have come from either an experimental investigation or more recently a complete numerical simulation by coupling finite element method and computational fluid dynamics analysis. Though such results are very accurate, can be obtained over a complete flight regime and can include "higher-order" phenomena and nonlinearities, they are also very expensive, especially so in the initial phase of design, when a number of design configurations may need to be analyzed.

For a restricted problem, it is advantageous to take into account simplifications which do not compromise the quality of the results. This would reduce the order of the problem while retaining high fidelity. Such a model would lend itself to an easier parameter identification and thus would be useful in design studies or in study of higher-order phenomenon.

The focus of this research was to analyze a high-aspect-ratio wing aircraft flying at low subsonic speeds. Such aircraft are designed for high-altitude, long-endurance

missions. Due to the high flexibility and associated wing deformation, accurate prediction of aircraft response requires use of nonlinear theories. Also strong interactions between flight dynamics and aeroelasticity are expected. To analyze such aircraft one needs to have an analysis tool which includes the various couplings and interactions. A theoretical basis has been established for a consistent analysis which takes into account, i) material anisotropy, ii) geometrical nonlinearities of the structure, iii) rigid-body motions, iv) unsteady flow behavior, and v) dynamic stall.

The airplane structure is modeled as a set of rigidly attached beams. Each of the beams is modeled using the geometrically exact mixed variational formulation, thus taking into account geometrical nonlinearities arising due to large displacements and rotations. The cross-sectional stiffnesses are obtained using an asymptotically exact analysis, which can model arbitrary cross sections and material properties. An aerodynamic model, consisting of a unified lift model, a consistent combination of finite-state inflow model and a modified ONERA dynamic stall model, is coupled to the structural system to determine the equations of motion.

Using finite element discretization, the formulation leads to a set of nonlinear partial differential equations which are first order in time. First, a steady-state solution for a given flight condition is obtained. The equations of motion can then be perturbed about this steady state to get the eigenvalues of the system, i.e., frequency and damping. The perturbed equations are in the state-space form and can be used for linear control synthesis. For time marching, space-time mixed finite elements are used to obtain a set of nonlinear algebraic equations which can be solved with the given initial conditions to get the solution after a time step.

The results obtained indicate the necessity of including nonlinear effects in aeroelastic analysis. Structural geometric nonlinearities result in drastic changes in aeroelastic characteristics, especially in case of high-aspect-ratio wings. The nonlinear stall

effect is the dominant factor in limiting the amplitude of oscillation for most wings. The limit cycle oscillation (LCO) phenomenon is also investigated. Post-flutter and pre-flutter LCOs are possible depending on the disturbance mode and amplitude. Finally, static output feedback (SOF) controllers are designed for flutter suppression and gust alleviation. SOF controllers are very simple and thus easy to implement. For the case considered, SOF controllers with proper choice of sensors give results comparable to full state feedback (linear quadratic regulator) designs.

Chapter 1

INTRODUCTION

The field of aerospace engineering is entering an era of high technology. Over the past decade there has been a great deal of progress in almost all the sub-fields in aeronautics. Control is becoming an integral part of all the sub-disciplines, thus leading to areas of research like control of flexible structures, flow control, and the fly-by-wire concept. Traditionally, designers sought to optimize the design for individual disciplines. For example, the design of the load-carrying member of a wing was the responsibility of the structural engineer, who had to do it within the constraint of an airfoil shape optimized by an aerodynamacist. The flight control system designer would then work on this design for the best performance and stability norms. Such a design does not always approach the global optimum, the solution to a coupled optimization problem.

Coupled optimization with realistic models is computationally very expensive. One could depend on historical data to constrain the system to the point that it is solvable. An alternative way is to construct low-order, high-fidelity models which contain most of the higher-order, nonlinear effects and couplings of the aircraft. This would not necessitate constraining of the system; thus it is open to newer designs for current flight requirements. Such a system model would give physical insight into the behavior of the problem, thus highlighting the kind of coupled behavior which is

sometimes favorable but can be disastrous at other times.

The last decade has seen an expansion of the flight envelope as well as an increase in the variety of flight missions. Aeroelastic tailoring of composite wings opened an era in which structural coupling was used favorably, making forward swept wings possible. Uninhabited aerial vehicles would take the human out of the aircraft. An increase in flight performance is likely due to the tolerance for high loads but would have to be accompanied by very robust and intelligent controllers. Here flight maneuvers which were once discarded due to their uncertainties could be used if accompanied by a controller based on an aircraft model (analysis) which possesses all the physical characteristics of the aircraft. Then stall could be a regular part of the flight trajectories, and control reversal could be used effectively as control augmentation. Again the need is for a model which takes into account the higher-order, nonlinear effects and the various couplings. Such a model could be used for parametric studies on an aircraft model and for optimization. One could augment this model with a more accurate analysis tool for final validation.

The aim of the proposed research is to develop such a low-order, high-fidelity model which includes various structural and aerodynamic nonlinearities and couplings. This model could give physical insight into the behavior of the system and would be useful in flight controller and flutter suppression system design. With the integration of the various disciplines, including structures, dynamics, aerodynamics, propulsion, flight mechanics and control, this model could also be used in a flight simulator as, say, a gust load alleviation model or as a test bed for nonlinear control design.

Chapter 2

LITERATURE SURVEY

Aeroelasticity is a vast field. Aeroelastic instabilities such as divergence and flutter have been the limiting factors for high speed flights. The development of theories for aeroelastic analyses, which started with simplistic models of linear modal analysis for structures and one-dimensional (1-D) quasi-steady aerodynamics, have come a long way to the point that tools based on coupling the Finite Element Method (FEM) and Computational Fluid Dynamics (CFD) are in current use. Yet many aeroelastic analysis tools and unsteady aerodynamics theories which were developed in the earlier part of the century are still in common use, e.g., modal analysis, Theodorsen's unsteady aerodynamics, the Doublet Lattice Method and the V-g method. The advent of high powered computers has only made it faster to get to the answer. It is not the aim of this chapter to go into the historical development of aeroelastic theories. Instead an overview of recent and ongoing research in related fields is presented. For putting the references in the right perspective, the literature survey is divided into various sections.

2.1 Aeroelastic Tailoring

Aeroelastic analysis of composite wings is the focus of an ever increasing body of literature. The interest stems from the possibility of using directional properties of composites to optimize a wing (i.e., aeroelastic tailoring). One of the earliest parametric studies on aeroelasticity of composite wings was done by Housner and Stein [1]. They presented a computer program for flutter analysis that calculated the variable stiffness properties by using a laminated, balanced-ply, filamentary composite plate theory. The parametric studies included the effect of filament orientation upon the flutter speed for wings with various sweep angles, mass ratios, and skin thicknesses.

Hollowell and Dugundji [2] analytically and experimentally investigated the flutter and divergence behavior of unswept, rectangular wings made of graphite/epoxy, modeled as cantilevered plates with various amounts of bending-twist coupling. Lottati [3] analytically investigated the flutter and divergence speeds of a cantilevered, composite, forward-swept rectangular wing, for various values of the bending-twist coupling. Green [4] concentrated on the aeroelastic problems of a transport aircraft with its high-aspect-ratio, aft-swept wings.

Shirk *et al.* [5] presents a historical background of aeroelastic tailoring and the theory underlying the technology. The paper provides historical perspective on the development of codes and the activities of various research groups up to that time. It is still true that in many studies, the structural deformation model used is a beam-like wing, since tailoring focuses on bend-twist deformation coupling. Restraining the freedom of the edgewise bending mode, which is often done, can result in substantially different natural frequencies and mode shapes for highly coupled laminates. The prudence of retaining rigid-body modes in flutter analysis during design iterations was also pointed out. Weisshaar [6] discussed static aeroelastic problems such as spanwise

lift redistribution, lift effectiveness, and aileron effectiveness. Two theoretical models are commonly used: (1) laminated plate theory with elementary strip theory airloads, (2) a more general representation of the laminated wing in matrix form, with discrete-element aerodynamics. In the latter case, the beam is characterized by bending stiffness EI, torsional stiffness GJ, and bending-twist coupling K.

The works described above use very simplified and unrealistic structural models compared to real wings. The models use either a plate-beam model or a "box-beam" composed of two rigidly attached plates. These models are sufficient to prove the concept of aeroelastic tailoring, but they are not suitable for designing real wings. Librescu and his co-workers [7, 8] analyzed the divergence instability of a swept-forward, composite wing modeled as a thin-walled, anisotropic, composite box beam. The model incorporates a number of non-classical effects, including anisotropy of the material, transverse shear deformation and warping effects. This type of model offers insight into the elastic coupling mechanisms. This model is representative of a wing-like geometry and includes "non-classical" effects in the beam model, but, it is still not suitable for a realistic, built-up structure.

Banerjee and his co-workers have been working on a similar problem and have investigated the optimization of a composite cantilevered box beam with frequency and aeroelastic constraints [9, 10]. The dynamic stiffness matrix method is used for modal analysis of the beam. In another study, parametric analysis of box beams with thick walls is conducted by Chattopadhyay and co-workers [11]. Here, higher-order laminate theory is used for each wall of the box beam. Aeroelastic tailoring of cantilevered composite box beams has been investigated by Cesnik, Hodges, and, Patil [12, 13]. The papers investigated the influence of ply angle layup on flutter and divergence speed of a high aspect ratio wing.

The aerodynamics used in all the above investigations is based upon simple

Theodorsen's strip theory. Aerodynamic loads can be obtained only if the reduced frequency (k) is specified. The drawback of k-type aerodynamics is that results for true aerodynamic damping at a given flight condition cannot be obtained, only the flutter condition is obtained accurately. In addition, important compressibility and finite aspect ratio effects are not accounted for in many models. Structurally the wing was clamped at one end thus neglecting the rigid body modes. The analyses were useful in indicating the strong influence of structural coupling, but were insufficient in terms of accuracy for practical configurations to be used for preliminary design or for control synthesis.

2.2 Nonlinear Aeroelasticity

Nonlinear aeroelastic analysis has gathered a lot of momentum in the last decade due to understanding of nonlinear dynamics as applied to complex systems, and the availability of the required mathematical tools. Boyd investigated the effect of edge-wise deformation and steady-state lift on the flutter of cantilevered wing [14]. He modeled a simple nonlinear structural coupling between torsion and bending arising due to moderately large deformation. Theodorsen's theory was used for aerodynamic analysis. The studies conducted by Dugundgi and his co-workers are a combination of analysis and experimental validation of the effects of structural couplings on aeroelastic instabilities for a simple cantilevered laminated plate wing [15, 16, 17]. Stall flutter is investigated using the ONERA stall model. Though the focus is on nonlinearities due to stall and some structural nonlinearities are also considered, none of this work considers realistic, built-up structural models.

Limit cycle oscillations

There are various modalities to analyze and predict limit cycle oscillations (LCO). Given below are a few which have been recently applied to aeroelastic LCO study.

The most common way of analyzing LCOs is via time marching. The system is simulated in time for various initial conditions. And the response is plotted in time or as a phase-plane plot to see if *i)* the response is diverging and *ii)* it converges to a LCO. This is very much computer time intensive and one needs to select a set of initial conditions relevant to the problem at hand. Tang *et al.* [18] used reduced order finite-state inflow model to analyze the nonlinear behavior of airfoil sections with free play nonlinearities. Tang and Dowell [19] have analyzed the nonlinear behavior of a flexible rotor blade due to structural, free-play and aerodynamic stall nonlinearities. The analytical results were compared with experimental observations. In both cases time-marching was used. Patil and Hodges [20] have presented results on the LCO observed in a stiff metallic wings. Finite elements in space and time were used for time integration.

In harmonic balance analysis the response is assumed to be a linear combination of a set number of harmonics. The solution is obtained by solving the nonlinear algebraic equations associated with all the harmonics. This type of analysis can often be improved by taking a larger number of harmonics. Unfortunately, it is not always possible to write the nonlinearities in terms of a set of harmonics, and even if it is, it may be too cumbersome. Dunn and Dugundji [16] used Fourier analysis to extract the relevant harmonics from the ONERA model and then used the harmonic balance method to predict LCO in a plate-like composite wing. The results obtained were compared with experimental data.

Wavelet filtering is a technique still under development and basically involves

running the time histories through a wavelet filter to get the Fourier components at various time steps. It is only a filtering (rather than analysis) technique and thus can take time histories from either experimental data or computation. It is useful in prediction of the onset of LCO. This analysis has been proposed by Lind, Snyder and Brenner [21], and has been used successfully to predict LCO using the nonlinear airfoil response data generated by Strganac and co-workers [22].

Apart from the experimental data for wing LCOs obtained by Tang and Dowell, and Dunn and Dugundji, O'Neil and Strganac [22] have obtained results for an airfoil on a nonlinear support system. A later theoretical analysis using the method of multiple scales by Gilliatt, Strganac and Kurdila [23] includes nonlinearities due to stall in a quasi-steady way. The objective is to predict internal resonance in such a model and to explore its effect as a LCO triggering mechanism.

2.3 Flight Dynamics of Flexible Aircraft

Aeroelastic characteristics of a highly flexible aircraft is investigated by van Schoor and von Flotow [24]. Natural mode shapes are obtained using finite element method and the corresponding unsteady forces are calculated using strip theory. It reiterates the necessity of modeling unsteady aerodynamics and flexibility to get the correct aircraft dynamics.

Waszak and Schmidt [25] used Lagrange's equation to derive the nonlinear equations of motion for a flexible aircraft. Generalized aerodynamic forces are added as closed form integrals. This form helps in identifying the effects of various parameters on the aircraft dynamics. Newman and Schmidt [26] discuss the method for reducing the order of a complete aircraft flight dynamics model. The reduction is accomplished by retaining all the modes that are critical in feedback system design. Frequency-weighted internally balanced reduction is compared with modal residual-

ization. Approximate literal expressions for the poles and zeroes of the system are also obtained. This method is good for a low order model and can give physical insight into the behavior of the system.

Linear aeroelastic and flight dynamic analysis results for a HALE aircraft are presented by Pendaries [27]. The results highlight the effect of rigid body modes on wing aeroelastic characteristics and the effect of wing flexibility on the aircraft flight dynamic characteristics.

Drela [28] has developed a nonlinear aeroelastic analysis code based on nonlinear finite elements for structural modeling and wind-aligned vortex wake for steady aerodynamic loads. Time marching is conducted by tracking the wake vortex sheet and calculating the influence on the wing. In the frequency domain unsteady aerodynamic loads are obtained for each space-time perturbation mode by using velocity influence coefficients for the frequency of the mode under consideration. A simplified approach using a locally-2D approximation is also presented.

2.4 Control of Aeroelastic Instability and Response

A survey paper by Noll [29] gives a good background on the subject of aeroservoelasticity. The feasibility of using feedback control systems for preventing aeroelastic instabilities on a forward swept wing was investigated by Noll *et al.* [30]. The design of a practical oscillation suppression system for an F/A-18 was done by Trame *et al.* [31].

A series of studies into control design for an aircraft based on its aeroelastic model have been conducted at NASA Langley. An experimental drone aircraft is used as a test case. Finite element method is used to model the structure and Doublet Lattice method is used to get the modal aerodynamic coefficients for various reduced frequencies. Newsom *et al.* [32] use a modified linear quadratic gaussian (LQG) method for

flutter suppression controller design. A reduced order controller is obtained by modal residualization and is evaluated on a complete system modal. This kind of design involves a lot of trial and error. Engineering judgment has to be used during selection of design parameters, relative noise gains and the states to be retained. Newsom and Mukhopadhyay [33] used the matrix singular values of the system return difference matrix to design a robust controller. The aim was to maximize the minimum singular value (unconstrained) or to constrain the singular values while minimizing the controller gains. Mukhopadhyay [34] extended the method to include shaping of the singular value spectrum (over the frequency). It is a four step procedure involving LQG controller design, optimization with singular value constraint, order reduction, followed by re-optimization with singular value constraint. Ref. [35] is a continuation of the work for a discrete time system. Here a digital robust controller is designed for gust load alleviation.

An active control system concept for an aeroelastic wind tunnel model with strong flight dynamic/aeroelastic interactions is developed by Rimer *et al.* [36]. A combination of a canard based stability augmentation system and an active flutter/divergence suppression system is used to get the desired flying qualities. The complete aircraft was modeled using few modes of vibration including rigid body modes.

Lin *et al.* [37, 38] have done a series of studies on using strain actuated aeroelastic wing control. Piezoelectric actuators were used for inducing strain. An experimental wing was designed and tested. A linear quadratic gaussian (LQG) control law was designed on the experimentally identified system for increased flutter dynamic pressure and decreases gust response.

Static output feedback

Static output feedback (SOF) gives one of the simplest possible controller design. Such a control design has been used in the present work for flutter suppression and gust load alleviation. Levine and Athans [39] first posed the linear quadratic SOF problem and found the control to be defined by the solution of two coupled Riccati equations. A computational solution procedure was also proposed. Since then there have been a lot of studies extending the results. A recent survey paper by Syrmos *et al.* [40] gives the current progress in the theory and solution techniques of SOF problems.

2.5 Other Relevant Literature

One does find in the literature a few dynamic aeroelasticity studies in which detailed structural formulations are considered. Guruswamy and co-workers have done a series of works in this area, including numerical solution of the 3-D unsteady Euler/Navier-Stokes equations [41], the study of wing-body aeroelastic response [42], and the solution of the Euler equations for flow over a wing assembled from plate finite elements [43]. Batina and co-workers have conducted similar work of coupling high-fidelity, computationally-expensive, time-domain aerodynamic codes with structural analysis. The work lead to the development of CAP-TSD (Computational Aeroelasticity Program-Transonic Small Disturbance) code [44, 45]. Here, the wing structure is represented by the natural modes. The aeroelastic analysis results are in good agreement with experimental data. Static aeroelastic results of a complete fighter configuration was obtained by Schuster [46] using ENS3DAE code [47]. ENS3DAE code is based on a complete three-dimensional Navier-Stokes algorithm. The studies discussed above are very accurate but far too complicated for use of linear control theory.

Rotor aeroelasticity is similar but much more complex as compared to fixed wing aeroelasticity. Analysis tools developed in both the fields have been frequently used in the other. The beam theory as well as the unsteady aerodynamics used in this research have been developed initially for helicopter aeroelasticity. Research conducted by Fulton [48] and Shang [49] form the basis for this research and is described below. Fulton and Hodges [50] coupled the mixed variational formulation for dynamics of beams [51] with 2-D quasi-steady aerodynamics and inflow calculated by momentum/blade element theory to develop a stability analysis for a hingeless, composite, isolated rotor in hover. The results were in good agreement with analytical as well as experimental results. Shang and Hodges [52] used state-space inflow theory developed by Peters and He [53] and coupled it with the mixed variational beam equations. Parametric studies were performed on rotors with advanced tip configurations, and on rotors with pretwist and initial curvature. Again the results were in good agreement with available analytical and experimental results.

Chapter 3

PRESENT WORK

In all the works described in the literature survey, although a few of them address some of the same concerns as proposed here, they either lack a sufficiently powerful structural model or a sufficiently powerful aerodynamic model. Some have considered various higher-order phenomena as a separate issue rather than in a unified framework. Some have included certain effects by adding *ad hoc* terms based on experience or intuition, while others have done trend analysis without proper consideration of physical constraints. There were some computationally intensive studies using the finite element method and CFD. While this leads to a very accurate aeroelastic analysis, it is computationally expensive, takes large amount of human resources to create accurate models and most importantly is not amenable to aeroservoelastic analysis, controller design and preliminary design.

Thus, the motivation for the proposed research stems from the lack of an aeroelastic model for an aircraft that has all the following capabilities:

1. able to model realistic wing structures of moderate to high aspect-ratio;

2. able to handle large rigid-body motion and geometrically nonlinear elastic deformation;

3. able to model representative flow about the wings without the complexity of

CFD;

4. able to obtain a sufficiently high degree of fidelity to ensure that the model provides an accurate physical insight into the behavior of the aircraft;

5. able to do so with a sufficiently low-order model to allow the use of linear control theory.

The goals of the present work necessitate the use of state-of-the-art, low-order, high-fidelity models. A brief description of the models used is presented below. A more detailed formulation of the aeroelastic analysis of a complete aircraft is presented in the next chapter.

3.1 Wing Structural Modeling

During the last nine years, a comprehensive framework has been developed for modeling of generally nonhomogeneous, anisotropic beams with arbitrary cross-sectional geometry and material distribution [54, 55]. With the modeling power of the finite element method, it takes a two-step modeling approach which facilitates the accurate treatment of complicated, built-up beam-like structures with a very small number of states. It is based on 3-D elasticity and is capable of modeling complex cross-sectional geometries (solid, built-up, or thin-walled; open or closed; airfoil shaped if necessary), including all possible couplings and deformation in an asymptotically correct manner. If further structural constraints are necessary, asymptotically correct 3-D strain/stress can be recovered at any point within the structure. Using this techniques, a moderate- to large-aspect-ratio wing can be modeled accurately as a beam. It should be noted that rather than always using the finite element method to extract the beam cross-sectional elastic constants, one can also solve for these constants in closed form if the structure is of thin-walled construction. An example of this sort of

analysis is found in Refs. [56] and [57]. Rehfield's model [56] is not asymptotically exact, but it analytically calculates the complete 6×6 stiffness matrix.

3.2 Large Rigid-Body Motion and Geometrically Nonlinear Deformation

The framework of structural analysis described in the earlier section also gives rise to a set of geometrically-exact nonlinear equations for the beam structural dynamics [51]. Thus, it provides a concise but accurate formulation for handling built-up, beam-like structures undergoing large motions with geometrically nonlinear deformation. It has been successfully applied to rotary-wing static and dynamic aeroelastic stability problems [50, 58], and aircraft composite wing aeroelastic analysis [12]. This formulation is ideally suited for large motion and geometrically nonlinear deformation of wings structures and will be used here.

3.3 Finite Element Discretization

By selecting the shape functions for the variational quantities in the formulation, one can choose between, *i)* finite elements in space leading to a set of ordinary nonlinear differential equations in time, *ii)* finite elements in space and time leading to a set of nonlinear algebraic equations.

3.4 Aerodynamics

A finite-state aerodynamic theory is well-suited for aeroelastic stability analysis, because the equations can easily be transformed into the s-plane for eigenanalysis. In order to have a state-space representation of the aerodynamic problem with a low number of states, the finite-state aerodynamic theory of Peters and co-workers

[59, 60] is a natural choice. It accounts for large frame motion and has generalized forces associated with generalized airfoil motion. The unsteady aerodynamics can be reduced to classical theories including trailing-edge flap deflection, *e.g.*, Theodorsen's theory [61] and Greenberg's theory [62]. The inflow model of Ref. [60] is responsible to provide the inflow states. The theory has been extended to include compressibility effects [63], and the ONERA stall model [59], thus increasing its validity over to a broader range of flight conditions.

3.5 Aeroelastic Analysis

By coupling the structural and aerodynamics models one gets the complete aeroelastic model. Using finite elements in space one can obtain the steady-state solution and calculate linearized equations of motion to do the stability analysis. This can also be used as a state-space representation for linear control synthesis. Finite elements in space and time will be used to march in time and get the dynamic nonlinear behavior of the system. This kind of analysis will be useful in finding the amplitudes of the limit cycle oscillations if the system is found to go unstable.

3.6 Control System Design

Once the state-space representation of the system has been achieved and the instability speed calculated, the next step is to increase the stability margin using active control. Here a simple static output feedback controller design is implemented [39]. Such a design is very easy to understand and implement. The simplicity of the controller coupled with the physical insight obtained from the aeroelastic model could lead to design of higher-order, physics-based controllers.

Chapter 4

THEORY

The theory is based on two separate works combined to give a consistent aeroelastic analysis, viz. *i)* mixed variational formulation based on exact intrinsic equations for dynamics of moving beams [51], and, *ii)* finite-state airloads for deformable airfoils on fixed and rotating wings [59, 63]. The former theory is a nonlinear intrinsic formulation for the dynamics of initially curved and twisted beams in a moving frame. There are no approximations to the geometry of the reference line of the deformed beam or to the orientation of the cross-sectional reference frame of the deformed beam. A compact mixed variational formulation can be derived from these equations which is well-suited for low-order beam finite element analysis based in part on the original paper by Hodges [51]. The latter work presents a state-space theory for the lift, drag, and all generalized forces of a deformable airfoil. Trailing edge flap deflections are included implicitly as a special case of generalized deformation. The theory allows for a thin airfoil which can undergo arbitrary small deformations with respect to a reference frame which can perform arbitrary large motions.

4.1 Nomenclature

b semichord

c_d	drag coefficient
D	drag per unit length
e_i	unit vectors in the i^{th} direction
f	external applied force
F	internal force
G	gravitational energy
h_n	generalized airfoil deformations
H	linear momentum
I	inertia matrix
K	kinetic energy
ℓ	wing length
L_n	lift distribution per unit length coefficients
m	external applied moment
M	internal moment
$\mathcal{M}$	mass
P	angular momentum
r	position vector from aircraft reference point
$\mathcal{S}$	6×6 stiffness matrix
u_0	aircraft forward speed
U	potential energy
v_n	generalized velocity perpendicular to airfoil
V	linear velocity
X	structural variables
Y	inflow variables
δ	variational operator
$\overline{\delta\mathcal{A}}$	virtual action

$\overline{\delta W}$ virtual work

Δ identity matrix

Δc_n reduction in generalized loads due to stall

γ strain

Γ circulation

κ curvature

λ_n inflow expansion coefficients

θ Rodrigues parameters

Ω angular velocity

ρ density of air

ξ mass offset

superscript

$\dot{(\,)}$ derivative with respect to time

$(\,)'$ derivative with respect to x_1

$\bar{(\,)}$ steady-state solution

$\check{(\,)}$ small perturbation about steady state

$\widetilde{(\,)}$ dual matrix

4.2 Structural Theory

The structural formulation derived in the present research is an extension of the mixed variational formulation for dynamics of moving beams. The original variational principle is modified and includes, global frame motion as variable and gravitational potential. Equations of motion are generated by including the appropriate energies in the variational principle followed by application of calculus of variation. Before describing the formulation, a few words have to be said about the notation and the reference frames used.

There is no difference, per se, between the symbols for scalars and those used for column matrices (the elements of which are measure numbers of vectors in a certain basis). The subscript in both the cases would indicate the object or the point referred to. In the case of a column matrix, a superscript might be added to indicate with which reference frame the measure numbers are associated. The rotation matrix would be denoted by C with the superscripts indicating the two reference frames in between which it transforms; e.g., $x^a = C^{ab}x^b$.

There are various reference frames used in the formulation: 'i' is the inertial reference frame, with i_3 vertically upward (needed to define the direction of gravitational forces); 'a' is a frame attached to the aircraft body, with a_2 pointing towards the nose, and a_3 pointing upward; 'b' is a series of frames attached to the undeformed beam (wing) reference line, b_1 is along the reference line; 'B' is the deformed beam reference frame.

The subscripts f and w refer to properties related to the fuselage and wing respectively. The subscripts 0 and b refer to points on the aircraft and beam reference line respectively. Note that the formulation is presented here assuming just one wing connected to a rigid fuselage for clarity. In actual implementation an user-defined number of "wings" are allowed, thus accounting for two wings, tail wings, vertical stabilizer, canard, or any other wing-like surfaces. A flexible fuselage or tail-boom (in HALE aircraft) is modeled as a purely structural beam.

The variational formulation is derived from Hamilton's extended principle and can be written as,

$$\int_{t_1}^{t_2} \left[\delta(K - U) + \overline{\delta W}\right] dt = \overline{\delta \mathcal{A}} \tag{4.1}$$

where t_1, t_2 specify the time interval over which the solution is required.

The kinetic energy of the system comes from the two subsystems which have mass,

viz., fuselage and wing. The kinetic energies can be represented as,

$$\begin{aligned} K_f &= \tfrac{1}{2}\left(\mathcal{M}_f V_0^{aT} V_0^a - 2\mathcal{M}_f \Omega_0^a \widetilde{V_0^a} \xi_f + \Omega_0^{aT} I_f \Omega_0^a\right) \\ K_w &= \tfrac{1}{2}\int_0^\ell \left(\mathcal{M}_w V_b^{BT} V_b^B - 2\mathcal{M}_w \Omega_b^B \widetilde{V_b^B} \xi_w + \Omega_b^{BT} I_w \Omega_b^B\right) dx_1 \end{aligned} \tag{4.2}$$

The gravitational potential energy can be written as

$$\begin{aligned} G_f &= \mathcal{M}_f g e_3^T C^{ia} \left(u_0^a + \xi_f\right) \\ G_w &= \int_0^\ell \mathcal{M}_w g e_3^T C^{ia} \left(u_0^a + r_b^a + u_b^a + C^{aB}\xi_w\right) dx_1 \end{aligned} \tag{4.3}$$

The strain energy due to elastic deformation of the wing is given by,

$$U = \tfrac{1}{2}\int_0^\ell \left\{ \begin{array}{c} \gamma \\ \kappa \end{array} \right\}^T [\,\mathcal{S}\,] \left\{ \begin{array}{c} \gamma \\ \kappa \end{array} \right\} dx_1 \tag{4.4}$$

The stiffness matrix for arbitrary cross section can be obtained from VABS (Variational Asymptotic Beam Sectional Analysis) [55].

Now taking the variation of individual energies, we get,

$$\delta K = \delta V_0^{aT} P_0^a + \delta \Omega_0^{aT} H_0^a + \int_0^\ell \left(\delta V_b^{BT} P_b^B + \delta \Omega_b^{BT} H_b^B\right) dx_1 \tag{4.5}$$

The expressions for P and H have been derived in Ref. [58] and are given by,

$$\begin{aligned} P &= \left(\frac{\partial K}{\partial V}\right)^T = \mathcal{M}\left(V - \widetilde{\xi}\Omega\right) \\ H &= \left(\frac{\partial K}{\partial \Omega}\right)^T = I\Omega + \mathcal{M}\widetilde{\xi} V \end{aligned} \tag{4.6}$$

Also,

$$\delta U = \delta G + \int_0^\ell \left(\delta\gamma^T F_b^B + \delta\kappa^T M_b^B\right) dx_1 \tag{4.7}$$

The expressions for F and M are obtained as

$$\left\{ \begin{array}{c} F \\ M \end{array} \right\} = \left\{ \begin{array}{c} \frac{\partial U}{\partial \gamma}^T \\ \frac{\partial U}{\partial \kappa}^T \end{array} \right\} = [\,\mathcal{S}\,] \left\{ \begin{array}{c} \gamma \\ \kappa \end{array} \right\} \tag{4.8}$$

The virtual work done on the system can be written as

$$\overline{\delta W} = \delta u_0^{aT} f_0^a + \overline{\delta \psi}_0^{aT} m_0^a + \int_0^\ell \left(\delta u_b^{aT} f_b^a + \overline{\delta \psi}_b^{aT} m_b^a \right) dx_1 \tag{4.9}$$

Now using the kinematic relationships derived in Ref. [51] and the transformed representation presented in Ref. [58], the expressions for the velocities and the generalized strains can be written as

$$\begin{aligned} V_0^a &= \dot{u}_0^a \\ \widetilde{\Omega}_0^a &= -\dot{C}^{ai} C^{aiT} \\ V_b^B &= C^{Ba} \left(V_0^a + \widetilde{\Omega}_0^a \left(r_b^a + u_b^a \right) + \dot{u}_b^a \right) \\ \widetilde{\Omega}_b^B &= -\dot{C}^{Ba} C^{BaT} + C^{Ba} \widetilde{\Omega}_0^a C^{BaT} \\ \gamma &= C^{Ba} \left(C^{ab} e_1 + u_b^{a\prime} \right) - e_1 \\ \widetilde{\kappa} &= \left(C^{bB} C^{Ba\prime} - C^{ba\prime} \right) C^{ab} \end{aligned} \tag{4.10}$$

Before proceeding any further, it is necessary to define rotational variables to represent the orientation of the aircraft and wing sections. The orientation of B frame with respect to a frame can be represented in terms of Rodrigues parameters. Rodrigues parameters have been applied to nonlinear beam problems with success. Thus, the expressions for the angular velocities and moment strain can be simplified

in terms of the parameters as

$$\begin{aligned}\Omega_b^B &= C^{ba}\left(\frac{\Delta - \frac{\widetilde{\theta}_b^a}{2}}{1+\frac{\theta_b^{aT}\theta_b^a}{4}}\right)\dot{\theta}_b^a + C^{Ba}\Omega_0^a \\ \kappa &= C^{ba}\left(\frac{\Delta - \frac{\widetilde{\theta}_b^a}{2}}{1+\frac{\theta_b^{aT}\theta_b^a}{4}}\right)\theta_b^{a\prime}\end{aligned} \tag{4.11}$$

For the orientation of the aircraft (i.e., of the a frame), the regular use of the Rodrigues parameters is insufficient because of a singularity at rotation of 180°. Thus, the direction cosines of a in i will be used as rotational variables. The expression for the angular velocity will automatically constrain the six additional unknowns.

Given above are the variational forms of all the energies, and the expressions for all the variables used therein. In the mixed formulation, the variable expressions are enforced as additional constraints using Lagrange multipliers. Denoting the expressions of all the variables by $()^*$, Hamilton's equation becomes,

$$\begin{aligned}&\int_{t_1}^{t_2}\Big\{\delta V_0^{a*T}P_0^a + \delta\Omega_0^{a*T}H_0^a + \delta u_0^{aT}f_0^a + \overline{\delta\psi}_0^{aT}m_0^a - \delta G - \delta V_0^{aT}(P_0^a - P_0^{a*}) \\ &\quad -\delta\Omega_0^{aT}(H_0^a - H_0^{a*}) - \delta P_0^{aT}(V_0^a - V_0^{a*}) - \delta H_0^{aT}(\Omega_0^a - \Omega_0^{a*}) + \int_0^\ell\Big[\delta V_b^{B*T}P_b^B \\ &\quad +\delta\Omega_b^{B*T}H_b^B - \delta\gamma^{*T}F_b^B - \delta\kappa^{*T}M_b^B + \delta u_b^{aT}f_b^a + \overline{\delta\psi}_b^{aT}m_b^a + \delta\gamma^T(F_b^B - F_b^{B*}) \\ &\quad +\delta\kappa^T(M_b^B - M_b^{B*}) - \delta V_b^{BT}(P_b^B - P_b^{B*}) - \delta\Omega_b^{BT}(H_b^B - H_b^{B*}) + \delta F_b^{BT}(\gamma - \gamma^*) \\ &\quad +\delta M_b^{BT}(\kappa - \kappa^*) - \delta P_b^{BT}(V_b^B - V_b^{B*}) - \delta H_b^{BT}(\Omega_b^B - \Omega_b^{B*})\Big]dx_1\Big\}dt = \overline{\delta\mathcal{A}}\end{aligned} \tag{4.12}$$

The expressions for various quantities and their variations can be substituted in the above equations to get a complete expression for the Hamilton's equation.

The external forces and moments in the above expressions are the various loads acting on the aircraft, including aerodynamic and propulsive loads. Propulsive loads

will be assumed as given. The aerodynamic loads will be calculated as described in the following section.

4.3 Aerodynamic Theory

In order to have a state-space representation of the aerodynamic problem with a low number of states, the finite-state aerodynamic theory of Peters and co-workers [59] is a natural choice. It accounts for large frame (airfoil) motion as well as small deformation of the airfoil in this frame, *e.g.*, trailing edge flap deflection. The theory has been extended to include compressibility effects [63], and gives good dynamic stall results when complemented with the ONERA stall model [59].

The aerodynamic loads used are as described in detail in Peters and Johnson [59]. The integro-differential airloads equations can be converted into ordinary differential equations (ODE) through a Glauert expansion. The ODEs are in terms of the expansion coefficients which are represented by a subscript n, so that

$$\begin{aligned}\tfrac{1}{2\pi\rho}\{L_n\} &= -b^2[M]\left\{\ddot{h_n} + \dot{v_n}\right\} - bu_0[C]\left\{\dot{h_n} + v_n - \lambda_0\right\} - {u_0}^2[K]\{h_n\} \\ &\quad -b[G]\{\dot{u_0}h_n + \bar{u_0}\zeta_n - u_0v_n + u_0\lambda_0\} \\ \tfrac{1}{2\pi\rho}\{D\} &= -b\left\{\dot{h_n} + v_n - \lambda_0\right\}^T[S]\left\{\dot{h_n} + v_n - \lambda_0\right\} + b\left\{\ddot{h_n} + \dot{v_n}\right\}^T[G]\{h_n\} \\ &\quad -u_0\left\{\dot{h_n} + v_n - \lambda_0\right\}^T[K-H]\{h_n\} + \{\dot{u_0}h_n + \bar{u_0}\zeta_n - u_ov_n + u_0\lambda_0\}^T[H]\{h_n\}\end{aligned} \tag{4.13}$$

where ρ, b are the air density and semichord respectively. The matrices denoted by $[K]$, $[C]$, $[G]$, $[S]$, $[H]$, $[M]$ are constant matrices whose expressions are given in Ref. [59]

The required airloads (viz., lift, moment about mid-chord, and hinge moment) are obtained as a linear combination of L_n. The theory described so far is basically a linear, thin-airfoil theory. But the theory lends itself to corrections and modifications

from experimental data. Thus, corrections such as thickness and Mach number can be incorporated very easily as described in Ref. [63].

4.3.1 Inflow theory

The inflow is obtained through the finite-state inflow theory [64]. The inflow (λ_0) is represented in terms of N states λ_1, λ_2, ..., λ_N as

$$\lambda_0 \approx \tfrac{1}{2} \sum_{n=1}^{N} b_n \lambda_n \tag{4.14}$$

where the b_n are found by least square method, and the λ_n are obtained by solving a set of N first-order differential equations [64] as,

$$\begin{aligned} &\dot{\lambda}_0 - \tfrac{1}{2}\dot{\lambda}_2 + \tfrac{u_T}{b}\lambda_1 = 2\dot{\bar{\Gamma}} \\ &\tfrac{1}{2n}\left(\dot{\lambda}_{n-1} - \dot{\lambda}_{n+1}\right) + \tfrac{u_T}{b}\lambda_n = \tfrac{2}{n}\dot{\bar{\Gamma}} \end{aligned} \tag{4.15}$$

where, $\bar{\Gamma}$ is the normalized circulation $\frac{\Gamma}{2\pi b}$. The expression for the normalized circulation is calculated based on the deformable airfoil model as

$$\bar{\Gamma} = \{1\}^T[C - G]\{h_n + v_n - \lambda_1\} + \tfrac{u_0}{b}\{1\}^T[K]\{h_n\} \tag{4.16}$$

4.3.2 Stall model

The airloads and inflow model can be modified to include the effects of dynamic stall according to the ONERA approach [65] as modified to couple with the present airloads model [59], so that

$$\begin{aligned} &L_{T_n} = L_n + \rho u_T \Gamma_n \qquad\qquad n \geq 1 \\ &\Gamma_T = \Gamma + \Gamma_\ell \end{aligned} \tag{4.17}$$

where

$$
\begin{aligned}
u_T &= \sqrt{{u_0}^2 + (v_0 + \dot{h_0} - \lambda_0)^2} \\
\ddot{\Gamma_n} + \tfrac{u_T}{b}\eta\dot{\Gamma_n} + \left(\tfrac{u_T}{b}\right)^2 \omega^2 \Gamma_n &= -\tfrac{\omega^2 {u_T}^3 \Delta c_n}{b} - \omega^2 e u_T \tfrac{d}{dt}\left(u_T \Delta c_n\right)
\end{aligned}
\tag{4.18}
$$

The parameters Δc_n, η, ω^2, and e must be identified for a particular airfoil. Γ_ℓ is the correction to the circulation obtained for Δc_ℓ. To calculate the correction to Lift ($-L_0$) and drag (D) the following equations are used, which also include the effect of skin friction drag; viz.,

$$
\begin{aligned}
L_{T_0} &= L_0 - \rho u_0 \Gamma_\ell - c_d u_T (v_0 + \dot{h_0} - \lambda_0)\rho b \\
D_T &= D - \rho(v_0 + \dot{h_0} - \lambda_0)\Gamma_\ell + c_d u_T u_0 \rho b
\end{aligned}
\tag{4.19}
$$

The airloads are inserted into Hamilton's principle to complete the aeroelastic model. Here a few comments need to be made regarding the validity of the aerodynamic model. The airloads model is based on thin airfoil theory and the inflow model is based on unsteady wake due to an oscillating airfoil. Thus, the theory does not take into account the steady or unsteady vortices shed due to spanwise variation of circulation. This implies that tip vortices and in general vortices in the freestream direction are neglected. Here it is assumed that due to the high aspect ratio, the three-dimensional inflow structure can be accurately approximated as a two-dimensional inflow at each spanwise airfoil except at the wing tips. It is further assumed that wing tip vortex effects will not change the overall behavior of the wing significantly. Thus, the results may be quantitatively off but would predict the overall qualitative behavior. Also, due to 2-D assumption any effect of vortices shed out of the plane due to curved wing are also not captured. Finally, the ONERA model is an semi-empirical model which gives accurate results for the flight conditions based on which the model

parameters are optimized. Any extrapolation of the model for conditions outside the range of design of the model would lead to inaccurate predictions.

4.4 Solution of the Aeroelastic System

Coupling the structural and aerodynamics models one gets the complete aeroelastic model. By selecting the shape functions for the variational quantities in the formulation, one can choose between, *i)* finite elements in space leading to a set of ordinary nonlinear differential equations in time, *ii)* finite elements in space and time leading to a set of nonlinear algebraic equations. Using finite elements in space one can obtain the steady-state solution and calculate linearized equations of motion about the steady state for stability analysis. This state-space representation can also be used for linear control synthesis. Finite elements in space and time are used to march in time and get the dynamic nonlinear behavior of the system. This kind of analysis is useful in finding the amplitudes of the limit cycle oscillations and checking the nonlinear system response.

Thus, three kinds of solutions are possible. *i)* nonlinear steady-state solution, *ii)* stability analysis of small motions about the steady state (by linearizing about the steady state); and *ii)* time-marching solution for nonlinear dynamics of the system.

For steady state and stability analysis, the formulation is converted to it weakest form in space, while retaining the time derivatives of variable. This is achieved by transferring the spatial derivatives of variables to the corresponding variation by integration by parts. Due to the formulation's weakest form, the simplest shape functions can be used [51].

$$
\begin{aligned}
&\delta u = \delta u_i(1-\xi) + \delta u_j \xi && u = u_i \\
&\overline{\delta\psi} = \overline{\delta\psi}_i(1-\xi) + \overline{\delta\psi}_j \xi && \theta = \theta_i \\
&\overline{\delta F} = \overline{\delta F}_i(1-\xi) + \overline{\delta F}_j \xi && F = F_i \\
&\overline{\delta M} = \overline{\delta M}_i(1-\xi) + \overline{\delta M}_j \xi && M = M_i \\
&\overline{\delta P} = \overline{\delta P}_i && P = P_i \\
&\overline{\delta H} = \overline{\delta H}_i && H = H_i
\end{aligned}
\tag{4.20}
$$

With these shape functions, the spatial integration in Eq. (4.12) can be performed explicitly to give a set of nonlinear equations.

The equation for the aircraft (rigid-body motion) can be written as,

$$
-\dot{P}^a - \widetilde{\Omega}^a P^a - m^a g C^{ai} e_3 + \textstyle\sum_{i=1}^{n}(-m^i g C^{ai} e_3 + C^{aw} f_a^i) = 0 \tag{4.21}
$$

$$
\begin{aligned}
&-\dot{H}^a - \widetilde{\Omega}^a H^a - \widetilde{V}^a P^a - m^a g \widetilde{\zeta}_{cg}^a C^{ai} e_3 + \textstyle\sum_{i=1}^{n}[m^i g \widetilde{C^{ai}} e_3 (r^i + u^i \\
&+ C^{aw}\widetilde{\zeta}_{cg}^i) + (\widetilde{r^i} + \widetilde{u}^i) C^{aw} f_a^i - C^{aw}\widetilde{\zeta}_{ac}^i f_a^i + C^{aw} m_a^i] = 0
\end{aligned}
\tag{4.22}
$$

The equations for the ith element of the wing can be written as,

$$
\begin{aligned}
&\tfrac{\Delta\ell}{2}[-C^{ab}(I - C^{bw})e_1 + C^{aw}\gamma]^i \\
&+u^i + \tfrac{\Delta\ell}{2}[-C^{ab}(I - C^{bw})e_1 + C^{aw}\gamma]^{i+1} - u^{i+1} = 0
\end{aligned}
\tag{4.23}
$$

$$
\frac{\Delta\ell}{2}[(I + \frac{\widetilde{\theta}}{2} + \frac{\theta\theta^T}{4})C^{ab}\kappa]^i + \theta^i + \frac{\Delta\ell}{2}[(I + \frac{\widetilde{\theta}}{2} + \frac{\theta\theta^T}{4})C^{ab}\kappa]^{i+1} - \theta^{i+1} = 0 \tag{4.24}
$$

$$
-\dot{P}^i - \widetilde{\Omega}^i P^i - m^i g C^{wi} e_3 + f_a^i + \Delta\ell(\widetilde{k}_b + \widetilde{\kappa})^i(\frac{F^- + F^+}{2}) + F^+ - F^- = 0 \tag{4.25}
$$

$$
\begin{aligned}
&-\dot{H}^i - \widetilde{\Omega}^i H^i - \widetilde{V}^i P^i - m^i g \widetilde{\zeta}_{cg}^i C^{wi} e_3 + \widetilde{\zeta}_{ac}^i f_a^i + m_a^i \\
&+\Delta\ell(\widetilde{e}_1 + \widetilde{\gamma}^i)(\tfrac{F^- + F^+}{2}) + \Delta\ell(\widetilde{k}_b + \widetilde{\kappa})^i(\tfrac{M^- + M^+}{2}) + M^+ - M^- = 0
\end{aligned}
\tag{4.26}
$$

$$
\dot{u}^i + V_0 + \widetilde{\Omega}_0(r_b^i + u^i) - C^{aw} V^i = 0 \tag{4.27}
$$

$$
\dot{\theta}^i + (I + \tfrac{\widetilde{\theta}}{2} + \tfrac{\theta\theta^T}{4})^i C^{ab}(C^{wa}\Omega_0 - \Omega^i) = 0 \tag{4.28}
$$

These equations can be separated into structural (F_S) and aerodynamic (F_L) terms and written as

$$F_S(X, \dot{X}) - F_L(X, Y, \dot{X}) = 0 \tag{4.29}$$

Similarly we can separate the inflow equations into an inflow component (F_I) and a downwash component (F_W) as

$$-F_W(\dot{X}) + F_I(Y, \dot{Y}) = 0 \tag{4.30}$$

The solutions of interest for the two coupled sets of equations (Eqs. 4.29 and 4.30) can be expressed in the form

$$\left\{ \begin{array}{c} X \\ Y \end{array} \right\} = \left\{ \begin{array}{c} \bar{X} \\ \bar{Y} \end{array} \right\} + \left\{ \begin{array}{c} \check{X}(t) \\ \check{Y}(t) \end{array} \right\} \tag{4.31}$$

For the steady-state solution one gets $\bar{Y}$ identically equal to zero (from Eq. 4.30). Thus, one has to solve a set of nonlinear equations given by

$$F_S(\bar{X}, 0) - F_L(\bar{X}, 0, 0) = 0 \tag{4.32}$$

The Jacobian matrix of the above set of nonlinear equations can be obtained analytically and is found to be very sparse [66]. The steady-state solution can be found very efficiently using Newton-Raphson method.

To get the divergence solution, Eq. (4.32) is transformed into an eigenvalue problem, the eigenvalues of which give the divergence dynamic pressure:

$$\left[\frac{\partial F_S}{\partial X}\right]_{X=\bar{X}} \{X\} = q_{div} \left[\frac{1}{q}\frac{\partial F_L}{\partial X}\right]_{X=\bar{X}} \{X\} \tag{4.33}$$

where q_{div} is the divergence dynamic pressure and both the Jacobian matrices are obtained at the calculated steady state.

By perturbing Eqs. (4.29) and (4.30) about the calculated steady state using Eq. (4.31), the transient solution is obtained from

$$\begin{bmatrix} \frac{\partial F_S}{\partial \dot{X}} - \frac{\partial F_L}{\partial \dot{X}} & 0 \\ -\frac{\partial F_W}{\partial \dot{X}} & \frac{\partial F_I}{\partial \dot{Y}} \end{bmatrix}_{\substack{X=\bar{X} \\ Y=0}} \begin{Bmatrix} \dot{\check{X}} \\ \dot{\check{Y}} \end{Bmatrix} + \begin{bmatrix} \frac{\partial F_S}{\partial X} - \frac{\partial F_L}{\partial X} & -\frac{\partial F_L}{\partial Y} \\ 0 & \frac{\partial F_I}{\partial Y} \end{bmatrix}_{\substack{X=\bar{X} \\ Y=0}} \begin{Bmatrix} \check{X} \\ \check{Y} \end{Bmatrix} = \begin{Bmatrix} 0 \\ 0 \end{Bmatrix} \tag{4.34}$$

Now assuming the dynamic modes to be of the form e^{st}, the above equations can be solved as an eigenvalue problem to get the modal damping, frequency and mode shape of the various modes. The stability condition of the aeroelastic system at various operating conditions is thus obtained.

To investigate the nonlinear dynamics of the aircraft a time history of aircraft motion has to be obtained. Space-time finite elements are used for time marching. This requires that the formulation be converted into its weakest form in space as well as time. Thus, the spatial and temporal derivatives are transferred to the variations. Again due to the weakest form of the variational statement, constant shape functions are used for the variables, and linear/bilinear shape functions are used for the test functions [67].

$$\begin{aligned}
&\delta u = \delta u_i(1-\xi)(1-\tau) + \delta u_j \xi(1-\tau) + \delta u_k \xi\tau + \delta u_l(1-\xi)\tau && u = u_i \\
&\overline{\delta\psi} = \overline{\delta\psi}_i(1-\xi)(1-\tau) + \overline{\delta\psi}_j \xi(1-\tau) + \overline{\delta\psi}_k \xi\tau + \overline{\delta\psi}_l(1-\xi)\tau && \theta = \theta_i \\
&\overline{\delta F} = \overline{\delta F}_i(1-\xi) + \overline{\delta F}_j \xi && F = F_i \\
&\overline{\delta M} = \overline{\delta M}_i(1-\xi) + \overline{\delta M}_j \xi && M = M_i \\
&\overline{\delta P} = \overline{\delta P}_i(1-\tau) + \overline{\delta P}_j \tau && P = P_i \\
&\overline{\delta H} = \overline{\delta H}_i(1-\tau) + \overline{\delta H}_j \tau && H = H_i
\end{aligned} \tag{4.35}$$

where τ and ξ are dimensionless elemental temporal and spatial co-ordinates. With these shape functions, Eqs. (4.29) and (4.30) take the form,

$$\begin{aligned} F_S(X_i, X_f) - F_L(X_i, X_f, Y) &= 0 \\ -F_W(X_i, X_f) + F_I(Y_i, Y_f) &= 0 \end{aligned} \tag{4.36}$$

where subscripts i, f, represent the variable values at the initial and final time. If the initial conditions and time interval are specified, the variable values at the final condition is obtained by solving the set of nonlinear equations.

4.5 Static Output Feedback Controller

Static Output Feedback (SOF) controllers are based on direct feedback of the sensor output. Unlike Linear Quadratic Regulator (LQR) controller, SOF does not have all the states for feedback, only a few linear combinations of system states are available. Optimal static output feedback is used for control synthesis.

Theory supporting the problem of optimal constant output feedback gains for linear multivariable systems was first presented by Levine and Athans [39]. A solution technique for solving the nonlinear matrix equations was also presented. A recent paper by Syrmos *et al.* [40] gives the survey of the various static output feedback techniques, including optimal SOF. The problem statement of Optimal Static Output Feedback is presented here briefly.

Given an n^{th}-order stabilizable system,

$$\begin{aligned} \dot{x}(t) &= Ax(t) + Bu(t) + Dw(t) \\ y(t) &= Cx(t) \end{aligned} \tag{4.37}$$

where, $x \in \Re^n$ are the system states, A is the system dynamics in state-space form, $u \in \Re^m$ are the actuator commands, B is the control actuation matrix, $y \in \Re^p$ are the

sensor measurement, C is the matrix relating the sensor measurements to the state variables, w is zero mean unit intensity white noise process, and D is the matrix of noise intensity.

Assuming,

$$u(t) = Ky(t) \tag{4.38}$$

one determines constant feedback gains K such that they minimize the quadratic performance measure given by,

$$J(K) = \lim_{t\to\infty} \mathcal{E}\left\{\frac{1}{t}\int_0^t \left[x^T(s)Qx(s) + u^T(s)Ru(s)\right] ds\right\} \tag{4.39}$$

with $Q \geq 0$ and $R > 0$, while stabilizing the closed-loop system.

The solution is given by,

$$K = -R^{-1}B^T SPC^T(CPC)^{-1} \tag{4.40}$$

where, P and S are given by a set of coupled nonlinear matrix equations in terms of system parameters and K. Thus, the solution involves the solution of three equations including the above equation for K and the equations given below,

$$\begin{aligned} 0 &= A_c^T S + SA_c + Q - C^T K^T RKC \\ 0 &= A_c P + PA_c^T + V \end{aligned} \tag{4.41}$$

where, $A_c = A + BKC$, and $V = DD^T$.

The solution of the above set of coupled nonlinear equations can be calculated using a variety of iterative algorithms. Only a few of these algorithms have been proved to be convergent to a local minimum. Many other algorithms, though not proved to be convergent, do converge in most of the practical cases. The computational effort required also varies. A detailed survey of the various computational

methods is presented by Makila and Toivonen [68]. Two algorithms have been used in results presented here, Newton BFGS [69] and an algorithm proposed by Moerder and Calise [70].

Before ending this section on control theory it should be noted that SOF controllers are used here as a demonstration of the applicability of control design techniques on the present model. Even though the SOF controller gives a good performance (as will be shown in the next chapter), there are many additional practical considerations that need to be included in the control design process in actual practice. The controller needs to be optimal within constrains imposed by controller and actuator. Limitations such as bandwidth of the actuator, rate limitations imposed by actuator and controller implementation and control saturation need to considered. More important is consideration of uncertainty in the modeling process. As discussed earlier there are many inaccuracies introduced in the model, especially in the unsteady aerodynamics at high angle of attack. There is also a possibility of variation in the actual model parameters as compared to the nominal system model under investigation. Thus, robustness of the controller to these uncertainties is very important and should be taken into account during design of practical controllers.

Chapter 5

RESULTS

In this chapter, different aspects of the aeroelastic stability of a high-aspect-ratio wing model are discussed. These include, the importance of using the right stiffness formulation in order to model material couplings, the effects of a structural geometric nonlinearity and aerodynamic stall nonlinearity on the aeroelastic stability of a slender wing, the effects of aeroelastic/flight dynamics interactions, and initiation and sustaining mechanisms for LCOs.

A modular computer code has been developed which is a direct implementation of the aforementioned structural and aerodynamic theories for a complete aircraft with high-aspect-ratio wing [71].

5.1 Test Cases and Linear Aeroelastic Results

The results are presented for three different wing/aircraft models. These models have a range of aspect ratios and flexibility thus allowing results for various configurations.

5.1.1 Case 1: Goland wing

The Goland wing is a low-aspect-ratio prismatic metallic wing. It has been extensively used for validation. The Goland wing data [72] is reproduced in Table 5.1. It is a structurally uncoupled wing with some inertial coupling. Fig. 5.1 shows the V-g

Table 5.1: Goland wing structural data

Wing half span = 20 ft
Wing chord = 6 ft
Mass per unit length = 0.746 slugs per ft
Radius of gyration of wing about mass center = 25 % of chord
Spanwise elastic axis of wing = 33 % of chord (from l.e.)
Center of gravity of wing = 43 % of chord (from l.e.)
Bending rigidity (EI_b) = 23.65×10^6 lb ft^2
Torsional rigidity (GJ) = 2.39×10^6 lb ft^2

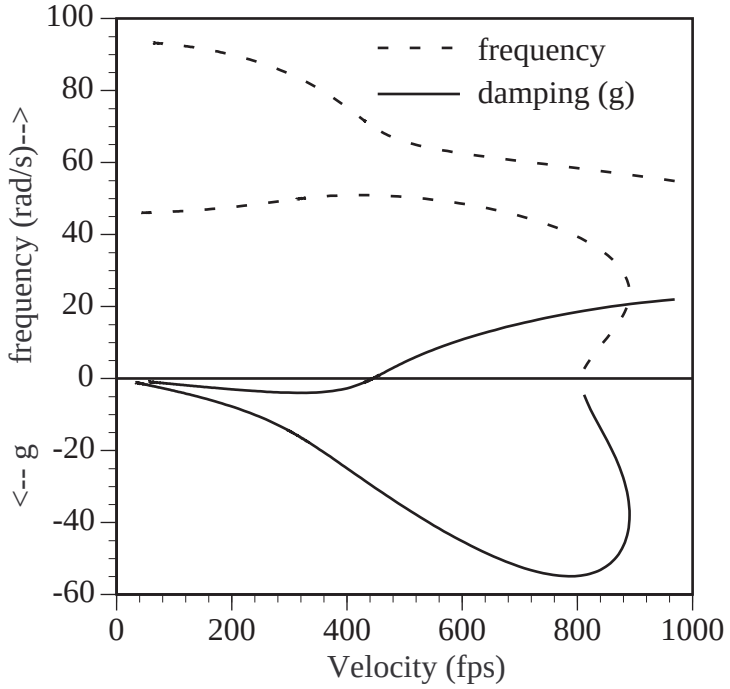

Figure 5.1: V-g plot for Goland's wing

Table 5.2: Comparison of flutter results for Goland wing

	Flutter Vel. (ft/sec)	Flutter Freq. (rad/s)
Present Analysis	445	70.2
Exact Solution	450	70.7
Galerkin Solution	445	70.7

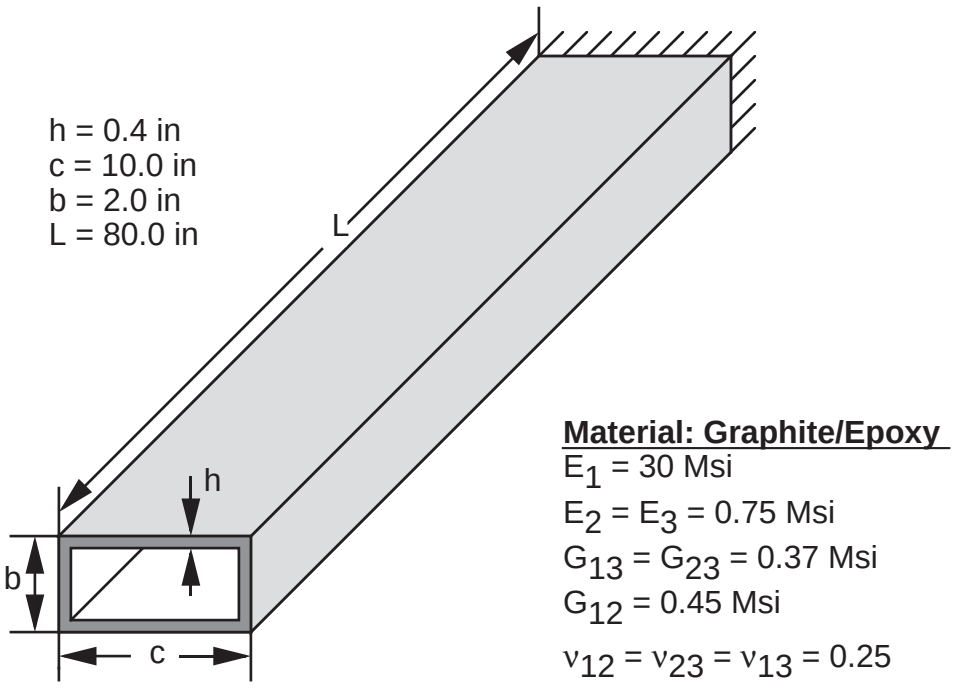

Figure 5.2: Geometry of box beam used by Librescu

plot obtained for this wing based on linear aeroelastic assumptions. Modal coalescence of the bending and torsion mode is observed and one mode goes unstable. The flutter and divergence point can be easily spotted. The present theory gives a flutter speed of 445 fps as compared to the exact flutter speed of 450 fps, and the flutter frequencies are, respectively, 70.2 rad/s and 70.7 rad/s (both with 1.0% relative error). (see Table 5.2)

5.1.2 Case 2: Librescu wing

The second test case is a composite box-beam wing of moderate aspect ratio. The wing model was defined in Ref. [7]. Fig. 5.2 shows a representation of this box beam. The wing dimensions and the properties of the laminate are also given in Table 5.3. The box beam is made of Graphite/Epoxy layers. The cross section is allowed to vary by changing the ply angle from $-90°$ to $90°$. The cross sections are organized into two

Table 5.3: Librescu wing structural data

Wing half span = 80 in
Wing box chord = 10 in
Wing box thickness = 2 in
Wing box laminate thickness = 0.4 in
LAMINATE: Graphite / Epoxy
E_1 = 30 Msi
$E_2 = E_3$ = 0.75 Msi
$G_{13} = G_{23}$ = 0.37 Msi
G_{12} = 0.45 Msi
$\nu_{12} = \nu_{23} = \nu_{13}$ = 0.25

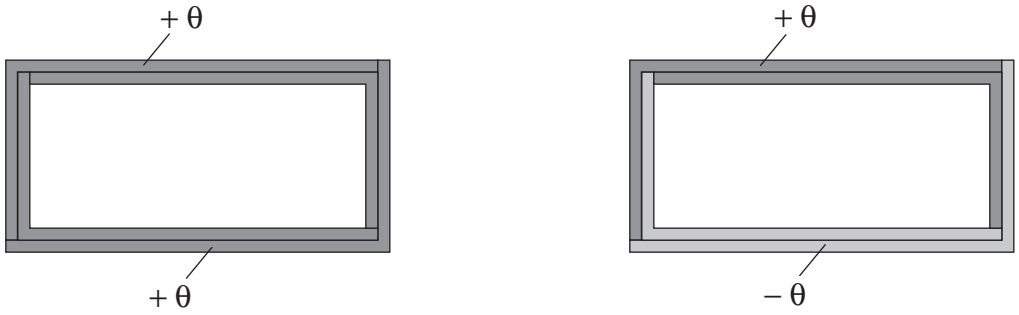

Figure 5.3: CUS (left) and CAS (right) configurations (Ply angle θ measured about the outward normal axis)

Table 5.4: HALE aircraft model data

WING
Half span = 16 m
Chord = 1 m
Mass per unit length = 0.75 kg/m
Mom. Inertia (50% chord) = 0.1 kg m
Spanwise elastic axis = 50% chord
Center of gravity = 50% chord
Bending rigidity = 2×10^4 N m^2
Torsional rigidity = 1×10^4 N m^2
Bending rigidity (edgewise) = 4×10^6 N m^2
PAYLOAD & TAILBOOM
Mass = 50 kg
Moment of Inertia = 200 kg m^2
Length of tail boom = 10 m
TAIL
Half span = 2.5 m
Chord = 0.5 m
Mass per unit length = 0.08 kg/m
Moment of Inertia = 0.01 kg m
Center of gravity = 50 % of chord

patterns, the circumferentially uniform cross section (CUS) and the circumferentially antisymmetric cross section (CAS), (Fig. 5.3). Aeroelastic tailoring is conducted for these two cross sections. The sweep angle Λ is also allowed to vary. A linearized code (achieved by assuming a zero steady state) is used for a aeroelastic tailoring study in order to allow a direct comparison with the results presented in Ref. [7]. The linear aeroelastic tailoring results obtained based on this case are presented in Section 5.2.

5.1.3 Case 3: HALE aircraft

Fig. 5.4 shows a sketch of the High-Altitude, Long-Endurance (HALE) aircraft under consideration. It has long slender wings to minimize drag and a tail boom to support the tail. Table 5.4 gives the structural and planform data for this aircraft.

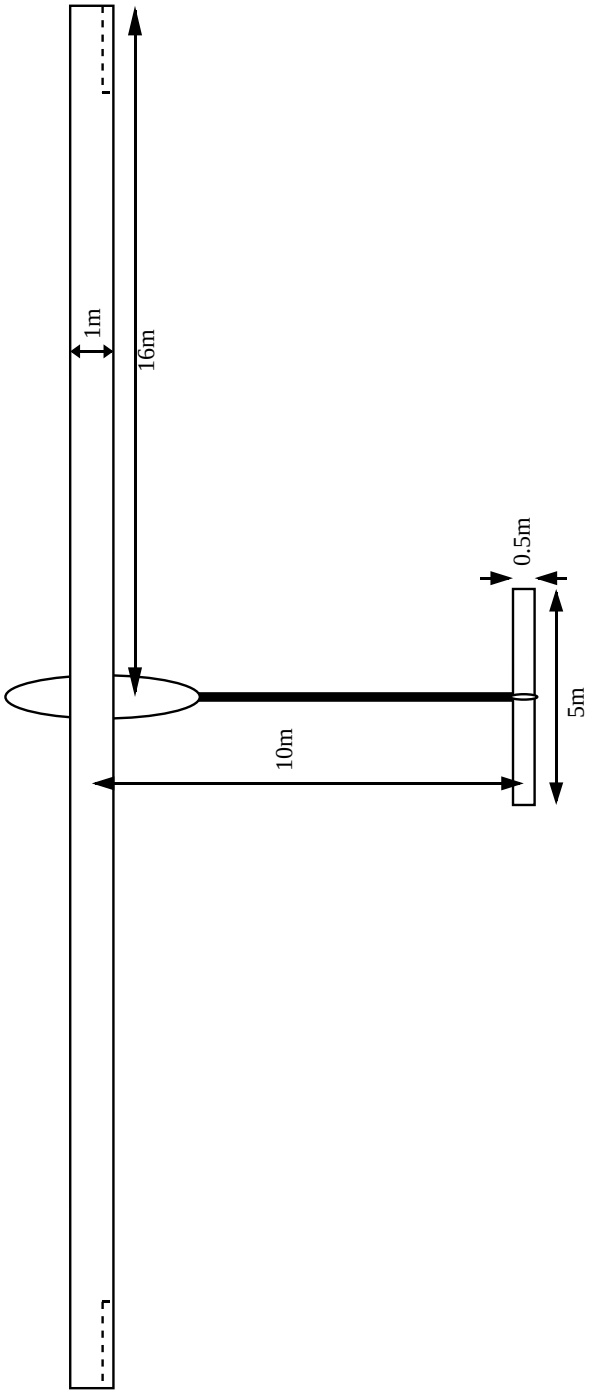

Figure 5.4: View of HALE aircraft model

Table 5.5: Comparison of linear frequency results (rad/s) for HALE wing

	Present Analysis	Analysis of Ref. [13]	% Error
1^{st} Flat. Bend.	2.247	2.243	+0.2
2^{nd} Flat. Bend.	14.606	14.056	+3.9
3^{rd} Flat. Bend.	44.012	39.356	+11.8
1^{st} Torsion	31.146	31.046	+0.3
1^{st} Edge. Bend.	31.739	31.718	+0.1

Table 5.6: Comparison of linear aeroelastic results for HALE wing

	Present Analysis	Analysis of Ref. [13]	% Diff.
Flut. Speed (m/s)	32.21	32.51	-0.9
Flut. Freq. (rad/s)	22.61	22.37	+1.1
Div. Speed (m/s)	37.29	37.15	+0.4

The data was obtained by modifying Daedalus data and is similar to the HALE kind of design.

Table 5.5 presents frequency results based on theories which are linearized about the undeformed state, i.e., the usual linear approach. The results for the present wing model were obtained using eight finite elements with all nonlinear effects suppressed. They are compared against the results obtained by theory of Ref. [13] which gives exact results for frequencies of a beam. The frequencies are very close except for the third flatwise bending mode. Error in the third bending mode is expected due to the low order discretization. But the third flatwise bending does not significantly influence the aeroelastic results and thus only eight finite elements are used.

Table 5.6 presents results from a linear calculation for flutter frequency and speed for the present wing model. As for the frequency results, the flutter results from

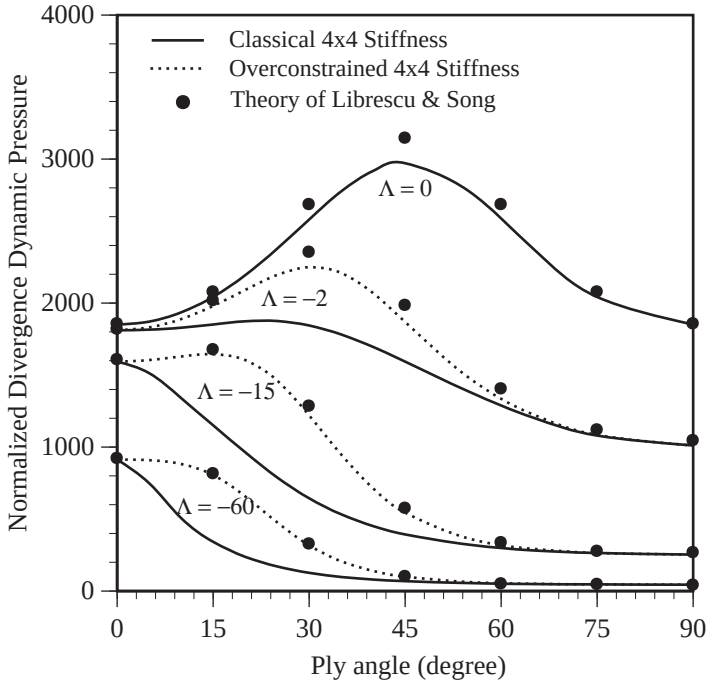

Figure 5.5: Variation of divergence dynamic pressure with ply angle for CUS configuration (normalized with respect to the divergence dynamic pressure for 0° ply angle)

the present analysis are obtained with all nonlinear effects suppressed. These are compared against the results obtained using theory of Ref. [13], which uses a Rayleigh-Ritz structural analysis with uncoupled beam mode shapes and Theodorsen's 2-D thin-airfoil theory for unsteady aerodynamics. The results are practically identical, indicating that eight finite elements are sufficient for the purposes of the present aeroelastic flutter calculations.

5.2 Aeroelastic Tailoring

Aeroelastic tailoring studies are conducted on Librescu's box-beam wing test case. Fig. 5.5 shows the variation of divergence dynamic pressure with ply angle for a circumferentially uniform stiffness (CUS) configuration, at different values of the sweep angle Λ. The CUS configuration produces extension-twist coupling and the fiber ori-

entation in the cross section is represented in Fig. 5.3 (left). When the authors of Ref. [7] studied this configuration, they were interested in the effects of transverse shear in the divergence speed. The symbols showed in Fig. 5.5 are samples of their numerical results without the inclusion of transverse shear. As discussed in Ref. [54], there are basically two ways to get a 4×4 stiffness model from a 6×6 stiffness formulation for the anisotropic beam. The first is achieved by just neglecting the transverse shear effects from the stiffness matrix. This does not lead to a correct 4×4 matrix, since it over-estimates some of the stiffness constants (see dotted lines in Fig. 5.5). The second approach is the consistent one, achieved by minimization of the strain energy with respect to the transverse shear measures (solid lines in Fig. 5.5). By doing so, the important contribution of the coupling terms between transverse shear and the classical measures are correctly accounted for. This result can be directly achieved by using an asymptotically correct classical formulation, as presented in Refs. [57] and [55].

For this particular example, the 6×6 cross-sectional stiffness constants were obtained by using Ref. [56]. Even though not described in Ref. [7], the results suggest that the authors used the first method of disregarding transverse shear effects. As one can see from Fig. 5.5, when the bending stiffness starts dominating (large sweep angles and $15^\circ \leq \theta \leq 60^\circ$), even the qualitative behavior of the wing are drastically different. The missing effects that are attributed to transverse shear [7] are in part caused by the reduction of the effective bending stiffness due to the bending-shear coupling (present in a CUS configuration). This just reinforces the fact that a consistent stiffness model is necessary for meaningful aeroelastic analysis.

Now for the composite box beam wing, consider the variation of the divergence and flutter speeds with ply angle for a circumferentially asymmetric stiffness (CAS) configuration. The CAS configuration produces vertical bending-twist coupling, the

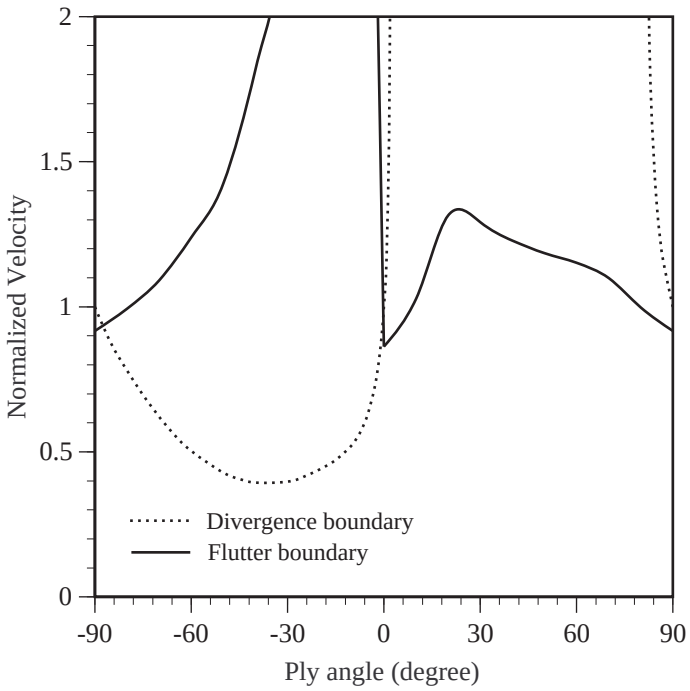

Figure 5.6: Variation of flutter and divergence velocities with ply angle for CAS configuration – normalized with respect to the divergence speed for 0° ply angle

fiber orientation in the cross section is represented in Fig. 5.3 (right). As for divergence, positive ply angles produce a favorable bending-twist coupling, leading to a very high divergence speed, whereas a negative ply angle shows lower divergence speed (see Fig. 5.6). The flutter results are more interesting and thought provoking. Flutter involves dynamic interaction of various modes. In the present study the normal modes of vibration of the composite beam change with ply angle, thus leading to a change in the flutter speed and mode shape. Unlike divergence, flutter is not directly associated with a single stiffness variable and thus much more complex. At any given speed there are various flutter speeds corresponding to various flutter modes. In Fig. 5.6, only the lowest flutter speed is represented. The plot is not smooth due to the changes of the lowest flutter mode shape. As can be seen large changes in flutter speed could be achieved sometimes by very small changes. Plots like these are useful

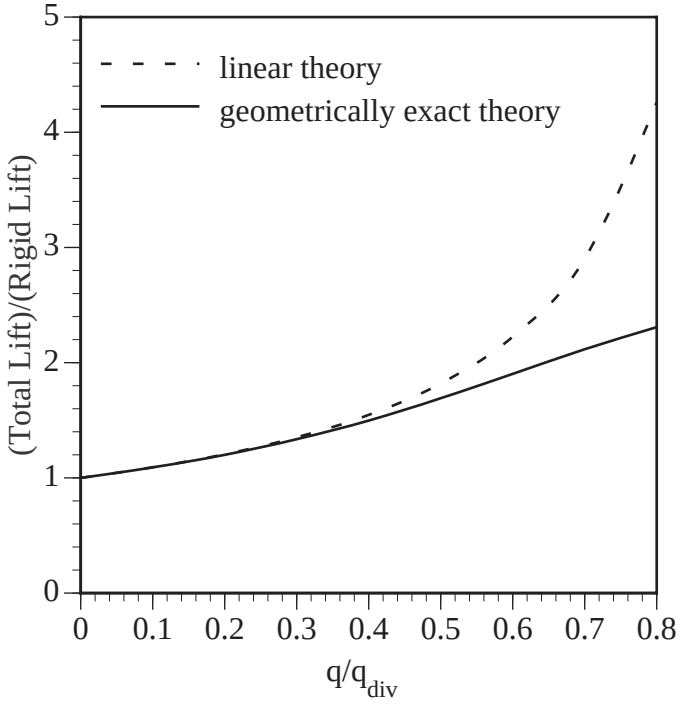

Figure 5.7: Variation of lift with the nonlinear steady state for Goland's wing

in understanding the effect of coupling on the aeroelastic characteristics and thus can be used during preliminary design.

5.3 Nonlinear Aeroelasticity

Nonlinear aeroelastic results have been obtained on the Goland's wing and the HALE wing. Nonlinear steady state and divergence characteristics are investigated first followed by nonlinear flutter and limit cycle oscillation studies. Analyzing nonlinear aeroelastic phenomena give a deeper insight into the inherent characteristics of the wing and give thumb rules for designers on taking these effects into account.

5.3.1 Steady state and nonlinear divergence

The effect of geometric nonlinearity on Goland's typical wing is illustrated in Figs. 5.7 and 5.8. These plots compare the variation of the ratio of total to rigid lift, and the

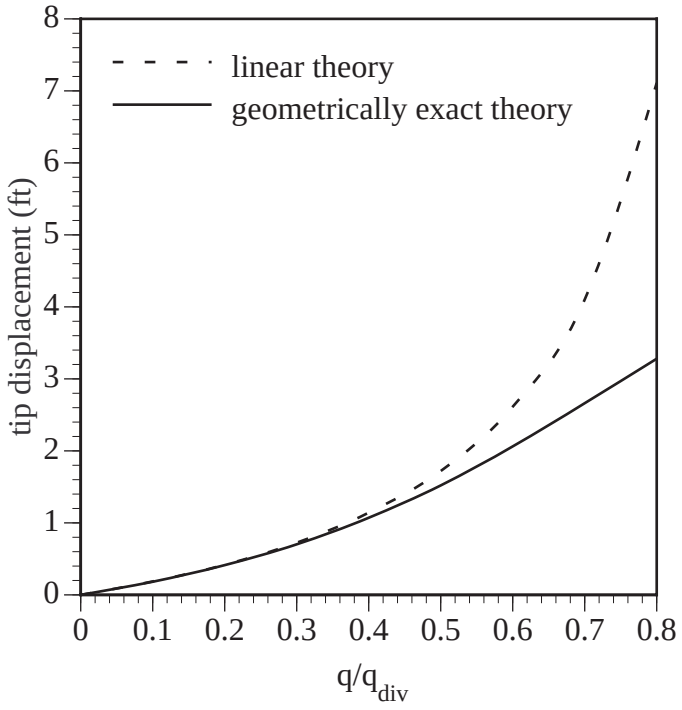

Figure 5.8: Variation of tip displacement with the nonlinear steady state for Goland's wing

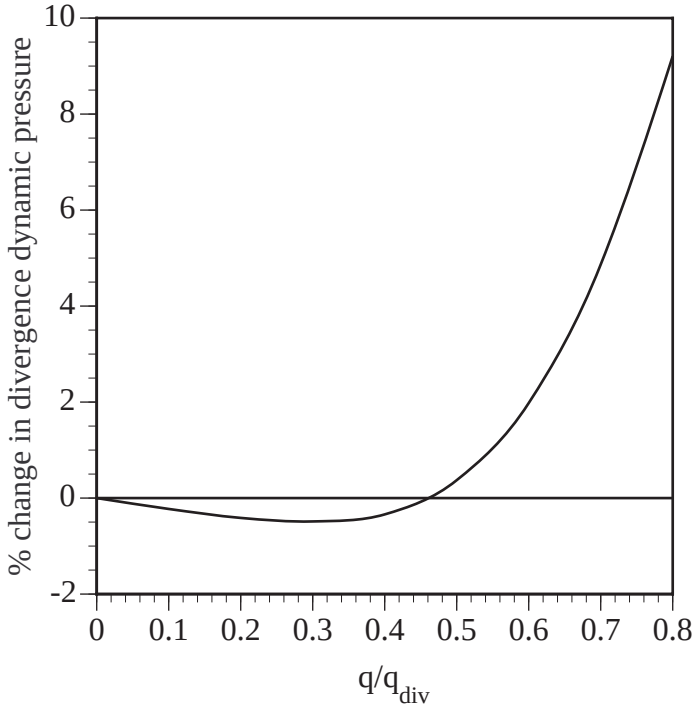

Figure 5.9: Variation of divergence dynamic pressure with the nonlinear steady state for Goland's wing

variation of tip displacement, respectively, with the dynamic pressure. The graphs show results obtained by the geometrically exact theory and its linearized form. Both total lift and tip displacement are over-predicted by the linear theory, and the difference increases with the dynamic pressure. At 80% of the linear divergence dynamic pressure, there is an error of about 100% for the total lift ratio, and even more for the tip displacement. This points to the fact that geometrically exact theory becomes increasingly important as one increases the dynamic pressure, and, therefore, the loads.

Divergence is a static instability that is calculated about a given equilibrium state. The linear approach takes the unloaded state and calculates its corresponding divergence dynamic pressure. But as the dynamic pressure increases (in the subcritical range), the wing deforms and different equilibrium positions are reached by the wing.

From this loaded equilibrium position, a new critical dynamic pressure may be calculated. Fig. 5.9 shows the increase in the divergence dynamic pressure for a loaded equilibrium state as function of the loading level (dynamic pressure). The critical dynamic pressure is unchanged up to 50% of the linear divergence dynamic pressure. The difference starts increasing and reaches more than 9% at 80% of the unloaded divergence dynamic pressure.

5.3.2 Effect of nonlinearities on flutter

Structural as well as aerodynamic nonlinearities are known to affect flutter. One of the goals of this research is to be able to determine up front those cases for which nonlinear models are essential for accuracy. Thus, nonlinear flutter analysis is conducted on the Goland cantilevered wing and HALE wing. As is presented herein, the nonlinear aeroelastic effects are completely different for these wings.

Goland wing

Nonlinear aeroelastic analysis has been conducted on the Goland's wing. To examine various nonlinear cases, the wing is given a specified root angle of attack. Due to the loads on the system, the wing deforms to a nonlinear equilibrium. Flutter analysis is then conducted by linearizing about the nonlinear steady state. The gravitational forces and skin friction drag are neglected in these results. Fig. 5.10 shows the variation of the flutter speed with increasing angle of attack. The results show the effect of structural nonlinearities, and dynamic stall nonlinearities on the flutter speed. As the angle of attack is increased, the aerodynamic load on the wing increases and so do the bending and torsional displacements. The flutter speed increases due to geometric stiffening. The plot shows that, the results including dynamic stall model are markedly different from those without. This is due to coupling between the structural

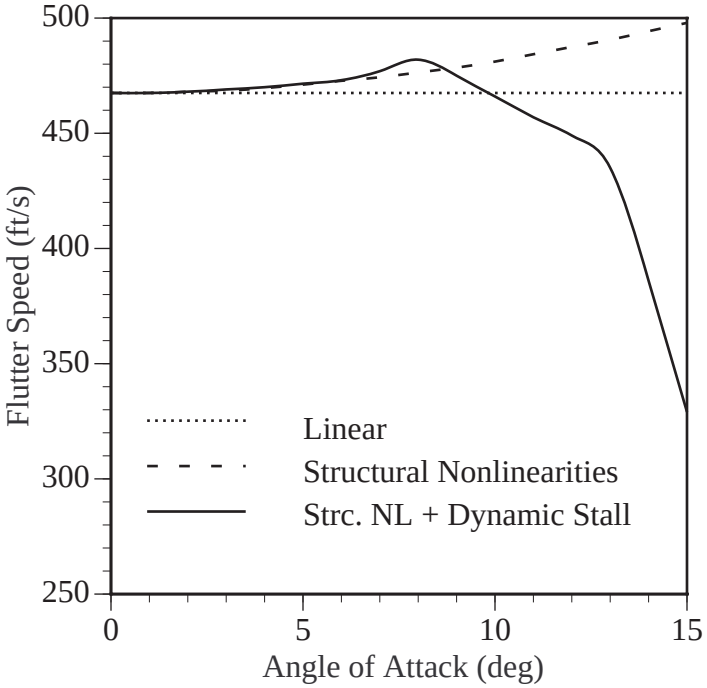

Figure 5.10: Variation of flutter speed with angle of attack for Goland's wing

and the stall states. The stall delay frequency of around 25 rad/sec interacts with the first two structural modes and leads to additional coupling and coalescence, and change in flutter mode. The flutter mode frequency shifts from around 70 rad/sec at 7° to 55 rad/sec at 12°. Also as the angle of attack is increased, wing stall occurs at lower speeds thus leading to possibility of flutter at lower speeds.

The effects of structural nonlinearities seem to be small in the above test case which is a relatively low aspect ratio conventional wing. The dominating nonlinearity is due to the change in aerodynamic characteristic due to dynamic stall phenomena.

HALE wing

Fig. 5.11 presents the nonlinear flutter results for the HALE wing model. It includes deformation due to gravity and aerodynamic forces. Unlike the Goland's wing case the present wing has a downward deflection due to gravity even at zero root angle

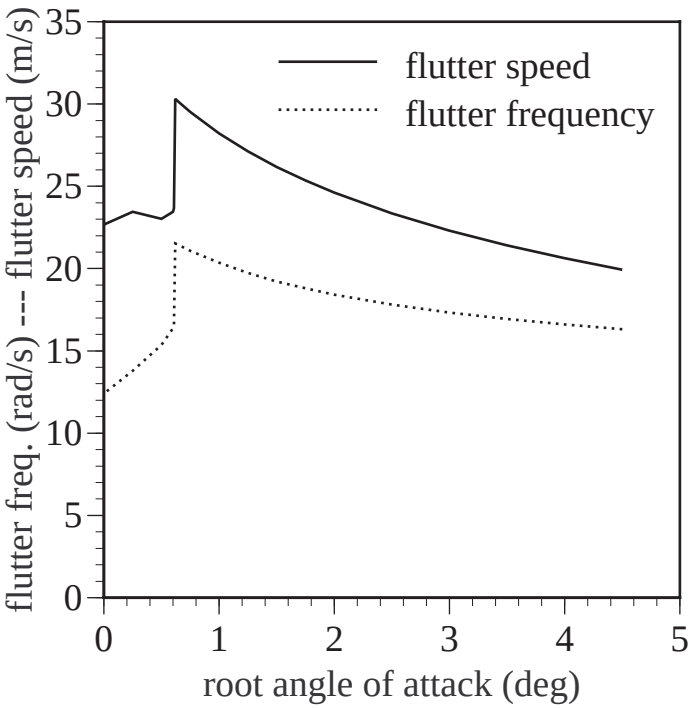

Figure 5.11: Variation of flutter speed with angle of attack for HALE wing

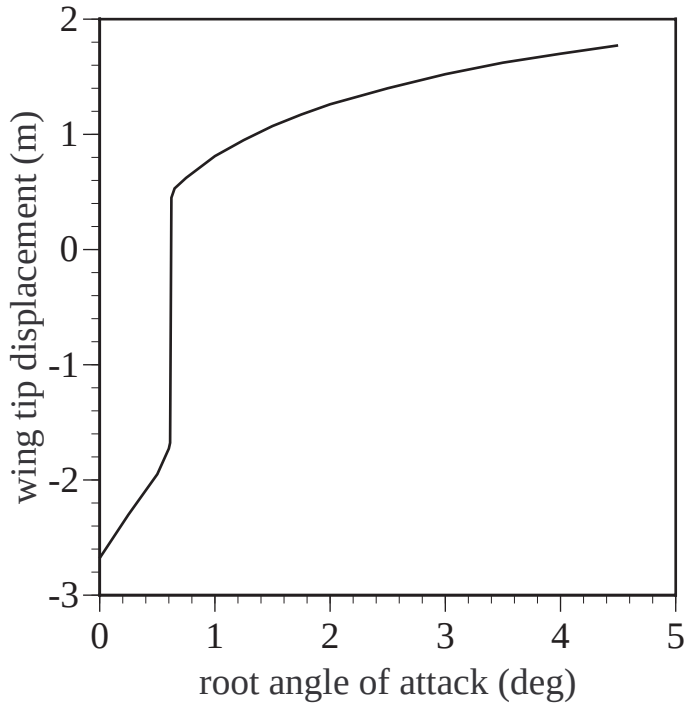

Figure 5.12: Flutter tip displacement at various root angles of attack for HALE wing

of attack. There are rapid changes in the flutter speed at low values of α_0, the root angle of attack. The nonlinear flutter speed and frequency are much lower than those estimated by the linear model. At around 0.61° there is a jump in the flutter speed and frequency. After the jump there is a smooth decrease in flutter speed and frequency. At around 4.5° the flutter speed again jumps, this time off the scale of the plot. Fig. 5.12 shows the tip displacement at the flutter speed. There is a discontinuity in the tip displacement which coincides with that in Fig. 5.11. A finite tip displacement seems to be favorable for flutter for this configuration. The next section goes deeper into the relationship between tip displacement and flutter to explain the behavior described above.

Flutter speed and tip displacement

There is a strong relationship between the wing-tip displacement and the flutter speed. In the example considered above, the drastic change in aeroelastic characteristics is due to changes in the structural characteristics of the wing due to bending (tip displacement). Unfortunately, this effect is not obvious due to additional velocity-tip displacement coupling introduced by α_0. Apart from flutter speed being a function of tip displacement, the tip displacement itself was a function of the speed of the aircraft.

In the case study presented in this section, a finite tip displacement is induced by applying a tip load and the analysis is conducted by linearizing about this curved beam state. The results for the structural frequencies versus wing-tip displacement are shown in Fig. 5.13. One observes a large decrease in the modal frequency for a coupled torsion/edgewise bending mode as tip displacement is increased. The flatwise bending modes are unaffected. Fig. 5.14 shows the corresponding drop in both flutter speed and flutter frequency with increase in tip displacement. To understand the

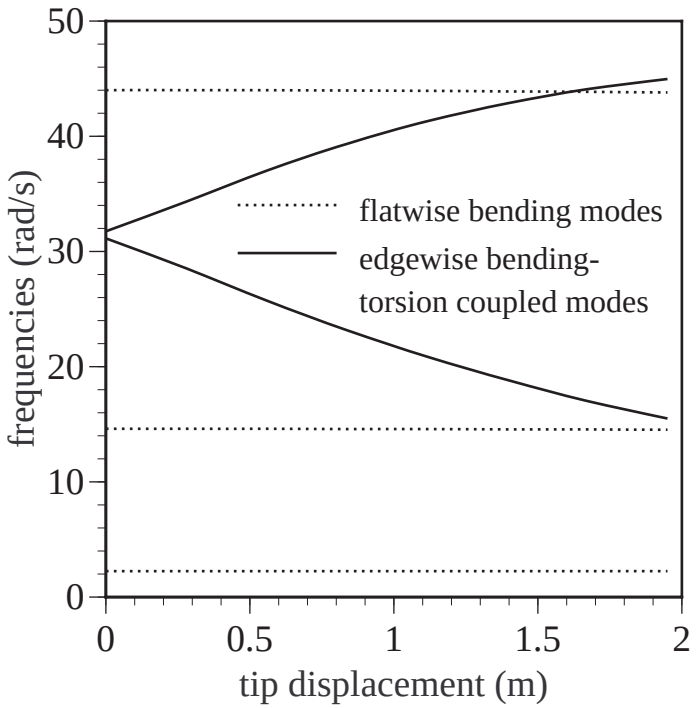

Figure 5.13: Variation of structural frequencies with tip displacement

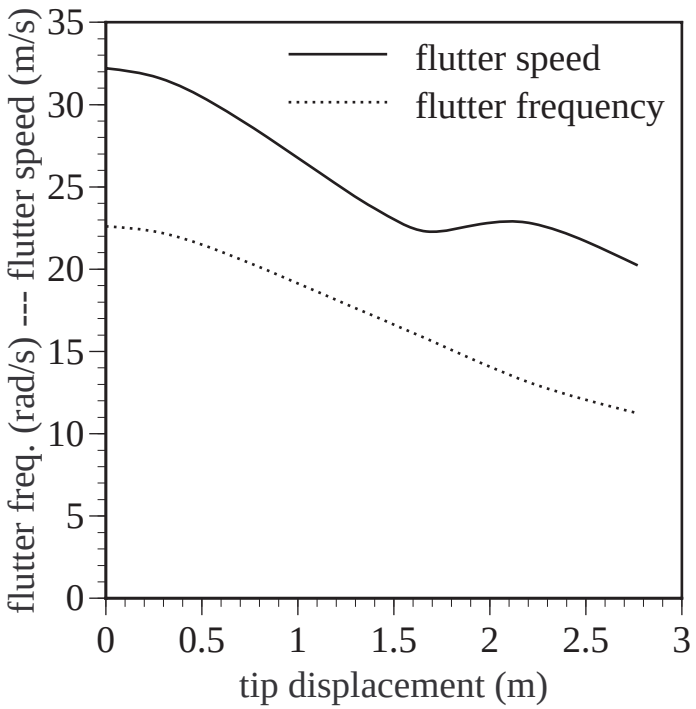

Figure 5.14: Variation of flutter speed and frequency with tip displacement

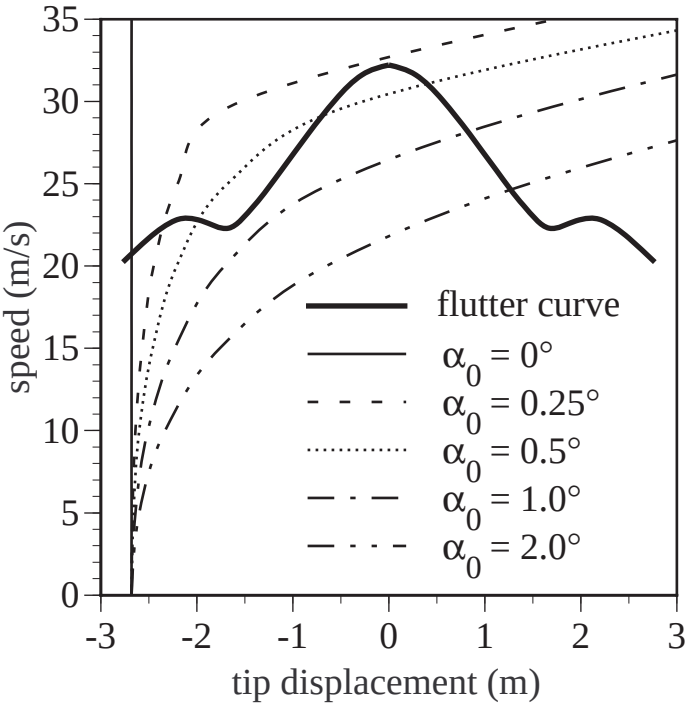

Figure 5.15: Correlation of flutter speed and wing tip displacement

results presented in the previous section one needs to do cross-matching.

Fig. 5.15 demonstrates how closely the wing tip displacement correlates with the flutter speed for various values of α_0 (Fig. 5.11). The thick line in the plot denotes the flutter speed with tip displacement (same as Fig. 5.14). The other curves represent the tip displacement due α_0 at various speeds. For example, the solid line for $\alpha_0 = 0°$ is just a straight line because the tip displacement is only due to gravity. For very small α_0, the flutter and tip displacement curves intersect at very small speeds and one gets very low flutter speeds. For slightly higher α_0 around 0.5° the flutter and tip displacement curves intersect three times. Thus, one observes that the wing flutters in a range of speeds, after which it is again stable for a range of speeds, then starts fluttering again. The first range of flutter speeds however decreases with increasing α_0. At around $\alpha_0 = 0.75°$, the first two intersection points collapse, the slopes of these curves are the same for a given value of α_0, and the flutter speed jumps to the

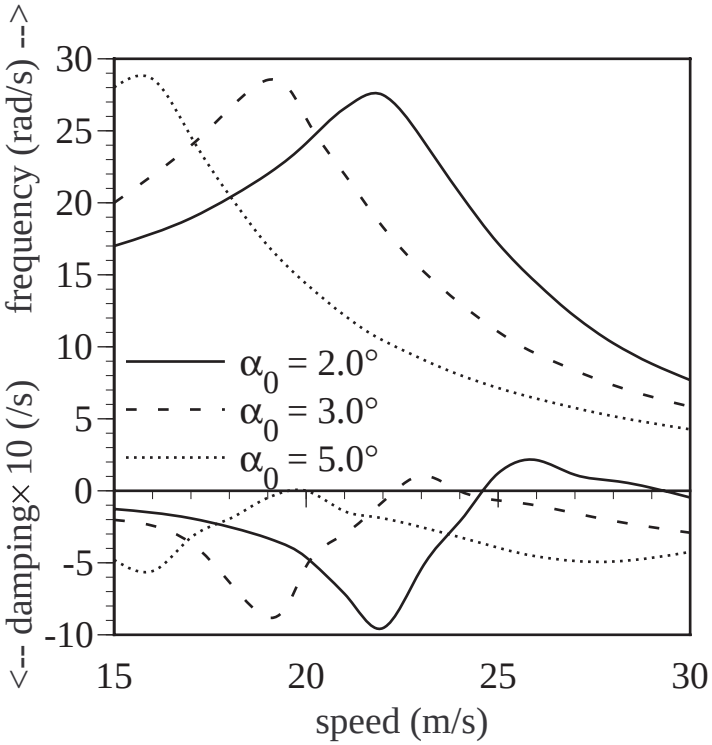

Figure 5.16: Flutter frequency and damping plots for various root angles of attack

next flutter range. For a tip displacement of around -1.5 m, one sees a jump in the flutter speed from approximately 22 m/s up to about 28 m/s, and a corresponding jump in frequency and tip displacement.

So, the nonlinear effects related to flutter boil down to the fact that the natural frequencies shift due to the changing equilibrium configuration. The nonlinear flutter solution about the deformed equilibrium condition is thus markedly different. This corresponds to the decrease in the flutter speed shown in Fig. 5.11. The results in this section qualitatively explain the aeroelastic behavior shown in Fig. 5.11. To get better quantitative results one would need to have the exact displacement shape matching.

The jump in flutter speed at $\alpha_0 = 4.5^\circ$ in Fig. 5.11 can also be explained by similar matching. Fig. 5.16 shows the frequency and damping plots for larger angles of attack. Again, flutter occurs in a small range above the flutter critical speed.

Though the flutter speed is decreasing with α_0, the strength and range of flutter is also decreasing. At around 4.5° the damping reverses its direction before reaching flutter condition, *i.e.*, damping does not reach zero.

Avoiding catastrophic decrease in flutter speed

From the earlier sections it is clear that large deflections in a slender wing can lead to dangerous aeroelastic repercussions. The wing curvature due to flatwise bending leads to torsion-edgewise bending coupled modes which can destabilize. Thus, it is important to control the torsion-edgewise bending coupling caused by curvature of the beam. One could either provide an inherent structural coupling that counteracts the coupling due to bending. Another way would be to pre-curve the wing downwards so that at nominal flight condition the wing is as close to a straight wing as possible. One could optimize the pre-curvature to give maximum flutter clearance over all expected flight conditions.

By efficiently designing the structural cross section one could provide some level of structural coupling. Fig. 5.17 shows the effect of structural coupling on the nonlinear aeroelastic characteristics of the wing. The parameter ψ is the coupling coefficient defined as the ratio of the coupling flexibility to the square-root of the product of the torsional and edgewise bending flexibility. It is assumed that a maximum coupling of ± 0.2 can be obtained by structural tailoring. As seen in the fig. 5.17, the coupling leads to shift of the nonlinear flutter plot. One can thus obtain around 10% increase in the flutter speed with such induced coupling.

To get complete recovery of linear results at a specific loading condition one could pre-curve the wing downward so that at the nominal flight condition the wing is approximately straight and would recover the high linear flutter speed. Fig. 5.18 shows the effect of pre-curvature on the nonlinear flutter results. It is necessary

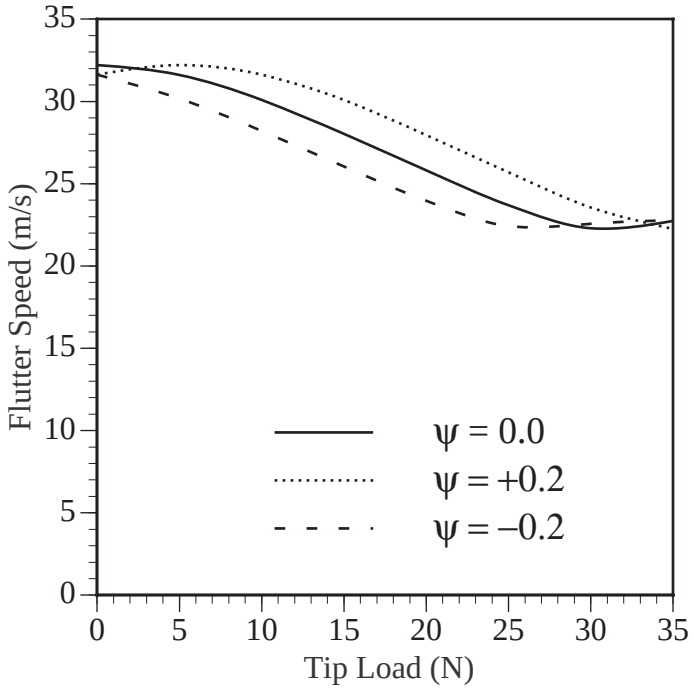

Figure 5.17: Effect of structural coupling on the nonlinear aeroelastic characteristics of the HALE wing

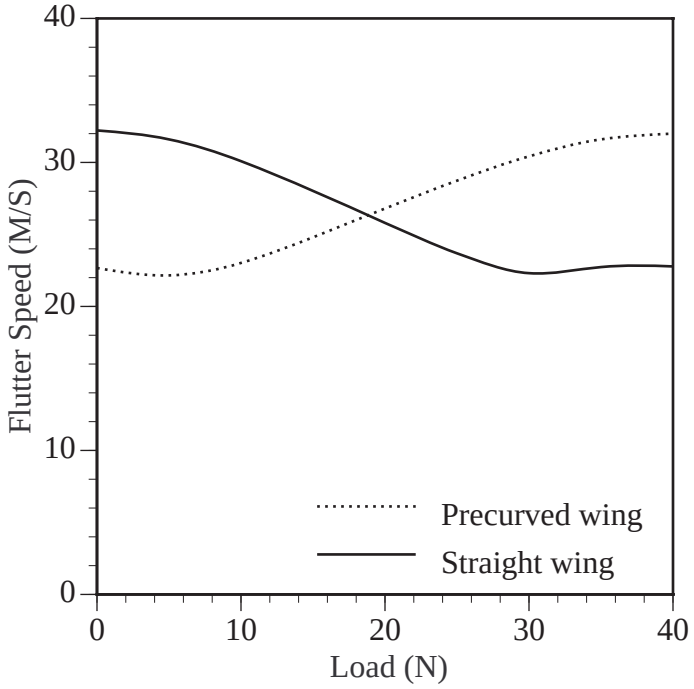

Figure 5.18: Effect of pre-curvature on the nonlinear aeroelastic characteristics of the HALE wing

here to point out that the cross-sectional coefficients change with curvature. Here, the curved beam analysis was conducted using the given cross-sectional coefficients for simplicity. For more consistent results one would need to use an appropriate cross-sectional analysis tool, *e.g.*, Ref. [73]. By introducing the pre-curvature, the linear straight wing results are partly recovered. There is 35% increase in the flutter speed at nominal condition. It is again seen that pre-curvature leads to decrease in the detrimental nonlinear effects of lift. Unlike in the coupling case, the pre-curved case is limited only by the ground clearance required of the wings. It is seen that one could tailor the curvature so as to get the maximum flutter clearance at the operating conditions.

5.3.3 Limit cycle oscillations

The linear theory of stability, when applied to aeroelasticity problems, typically leads to a set of eigenvalues. It predicts that small disturbances applied to a system at an unstable equilibrium grow exponentially. Within its valid range, linear theory is correct, *i.e.*, *small* disturbances *do* grow exponentially – at least *at first*. However, one should not regard the results of linear theory to have any significance whatsoever regarding the behavior of a system subjected to large disturbances, or after a long time elapses from an initial small disturbance. For example, according to linear theory the system response will diverge from the unstable equilibrium to infinity (or material failure). This does not always comport with experimental evidence, and nonlinear analysis methodology has been developed to remedy this problem [74].

If a system has a nonlinear stiffening term, then in most occasions the amplitude of oscillations will grow until a LCO is reached. LCOs, though stable in the sense of Lyapunov, are not asymptotically stable. That is, although the final state is bounded, the system will not asymptotically approach its original equilibrium state

as time grows. Moreover, LCOs are not necessarily a result of a linear instability. LCOs can be induced by certain disturbances, if sufficiently large, even when the given equilibrium state is stable. Basically, if the disturbances are not small, then the response cannot be predicted by theories that are linearized about a nonlinear steady state. Depending on the amplitude of the LCO, the structure may or may not experience immediate failure. However, for an aircraft, LCOs pose significant problems in their own right. The vibration caused by LCOs causes fatigue, reducing the useful life of the structure. Thus, efficient prediction of LCOs is very important during design, especially for aircraft flying near the limits of the linear assumptions.

Theoretical investigation of parameters affecting LCOs in an aircraft is a difficult task, even for very low-order systems. The investigation of a realistic wing with an accurate representation of the aerodynamics leads to a very computationally intensive task. Presently, computational methods which simulate the system behavior are used to obtain time histories of motion, which are then used to study any observed LCO. It is necessary to investigate LCO in the best possible way so as to get a deeper understanding of its initiation and sustaining mechanisms. LCOs are studied for the Goland's wing and HALE wing case below. Again, a qualitative difference in behavior is observed.

Post-flutter LCO in Goland wing

The Goland wing at zero steady-state angle of attack and a speed of 500 ft/sec (V_F = 468 ft/sec) was disturbed by a small disturbance and the time history of oscillations was obtained. The tip displacement, tip rotation and the total energy (sum of kinetic and potential energy) are plotted against time in Fig. 5.19. The tip displacement and rotation increase exponentially when the amplitude of vibration is small, *i.e.* the nonlinearities are negligible. As the amplitude of vibration increases,

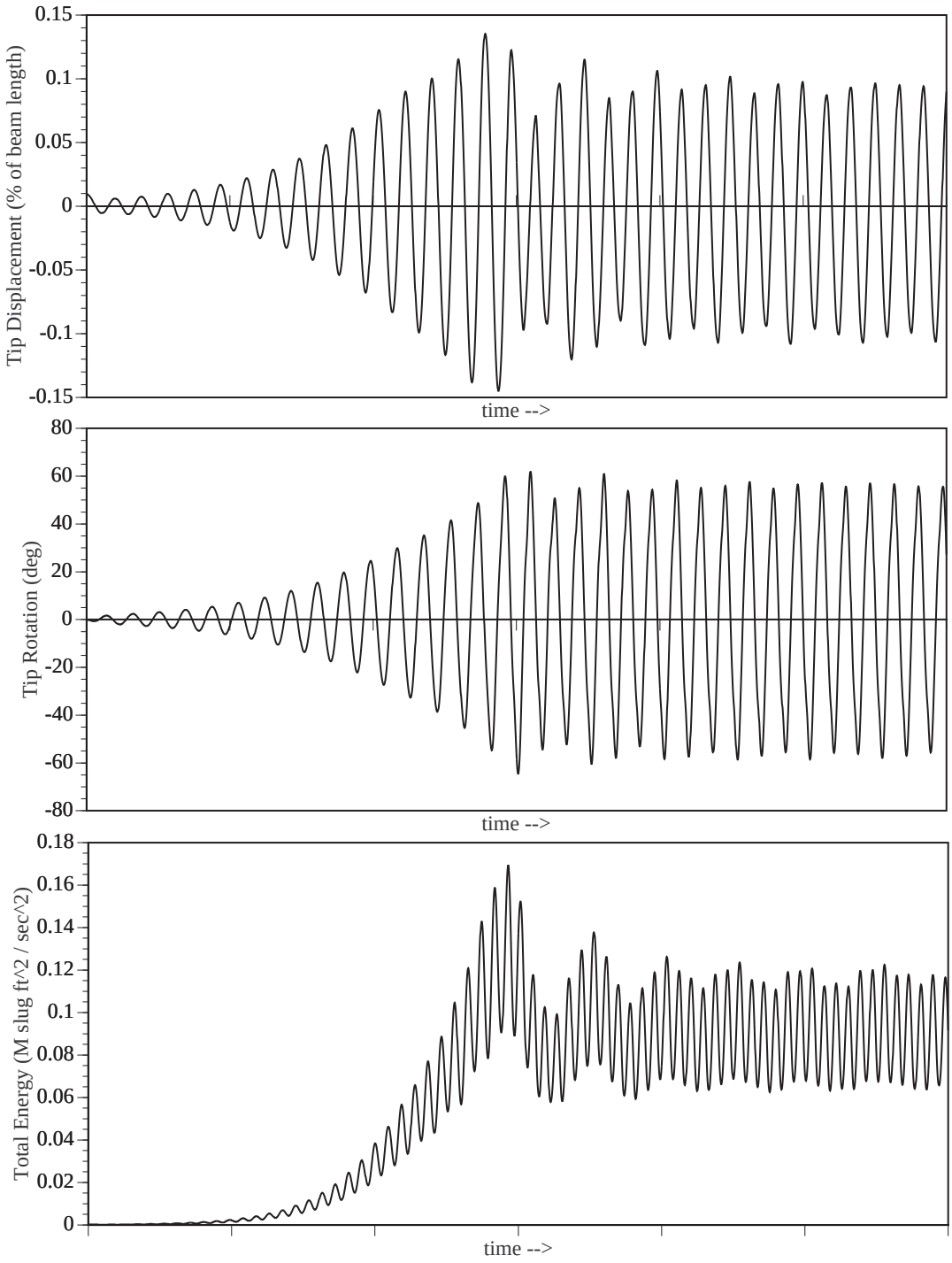

Figure 5.19: Time history showing LCO above flutter speed for Goland's wing

nonlinearities due to stall become important and in fact dominant. The aerodynamic forces drops and thus can no longer pump the required amount of energy into the structure and the amplitude of oscillation and the total energy levels out.

Another way of investigating LCOs is via a phase plane plot. Here two variables of the system are plotted against each other to give an insight into the mode shape of oscillation. Fig. 5.21A shows the plot of tip displacement versus tip rotation. One can clearly see the changes in the mode shape as the amplitude increases, and eventually settles into a LCO.

Effect of large disturbances on Goland wing

Stability as calculated by eigenvalues is a linear concept, and thus is valid for small disturbances about the steady state. The flutter speeds calculated above predict that small disturbances grow for speeds higher than the flutter speed and decay for lower speeds. But the disturbances encountered by an aircraft depend completely on its mission and environment, *e.g.* maneuvers, gust amplitudes. A nonlinear system found to be stable under small disturbances may not necessarily maintain stability for higher amplitudes of disturbances. In fact the dynamics of the system can be completely different for varying initial conditions.

Consider the Goland wing at 10° steady-state angle of attack flying with a speed of 450 ft/sec (V_F = 466 ft/sec). Fig. 5.20 shows the response of the system for various initial conditions. The initial conditions are obtained by deforming the wing with tip forces and moments. "S" denotes a stable response, "L" denotes a mode which is either a LCO or very lightly damped oscillation, and "U" denotes that the initial mode shape is unstable, and thus the amplitude of oscillation increases and finally settles into a new higher-amplitude LCO. The reason to distinguish between the latter two responses is that the first one has a small amplitude and most likely will

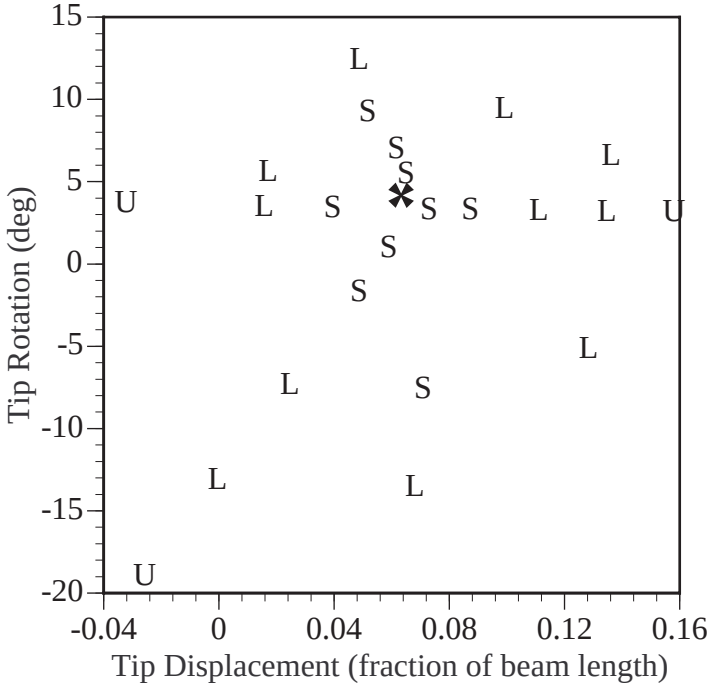

Figure 5.20: Stability at various initial conditions for Goland's wing

not result in structural failure. The plot shows that depending on the disturbance, the wing may go into a flutter / LCO even at speeds lower than the flutter speed.

The mode shapes in the phase plane are given in Fig. 5.21. Plot 5.21B, shows the behavior of the system for small disturbances. It is lightly damped and the mode shape is that obtained by linear eigenvalue solution. Plot 5.21C and Plot 5.21D, show the kind of responses for medium level disturbances. The mode shape is nonlinear (non sinusoidal), and depending on the disturbance the damping is either zero or very close to it (5.21D) or small (5.21C). Plot 5.21E and Plot 5.21F show the initial and final mode shape for high power disturbance. Two plots have been made for easier visualization. Plot 5.21E clearly shows that the amplitude of vibration is increasing, and Plot 5.21F shows the final converged large amplitude LCO.

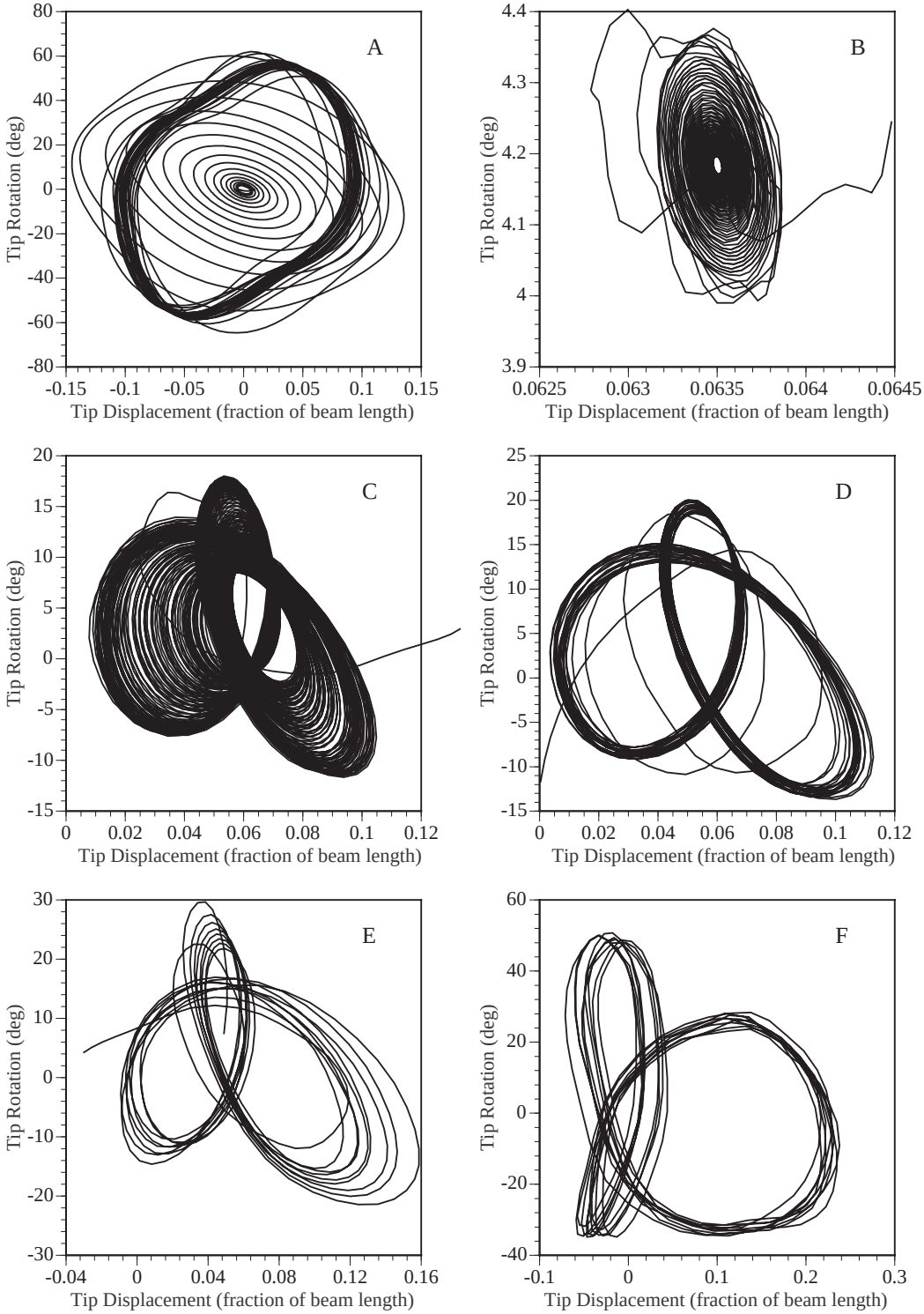

Figure 5.21: Phase-Plane Diagrams for various initial disturbances for Goland's wing

Post-flutter behavior of HALE wing

The time history of the tip displacement, tip twist and total energy of the wing are plotted in Fig. 5.22 for a flight speed of 35 m/s (slightly above the flutter speed). The time history and phase-plane plots have been obtained by giving a small initial disturbance of 0.01 m at the tip in the vertical direction. The plots of time history clearly show that the amplitude of oscillation initially increases exponentially, but eventually settles into a limited amplitude oscillation. But this LCO is not stable and the oscillations become quite different. This phenomenon is initiated by a drastic change in the tip displacement response. Instead of oscillating about tip displacement values near zero, the oscillations are shifted. The oscillations are of the order of 1.5 ± 1.0 m. The response is still very much physical but chaotic due to the strong geometric nonlinearities associated with 1.0 m oscillations. The geometric nonlinearities due to tip displacement and its effect on aeroelastic response in explained in detail in the following section.

Figs. 5.23 show the phase-plane plot of the oscillation after the limiting amplitude oscillations are reached at speed of 35 m/s. It is again observed that the oscillations are aperiodic and quite chaotic.

LCO and tip displacement

As seen in Fig. 5.14 previously, the flutter speed and frequency change drastically with tip displacement. The results are obtained by applying a tip load and conducting flutter analysis about the deformed state. There is a drastic decrease in the flutter speed with tip displacement. This is due to a decrease in the frequency of the torsion/edgewise bending mode as discussed in an earlier section.

Fig. 5.24 shows the changes in frequency and damping of the significant aeroelas-

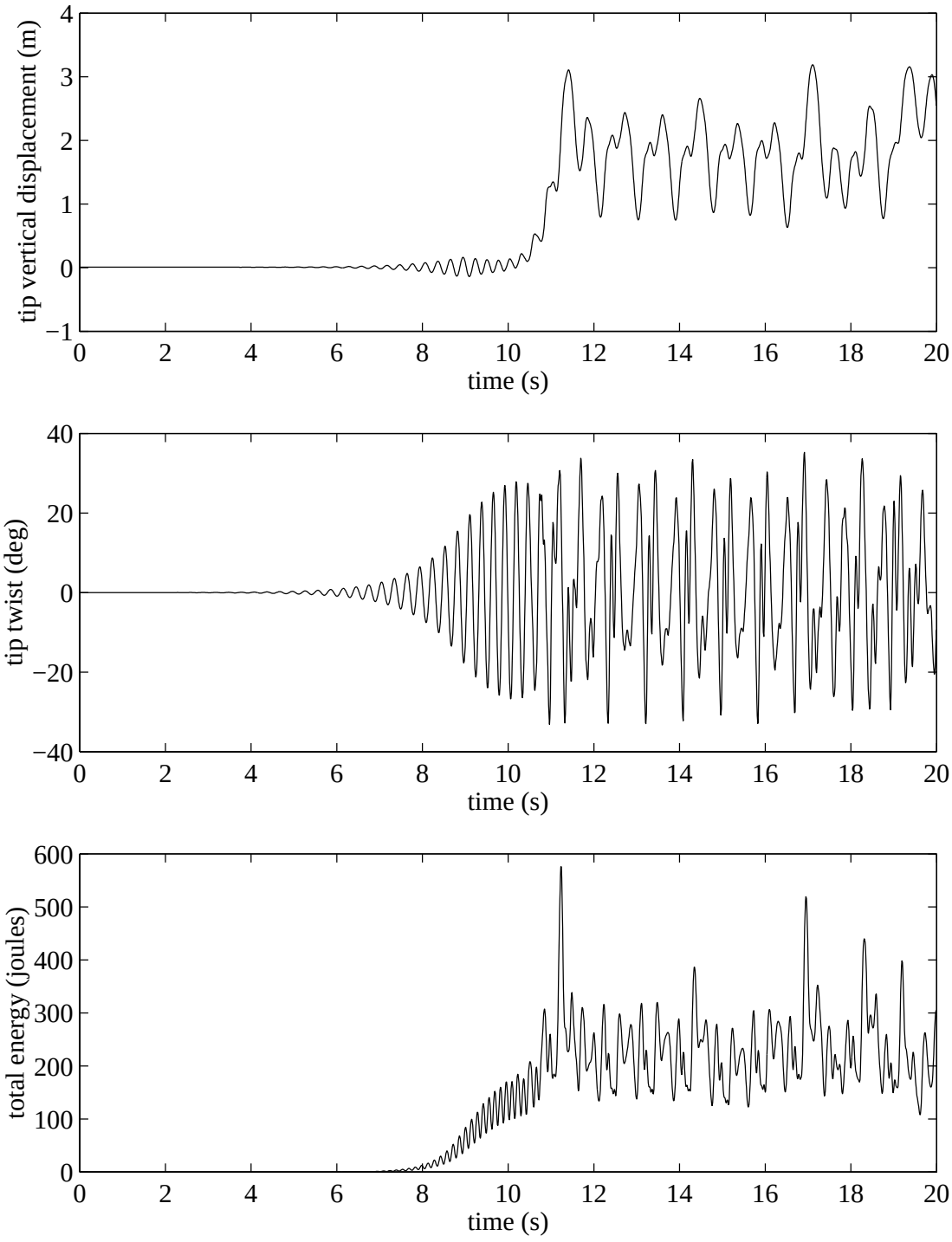

Figure 5.22: Time history showing LCO above flutter speed (speed = 35 m/s) for HALE wing

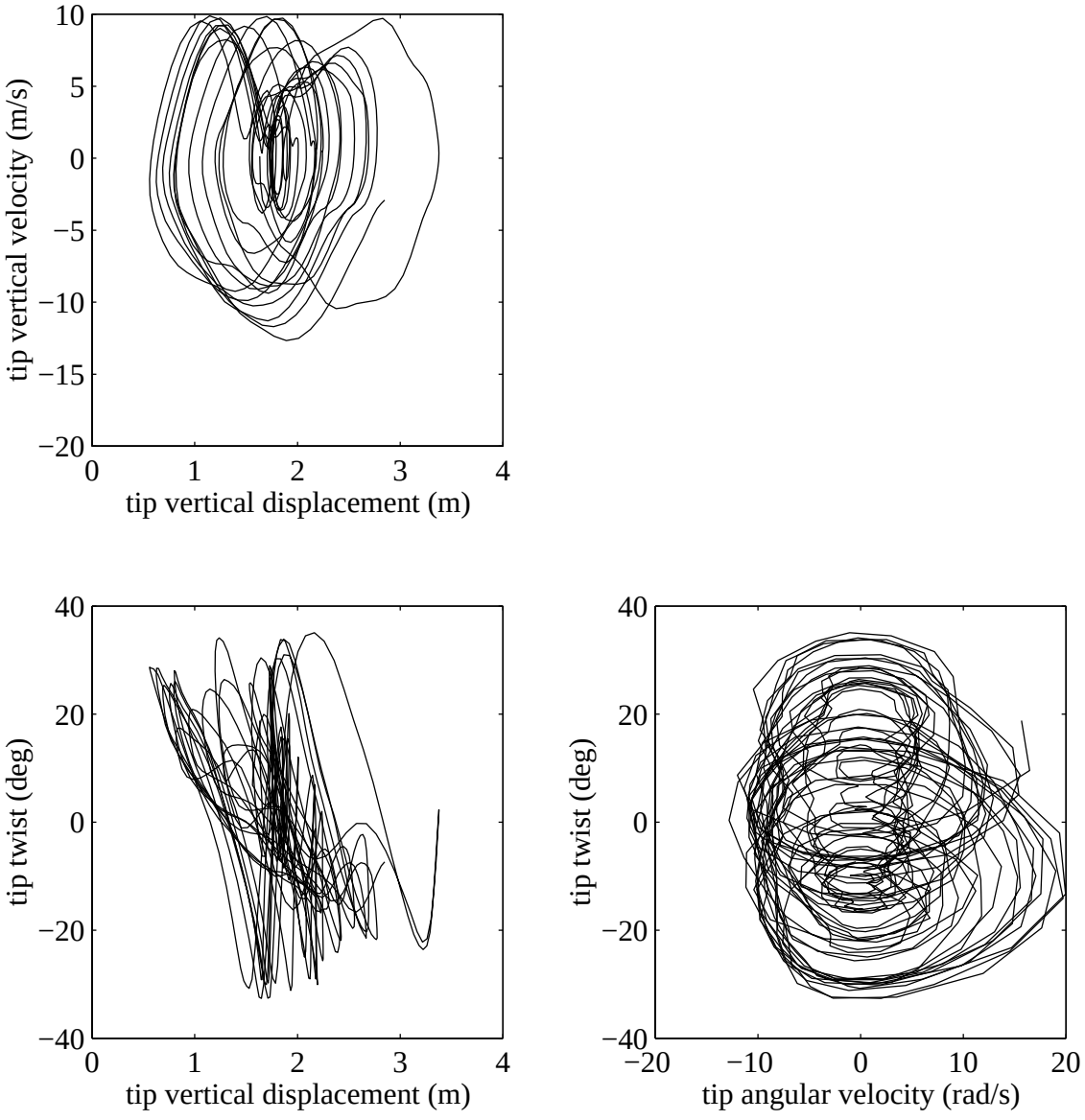

Figure 5.23: Various phase-plane plots at speed = 35 m/s

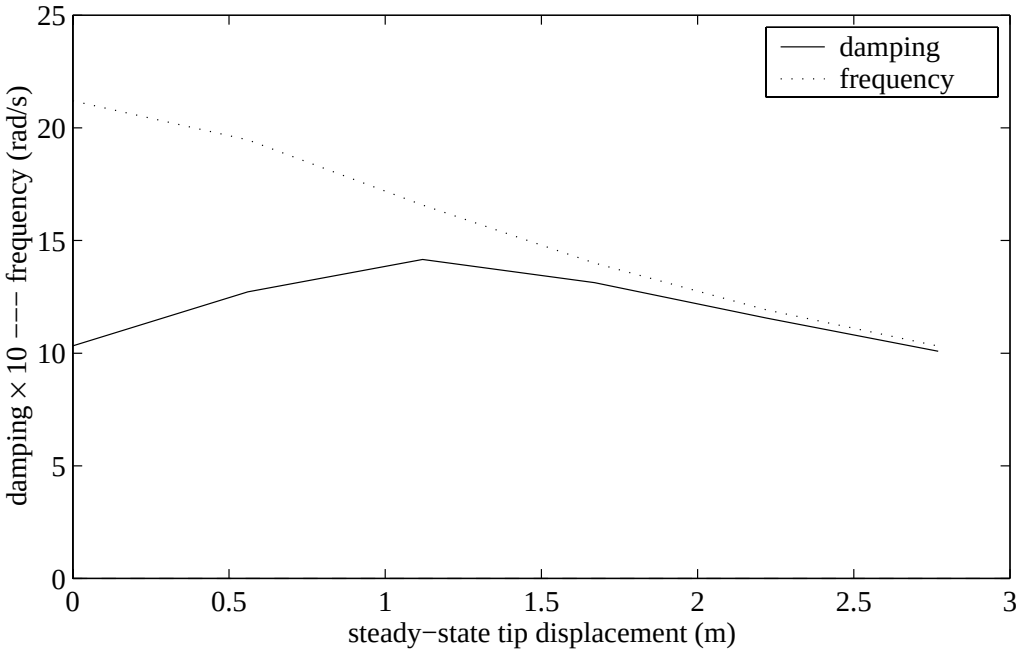

Figure 5.24: Variation of damping and frequency with tip displacement at flight speed of 35 m/s

tic mode with tip displacement. One can see the positive slope of damping with tip displacement, *i.e.*, the instability becomes more pronounced. This is a very important phenomenon and could be the root cause of most of nonlinear aeroelastic behavior presented here. The system instability becomes stronger by having a mean tip displacement, so that there is a greater flow of energy from the surrounding air into the wing. For the system to go into the stronger instability, a mean tip displacement should be maintained. The system needs to dynamically satisfy the mean deformation shape by appropriately providing a mean force. If such a force could be easily provided then it would mean an easy transition into a state with stronger instability.

Pre-flutter LCO

In the previous section, the LCO tends to have a mean at a finite displacement even though there is no static equilibrium point. As shown in Fig. 5.14, the flutter speed for a wing displaced from the no loads equilibrium straight configuration is much lower then the linear flutter speed. It is thus obvious that if the wing under loads is deformed then at lower speeds one could get instability and most possibly a LCO. But an interesting case is if the wing is given an initial deflection into the unstable regime, *i.e.*, like a gust induced temporary deflection, and then observed to see if the wing regains it equilibrium position. Fig. 5.25 shows the time history of a wing at 30 m/s given an initial disturbance of 2m. It is seen that as the bending mode decays, the torsional mode which is unstable for a deflected state is excited and it goes into a LCO.

The damping-tip displacement relationship (Fig. 5.26) might again be used to explain this behavior. From the plots it is clear that at high tip displacements, the damping is positive. As the system tries to come back to a zero deflection steady state, it is passing through a dynamically unstable state, and thus the system is

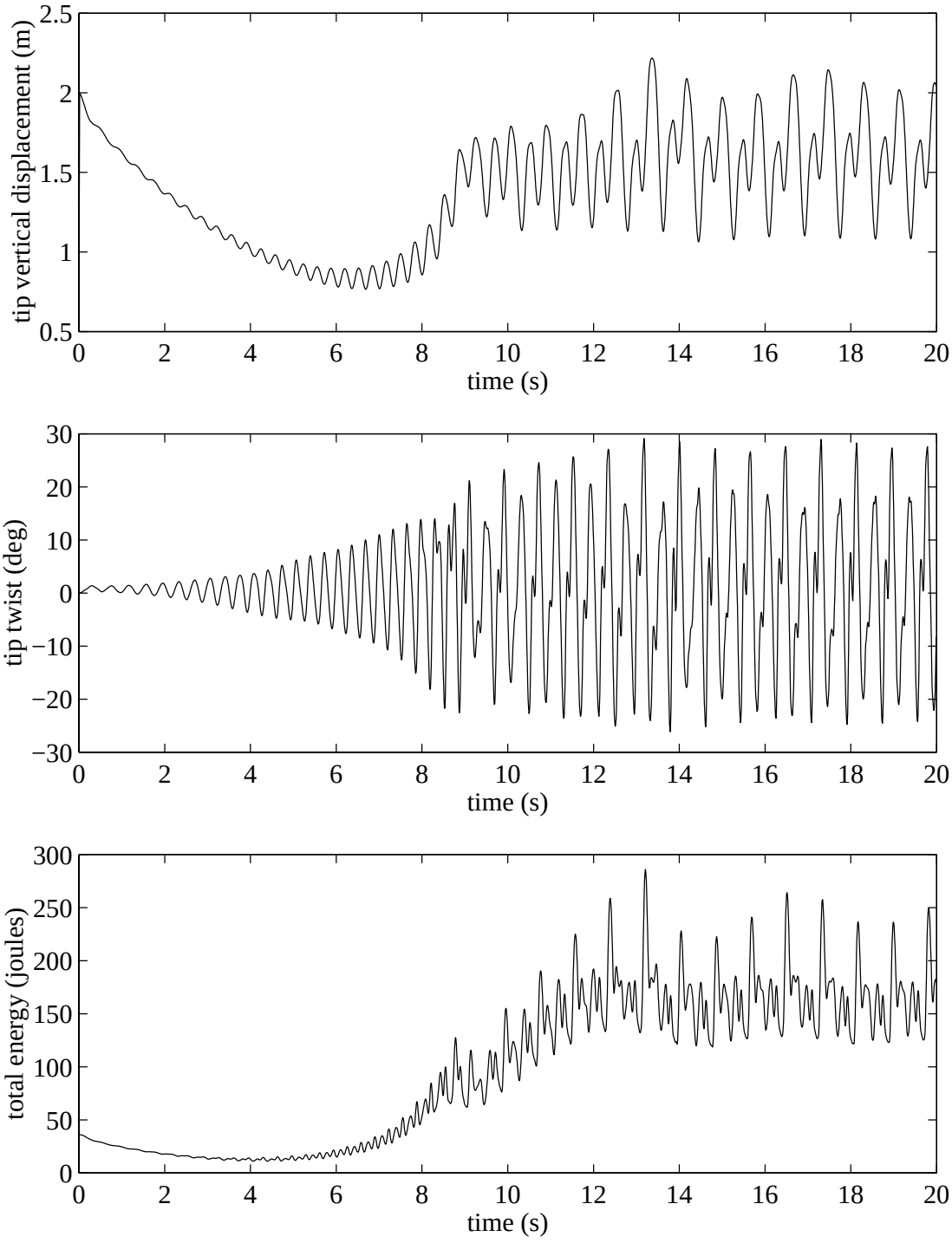

Figure 5.25: Time history showing LCO below Flutter speed (speed = 30 m/s) for HALE wing

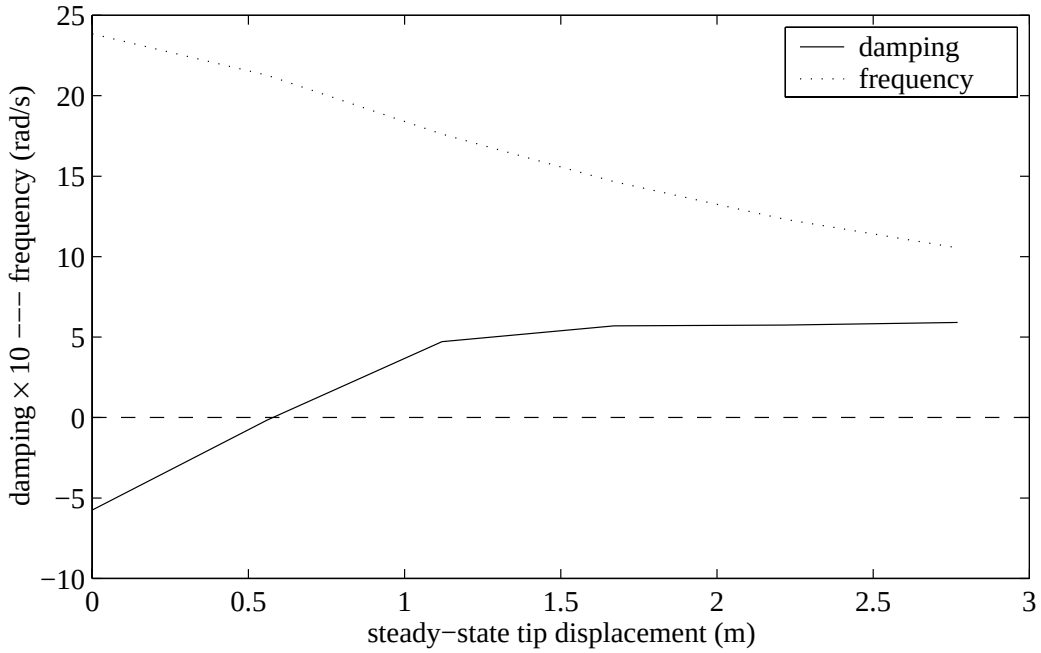

Figure 5.26: Variation of damping and frequency with tip displacement at flight speed of 30 m/s

dynamically absorbing energy. If the system absorbs more than a critical amount of energy before it reaches the zero steady state, it then jumps to a high energy unstable state (oscillating about a non-equilibrium deformed state) and dynamically provides the forces required to maintain a mean deformed state (required to stay unstable).

The LCO that the wing goes into is very different from the one seen at 35 m/s. The phase-plane plots (Fig. 5.27) show that the motion is composed of several sub-harmonics. Subharmonics lead to increase in period for the system to return to a given position, and is seen in a phase-plane plots as loops. The LCO is complex but periodic as opposed to LCOs at 35 m/s which seem chaotic.

LCOs dependence on disturbance for the HALE wing

As seen in Fig. 5.14 the flutter speed is much lower for a finite tip displacement. Thus, to excite the flutter modes below the flutter speed a finite disturbance is required. Fig. 5.28 presents the system response at 30 m/s given various initial tip disturbances. It is observed that a critical magnitude of disturbance is required to excite a LCO at a given speed, but above the critical condition the LCO does not change in character. Fig. 5.29 on the other hand, presents the system response at various speeds given an initial disturbance amplitude of 4m. It is seen that at 28 m/s and 31 m/s the system goes into a LCO, whereas at 25 m/s, the system is unable to accumulate enough energy to jump to a unstable state about a deformed state. Thus, a critical speed is required to excite the LCO for a given disturbance. Above the critical speed one observes different and higher amplitude LCO with increasing speed.

The transition of LCO behavior with speed for HALE wing

From the previous sections it is observed that LCOs are possible at various speeds. The LCO type was drastically different for the the pre-flutter and post flutter case.

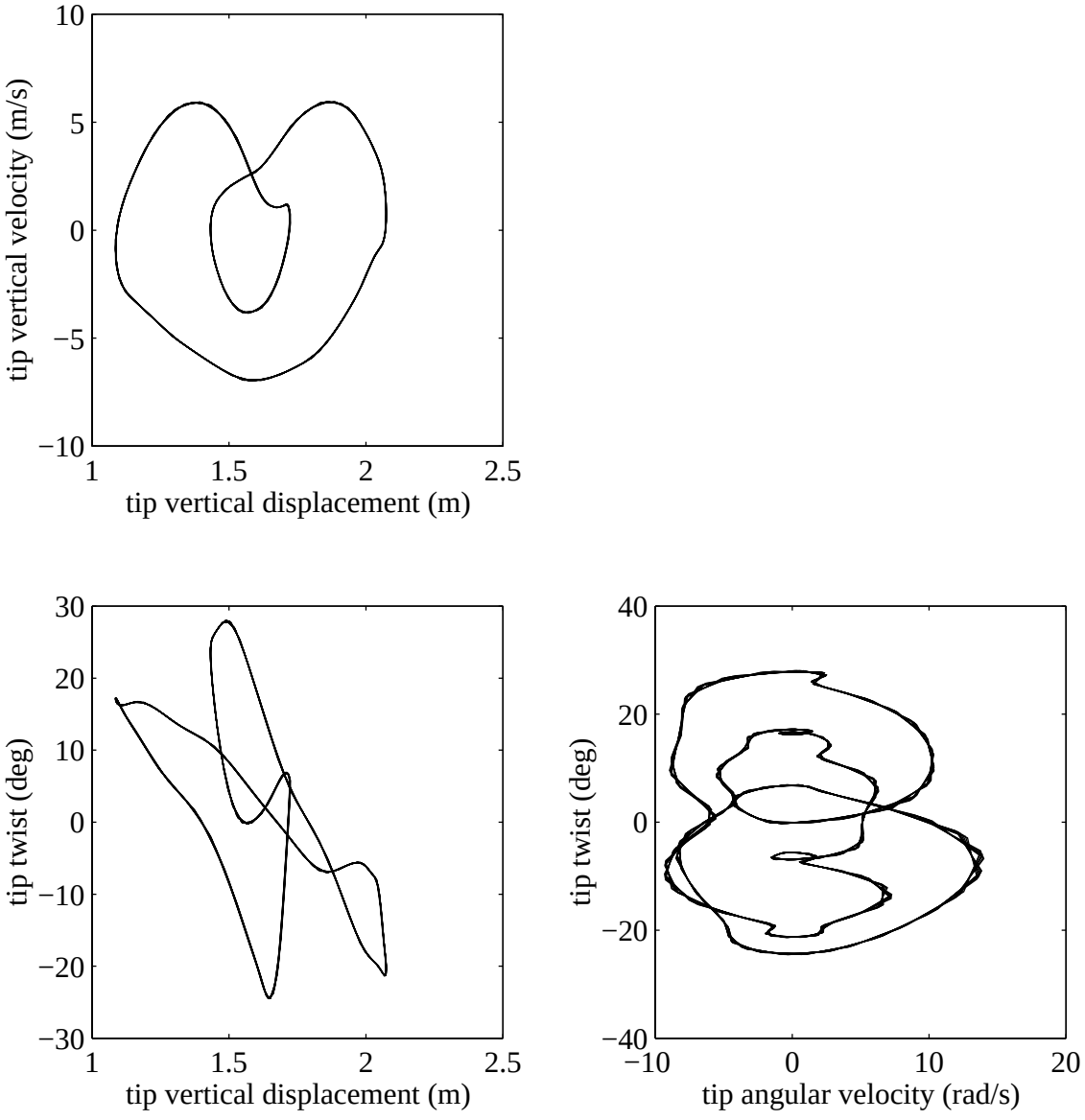

Figure 5.27: Various phase-plane plots for speed = 30 m/s (init. dist. = 2 m)

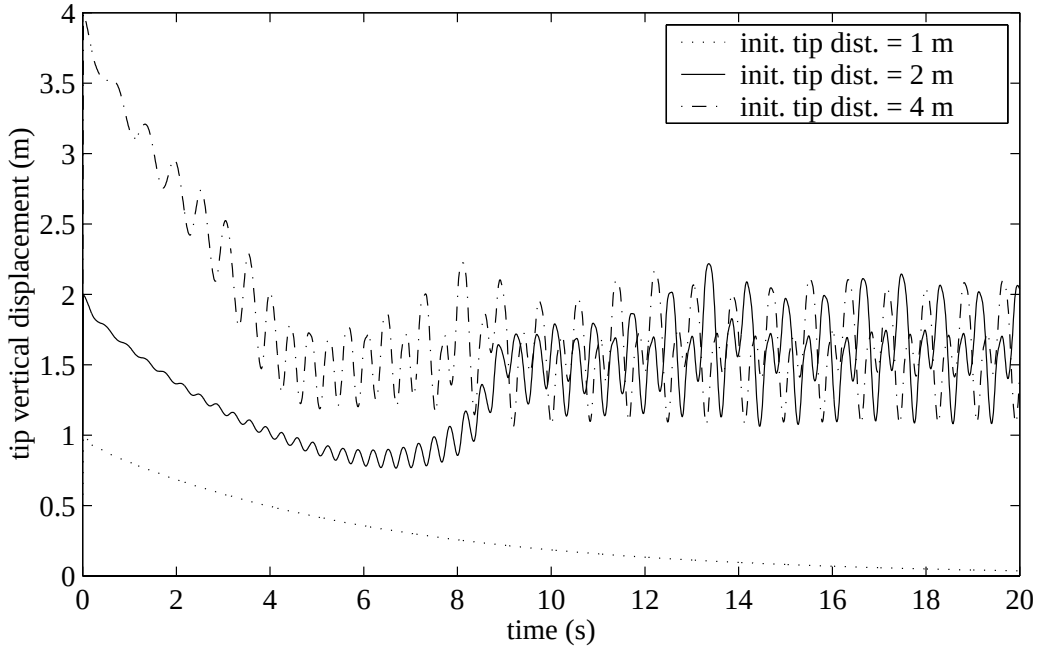

Figure 5.28: Response of the wing at 30 m/s for various initial disturbances

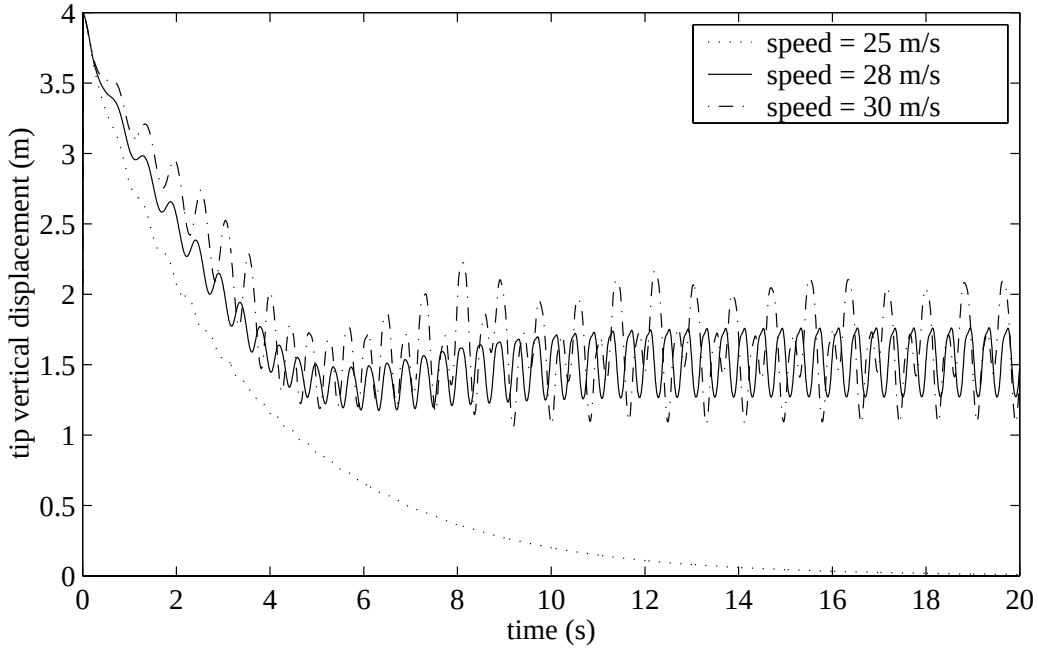

Figure 5.29: Response of the wing at various velocities for an initial disturbances of 4m

In this section the LCO behavior is investigated at various other velocities. The wing is attracted to a LCO if a critical disturbance is provided.

At flight speed of 25 m/s the wing does not go into a LCO even for large bending displacements. From the flutter versus tip displacement plot (fig. 5.14) it is clear that the lowest flutter speed at a deflection of around 3m is about 22 m/s. Thus, it is likely that LCOs exist at 25 m/s. A effective initial disturbance mode-shape can be calculated by considering a snapshot of LCO at higher speed. Using such an initial condition, the wing time history is calculated. Fig. 5.30 shows the phase-plane plot of LCO at 25 m/s. The LCO seems to be almost sinusoidal. It seems to have a higher harmonic component obvious in the shape of the phase-plane plot. An easier way to determine frequency content and thus complexity of the motion is via a frequency spectrum of the LCO. Fig. 5.31 shows the frequency spectrum of LCO at 25 m/s. As can be seen there a dominant frequency at around 16 rad/s and then there are superharmonics.

At speed of 28 m/s, the phase plane plot (Fig. 5.32) shows that the LCO is little more complex. The looping of the phase-plane suggests that there is period doubling, *i.e.*, the system returns to its original state after two periods. Fig. 5.33 shows the corresponding frequency spectrum. Here the phenomenon of period doubling is clearly seen in the subharmonic peak. At flight speed of 31 m/s, there is further increase in the complexity of the LCO. Fig. 5.34 shows the phase-plane plot at 31 m/s. Many more loops are observed. The LCO has a very large period. Fig. 5.35 shows the corresponding frequency spectrum. In the frequency spectrum it is clear that the period is further tripled. It thus takes six periods to come back to the original state.

At speeds close to or higher than the flutter speed the periodic pattern is lost. Fig. 5.36 shows the phase-plane plots at speed of 33 m/s. There is no periodicity, *i.e.*, the period is infinite. This is seen in the frequency spectrum (Fig. 5.37) as a

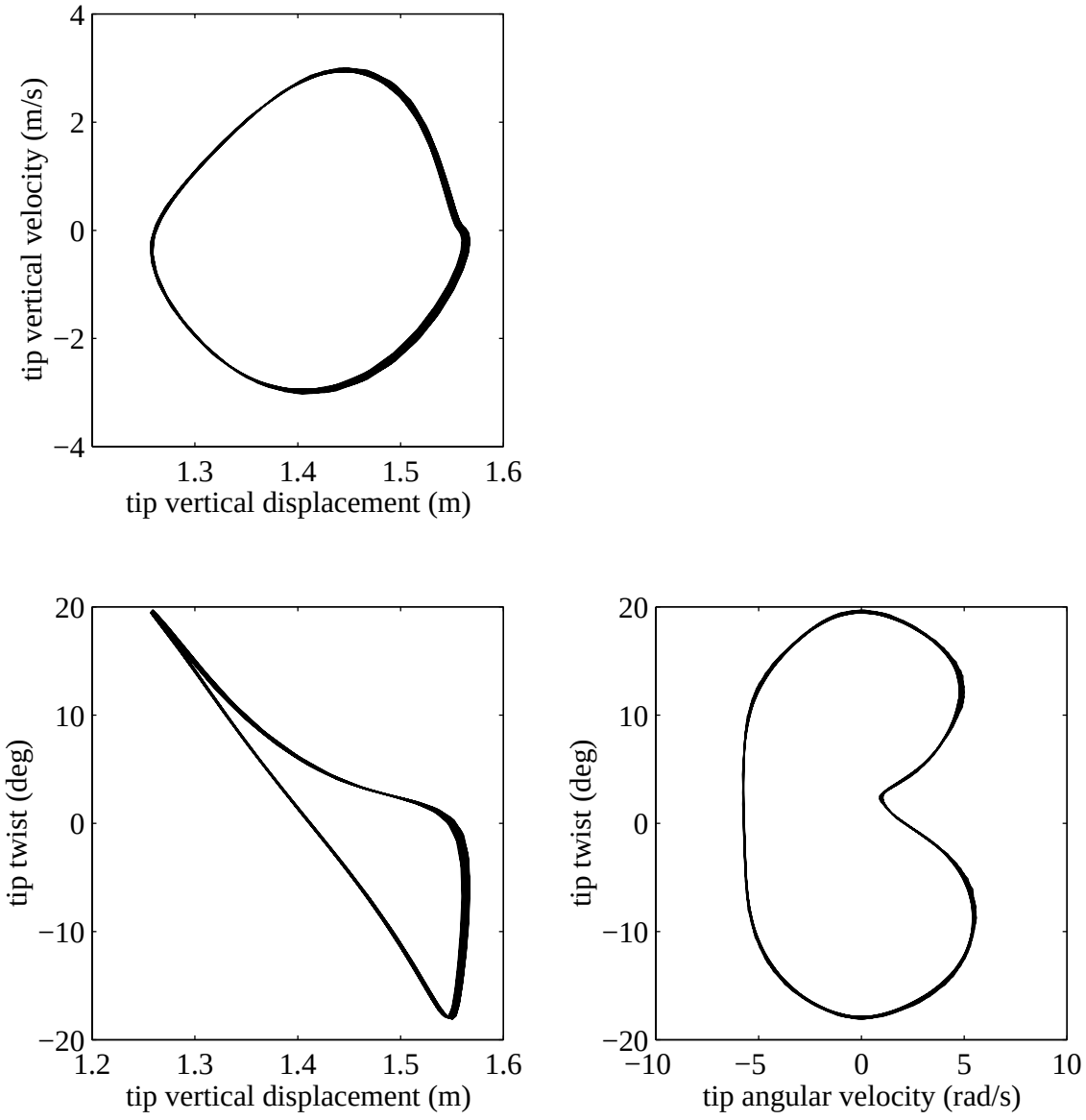

Figure 5.30: Various phase-plane plots for speed = 25 m/s (initial disturbance is a prior flutter condition)

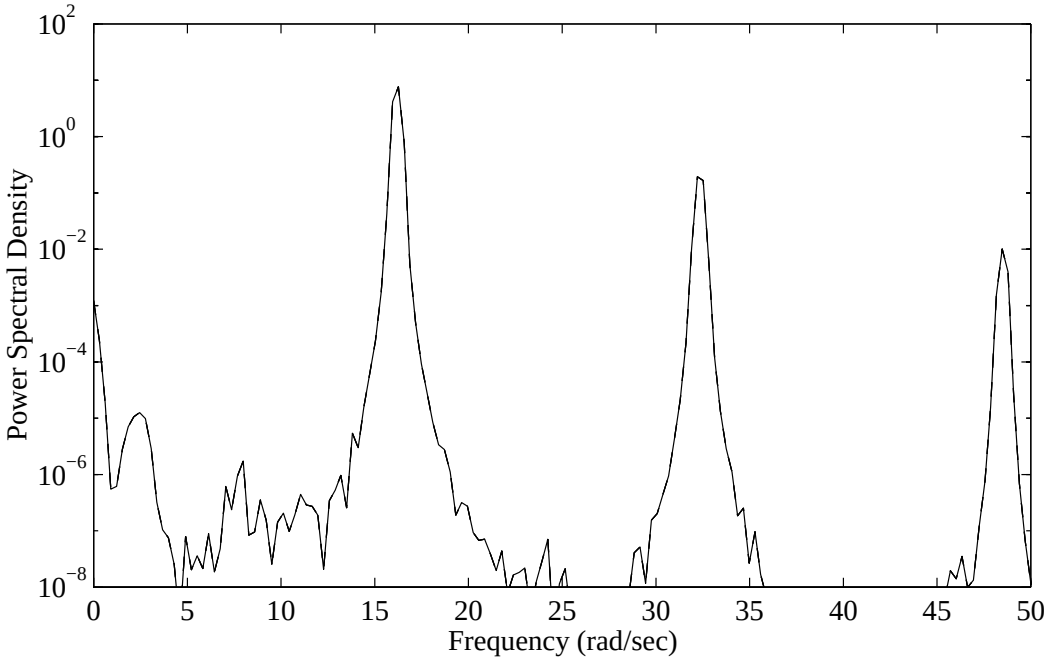

Figure 5.31: Power spectral density for speed = 25 m/s (initial disturbance is a prior flutter condition)

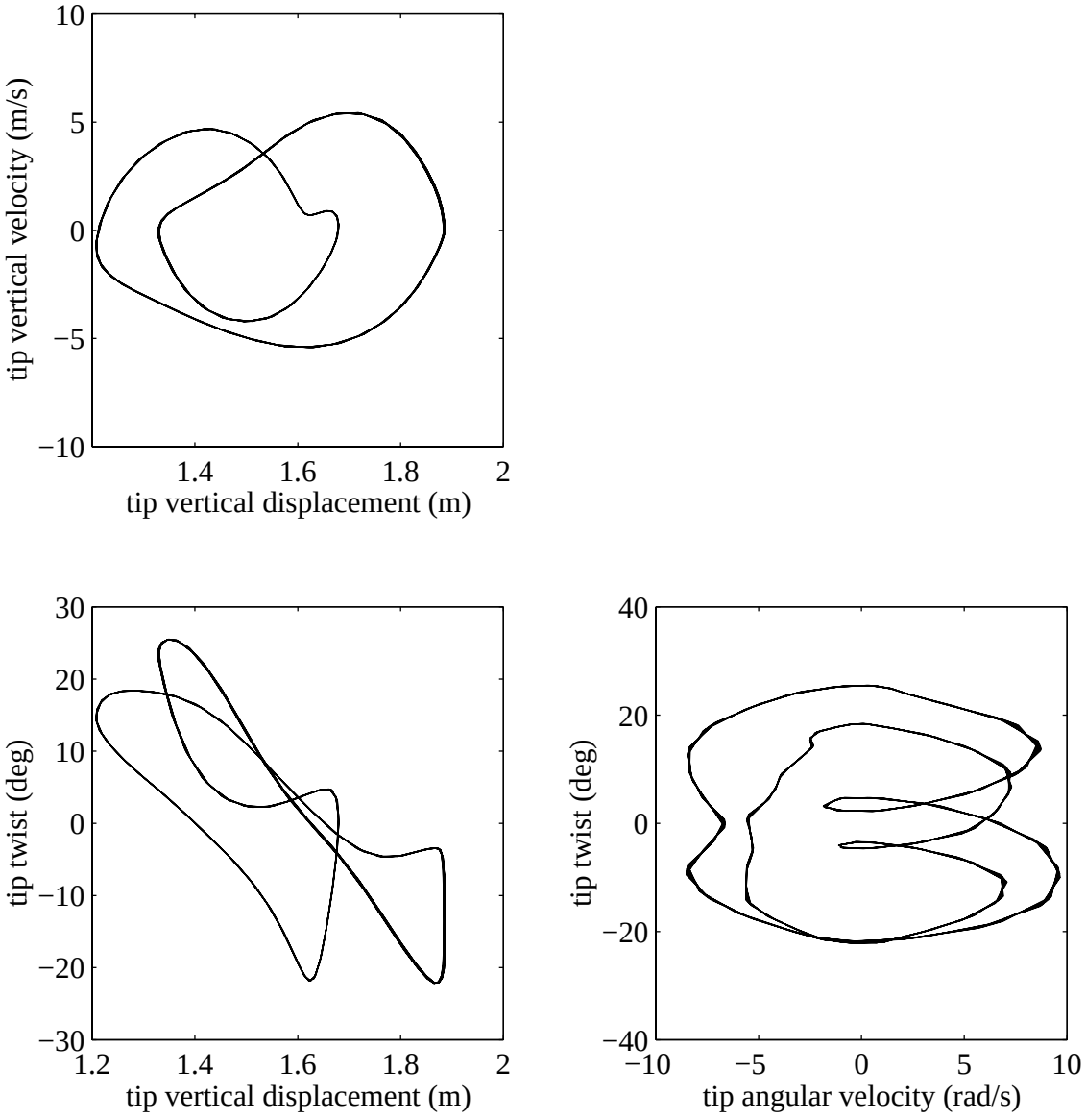

Figure 5.32: Various phase-plane plots for speed = 28 m/s (initial disturbance = 4 m)

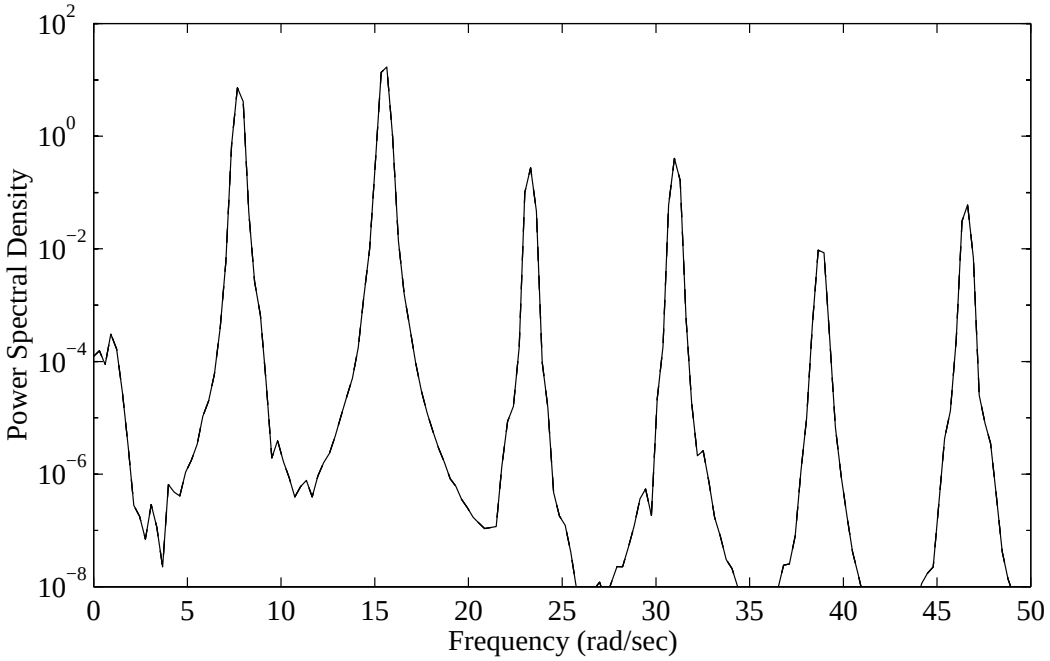

Figure 5.33: Power spectral density for speed = 28 m/s (initial disturbance = 4 m)

broadening of the spectrum.

If one looks at all the phase-plane plots, one sees a clear increase in complexity of the LCO with speed. Period doubling occurs between 25 m/s and 28 m/s; the complexity increases after 31 m/s and at around 32 m/s the response starts losing its periodicity (though it still is bounded). Observing the LCO phase-planes at other speeds presented earlier (Fig. 5.27 and Fig. 5.23), there is close to a continuous increase in complexity, and post-flutter behavior seems quite chaotic. The initial frequency doubling followed by the broadening of the spectrum is more obvious in the frequency spectra. This is a tell-tale sign of chaotic behavior. At 25 m/s there were only superharmonics to the dominant flutter / LCO frequency of around 16 rad/s, whereas at 28 m/s there is a subharmonic of half the frequency. Thus, the frequency spectrum changes from a 1,2,3 ... spectrum to a 1/2,1,3/2,2,5/2,3 ... spectrum. At

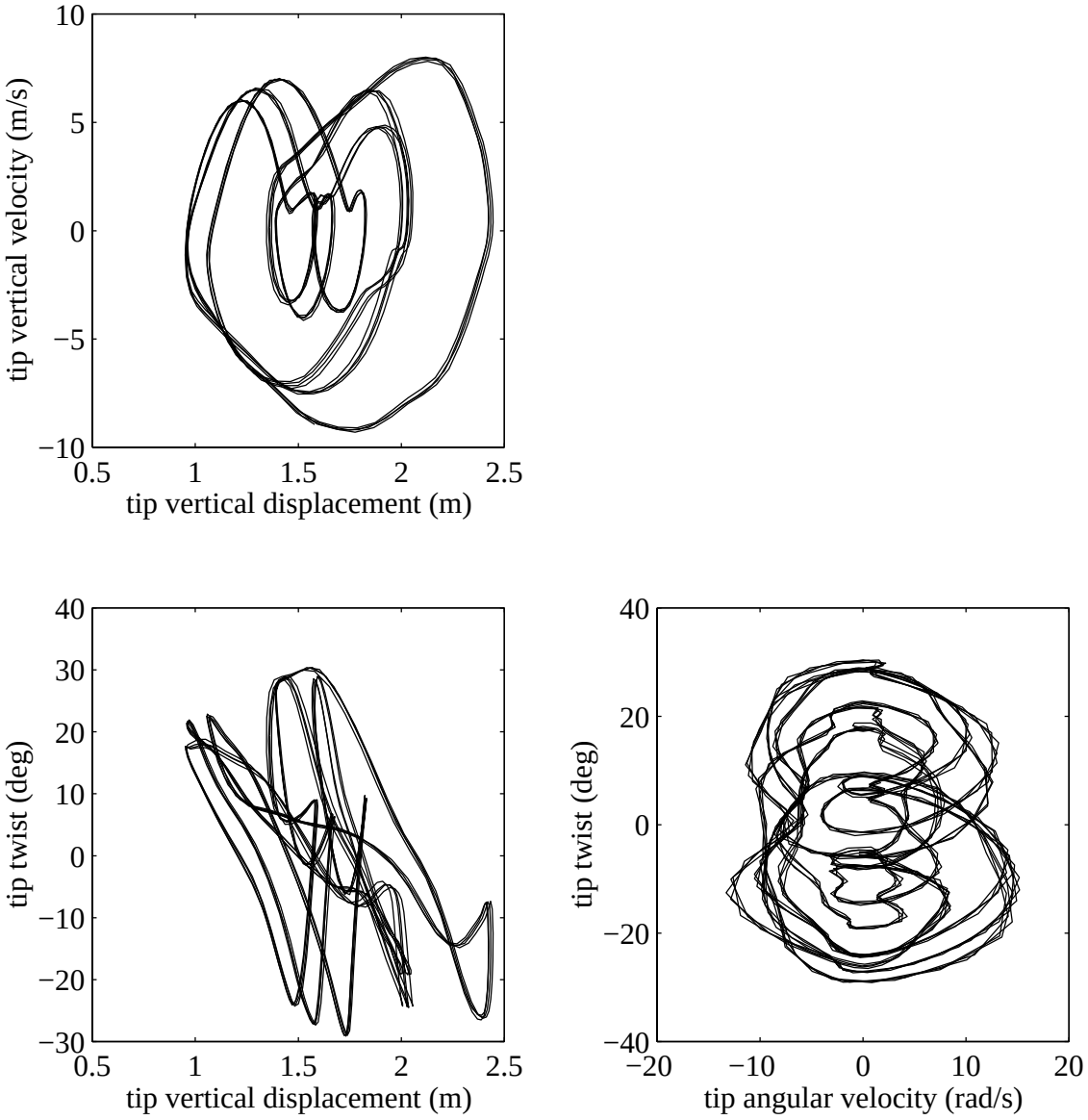

Figure 5.34: Various phase-plane plots for speed = 31 m/s (initial disturbance = 2 m)

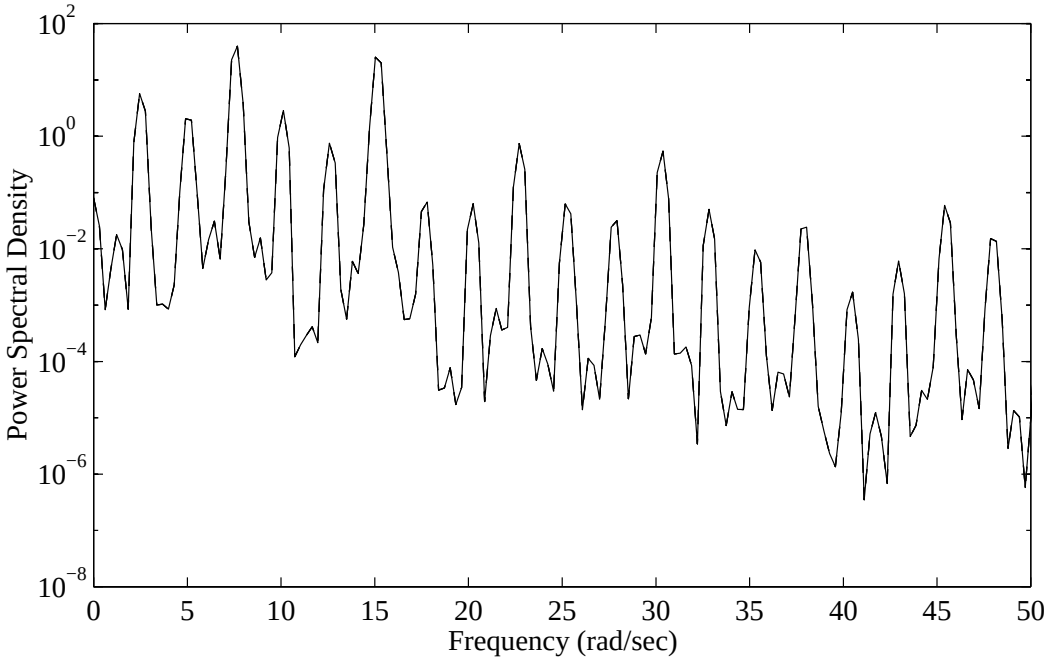

Figure 5.35: Power spectral density for speed = 31 m/s (initial disturbance = 2 m)

31 m/s, the frequency spectrum undergoes a further period tripling. Thus, there are six subharmonics at 31 m/s and the spectrum thus has a 1/6, 2/6, 3/6, 4/6, 5/6, 1, 7/6, ... spectrum. The frequency content of the LCO further increases with speed and thus broadening of the frequency peaks is observed at 32 m/s and finally a broad spectrum is obtained at 33 m/s.

Table. 5.7 summarizes the results for LCO obtained on the HALE wing. Thus, depending on the level of disturbance expected in flight, the designer would need to take into account a LCO boundary, *i.e.*, the maximum flight speed possible without the possibility of LCO at the assumed level of disturbance.

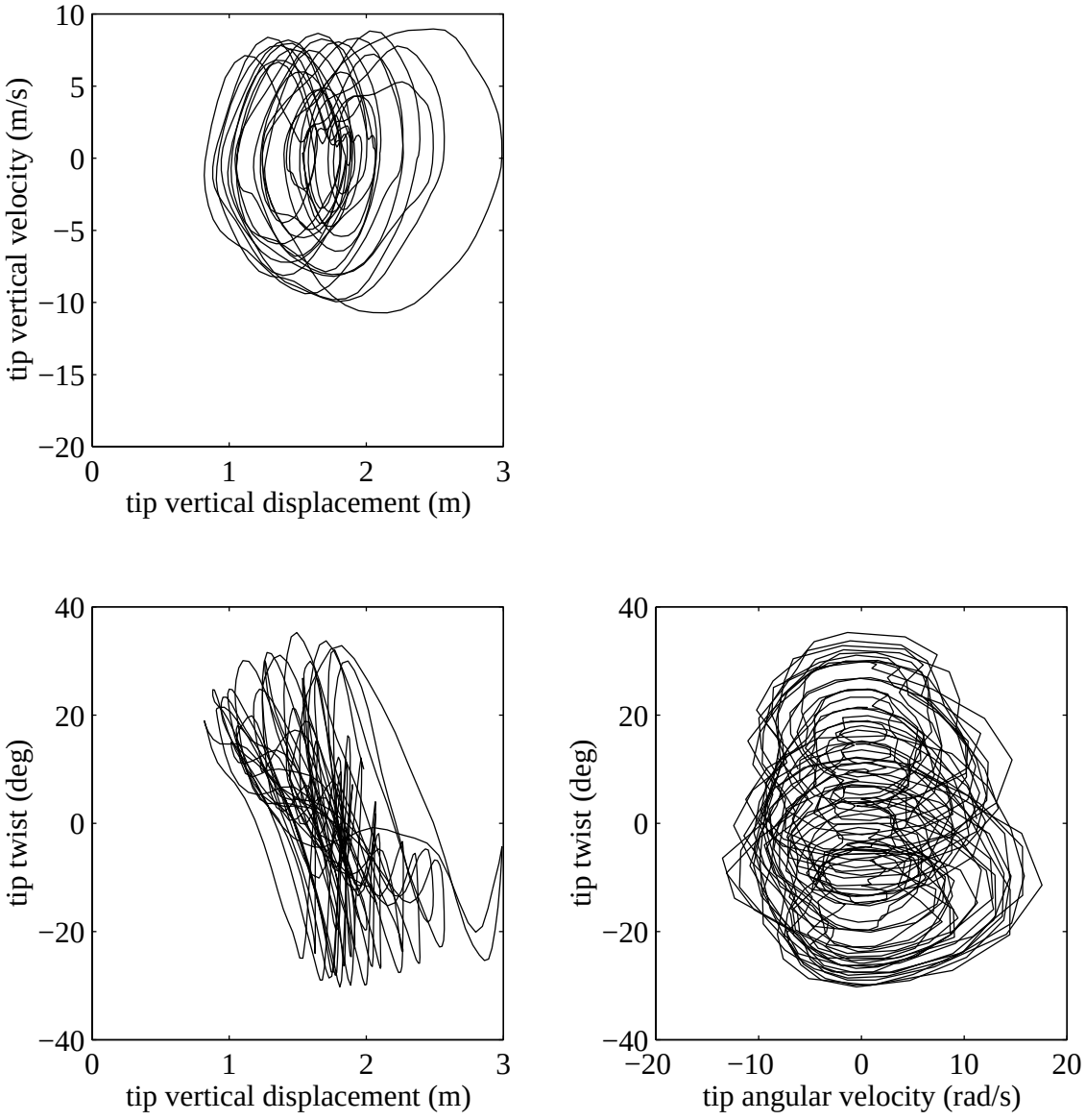

Figure 5.36: Various phase-plane plots for speed = 33 m/s (initial disturbance = 0.01 m)

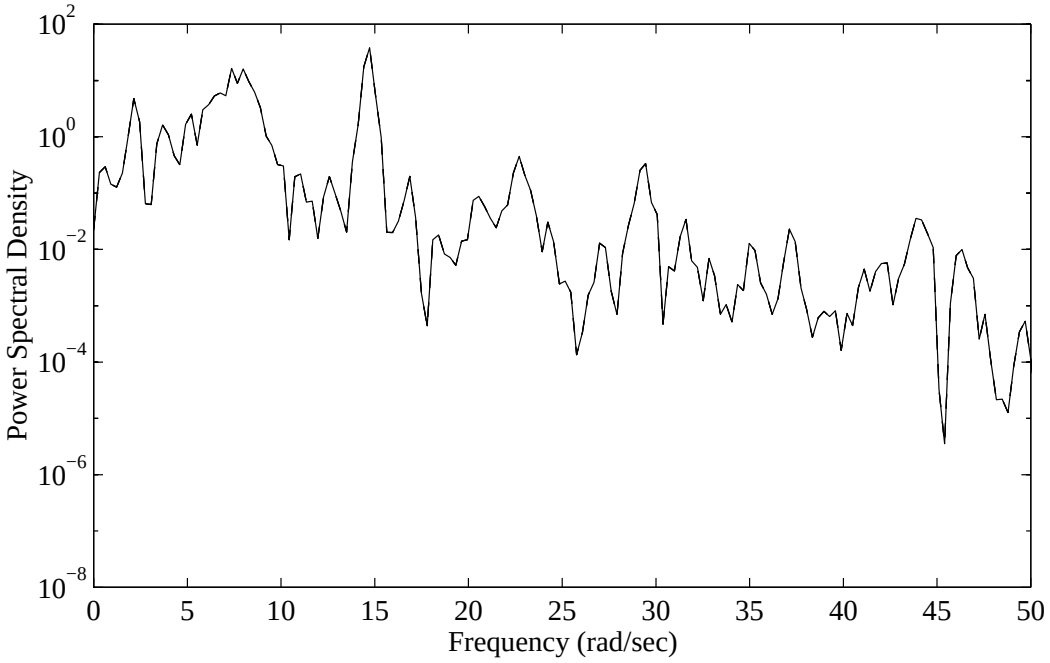

Figure 5.37: Power spectral density for speed = 33 m/s (initial disturbance = 0.01 m)

Table 5.7: Observed LCO chart for HALE wing

Initial Dist.	25 m/s	28 m/s	30 m/s	31 m/s	32 m/s	35 m/s
0.01 m	Stab.	Stab.	Stab.	Stab.	Stab.	LCO
1 m	Stab.	Stab.	Stab.	Stab.	LCO	LCO
2 m	Stab.	Stab.	LCO	LCO	LCO	LCO
4 m	Stab.	LCO	LCO	LCO	LCO	LCO
6 m	Stab.	LCO	LCO	LCO	LCO	LCO
Flutter	LCO	LCO	LCO	LCO	LCO	LCO
Type	Periodic				Chaotic	
Periodicity	1, 2 ...	1/2, 1, 3/2, 2, ...		1/6, 2/6, ...		

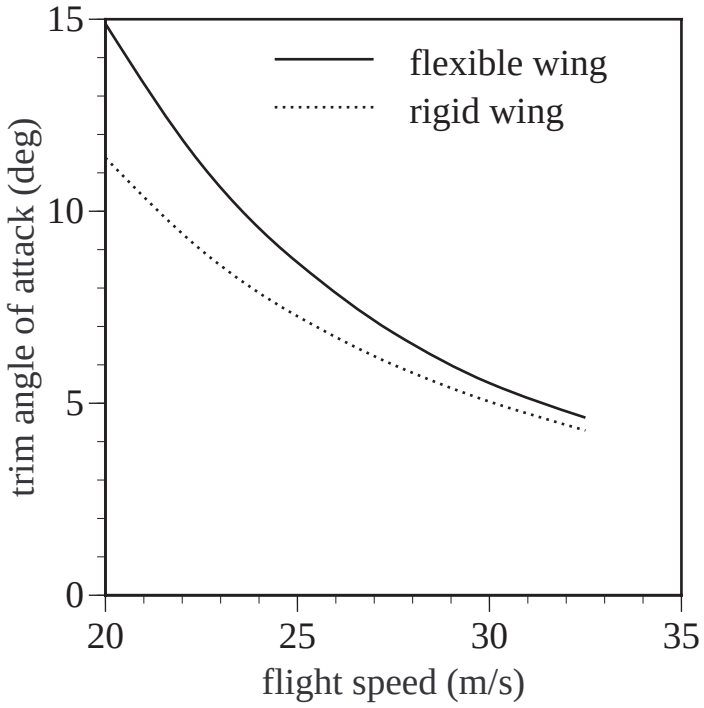

Figure 5.38: Variation of $\overline{\alpha}_0$ with flight speed for HALE aircraft

5.4 Flight Dynamics and Aeroelasticity

HALE aircraft are expected to have large flight dynamics-aeroelasticity interactions due to the high flexibility (thus low structural frequencies) of such aircraft. Flight dynamic calculations done on the complete HALE aircraft model are presented below.

5.4.1 Trim results

Fig. 5.38 shows the trim angle of attack, $\overline{\alpha}_0$ at various flight speeds. The value of $\overline{\alpha}_0$ required from a flexible wing is more than that from a rigid one. This is not expected based on linear aeroelastic theory. Linear aeroelastic theory predicts that at a given $\overline{\alpha}_0$ the lift generated by flexible wing is higher than a rigid wing and thus the trim $\overline{\alpha}_0$ required is lower for the flexible wing. The opposite results observed here are due to large flatwise bending induced by lift. This bending causes the lift

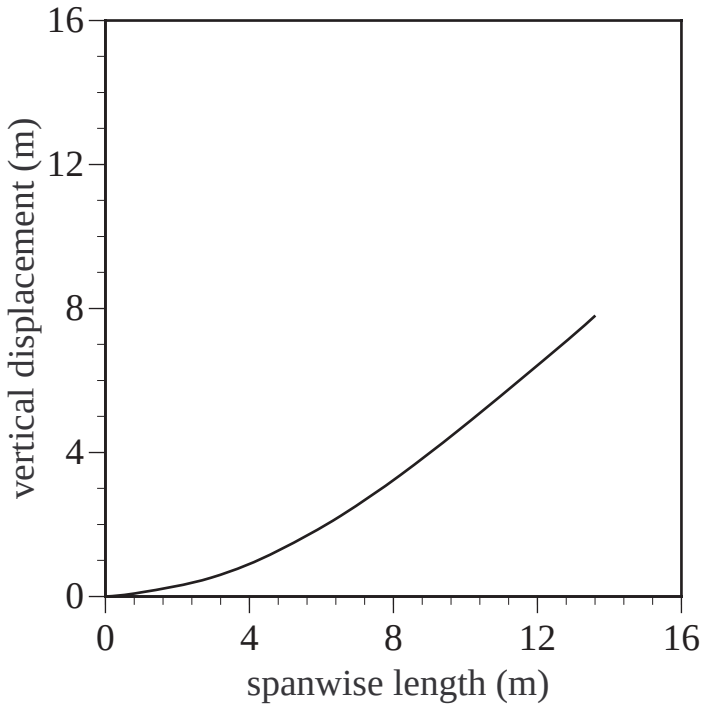

Figure 5.39: HALE wing displacement at 25 m/s

vector, which is perpendicular to the flow and the wing reference line, to not act in the vertical direction. This tilt of lift vector can be understood from the plot of the deformed wing shape. Fig. 5.39 shows the displacement shape of the wing at 25 m/s forward speed trim condition. The deflection of the wing is very large and outside the region of applicability of linear theory. This high deformation and associated loss of aerodynamic force in the vertical direction leads to the requirement of a higher value of $\overline{\alpha}_0$.

Fig. 5.40 plots the ratio of total lift (force in vertical direction perpendicular to the flight velocity and span) to rigid lift. The drastic loss of effective vertical lift is clearly observed as compared to linear results. The main significance of this result lies in the fact that, if stall angle is around 12°, then the rigid-wing analysis predicts the stall speed to be 20 m/s, whereas the actual flexible aircraft would stall at much higher flight speed of around 25 m/s. This would mean reduction in the actual flight

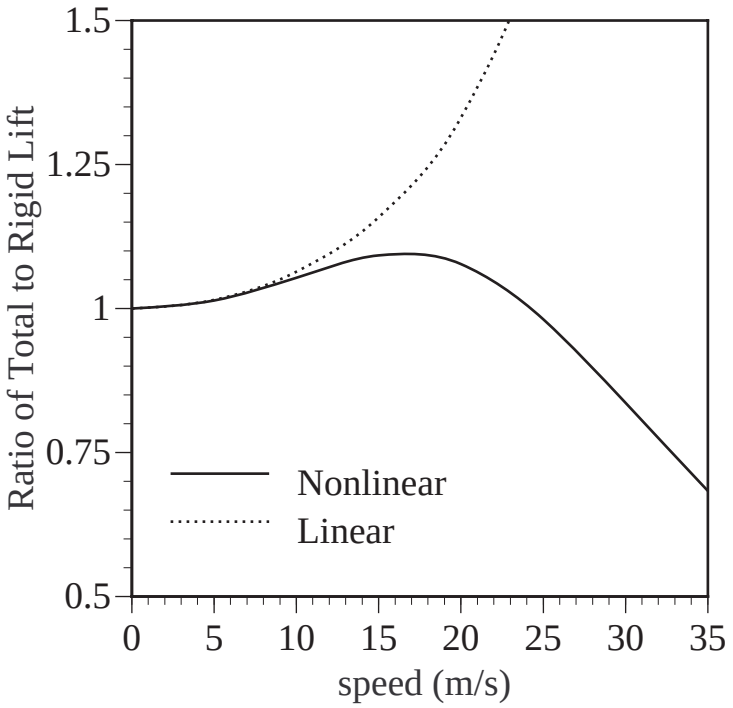

Figure 5.40: Total lift to rigid lift ratio at $\alpha_0 = 5°$

envelope.

5.4.2 Rigid aircraft flight dynamics

Table 5.8 shows the the phugoid- and short-period-modal frequencies and dampings obtained by the present analysis, assuming a rigid wing. These results are compared against the frequencies obtained by the simple rigid aircraft analysis given in Roskam [75]. One sees that results from the present analysis are essentially identical

Table 5.8: Comparison of rigid aircraft flight dynamics for HALE aircraft

	Present Analysis	Analysis of Ref. [75]	% Diff.
Phug. Freq. ω_{n_P}	0.320	0.319	+0.3
Phug. Damp. ζ_P	0.0702	0.0709	-1.0
S.P. Freq. $\omega_{n_{SP}}$	5.47	5.67	-3.5
S.P. Damp. ζ_{SP}	0.910	0.905	+0.6

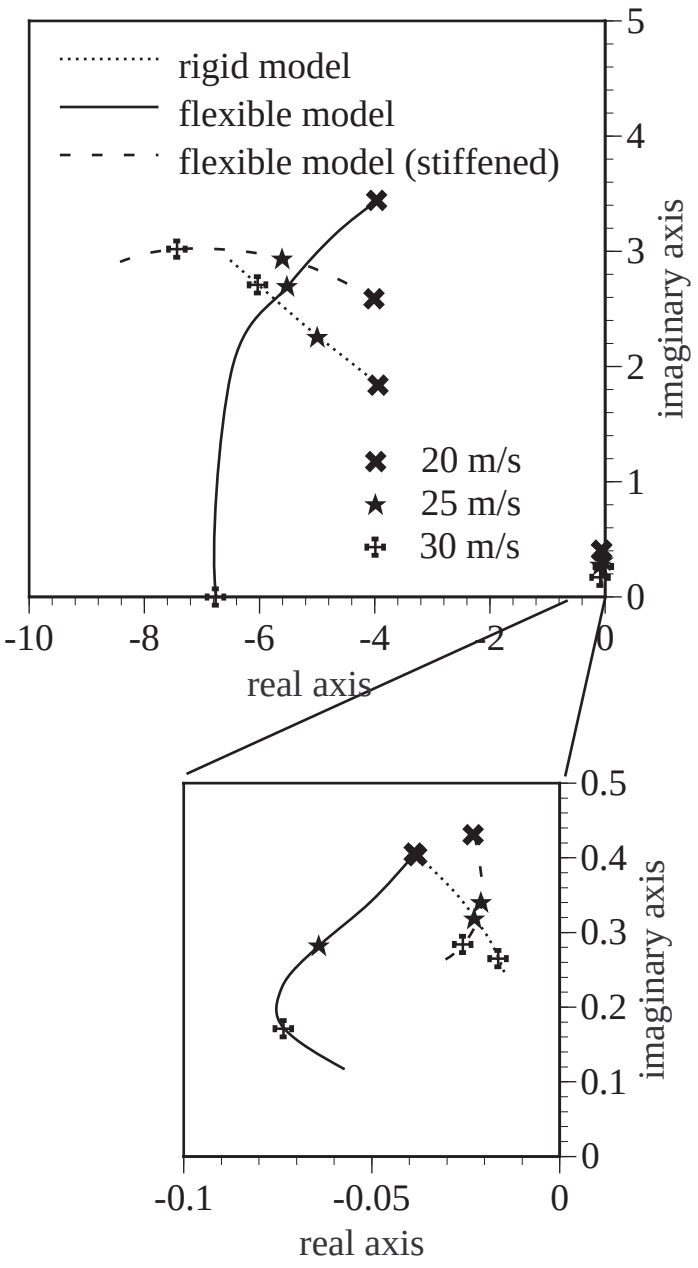

Figure 5.41: Root locus plot showing the HALE flight dynamics roots, with a magnified section showing the roots nearest the origin

to published results.

5.4.3 Stability of complete flexible aircraft

When flexibility effects are taken into account in the flight dynamic analysis, the behavior is distinctly different from that of a rigid aircraft. Fig. 5.41, compares the flight dynamics frequencies obtained with and without wing flexibility. The phugoid as well as the short period mode are affected by wing flexibility.

On the other hand, flight dynamic roots affect the aeroelastic behavior of the wing. Fig. 5.42 compares the root locus plot for the complete aircraft with those obtained by using linear wing aeroelastic analysis and nonlinear wing aeroelastic analysis. The nonlinear wing aeroelastic analysis uses the known flight trim angle of attack. A magnified plot is inserted which shows the qualitative differences in more detail. It is clear that the low-frequency modes which involve flexibility are completely coupled to the flight dynamic modes changing the behavior completely. On the other hand, the high-frequency modes, one of which linear analysis predicts to be unstable at 34.21 m/s, are only affected by the nonlinearity. Thus, if the trim solution is properly taken into account then the nonlinear wing analysis gives a good estimate of the actual wing plus aircraft combination modes.

5.5 Aeroelastic Control

One of the motivations for the present work was to develop an aeroelastic analysis tool amenable to control design. To make the model control compatible, the model should be able to be transformed to a state-space form. One could then use any of the available linear control design techniques. The aim was to design a simple and effective controller for flutter suppression and gust load alleviation. A series of optimal Static Output Feedback (SOF) controllers are designed for improving aeroelastic

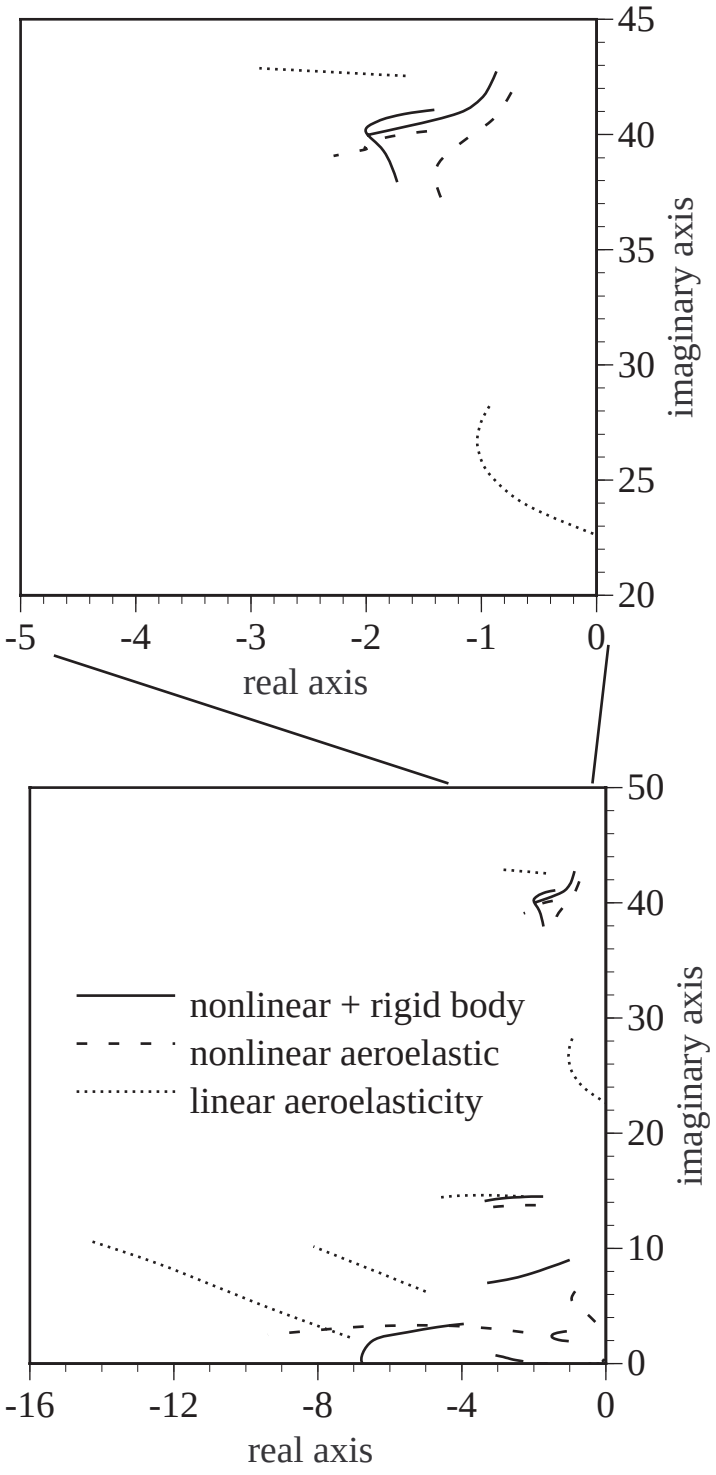

Figure 5.42: Expanded root locus plot with magnified section inserted which depicts roots in vicinity of the unstable root

characteristics. A brief background on model order reduction is presented in the next section followed by a section describing the case studies of control design, open and closed loop results and comparison with the Linear Quadratic Regulator (LQR) and the Linear Quadratic Gaussian (LQG) regulator.

5.5.1 Transforming present model to a low-order state-space form

Before a control is designed for the aeroelastic system, the system needs to be converted to a linear, state-space form. The original total number of variables of the complete nonlinear system is around $30 \times n$, where n is the number of finite elements. The break up of the 30 variables is, 3 each for displacement (u), rotation (θ), internal force (F), internal moment (M), linear momentum (P), angular momentum (H), and 6 each for inflow states (λ) and stall states. For an eight element wing this total is 240, which is very large. In addition, some of the equations, *e.g.*, strain – displacement relation, are static equations with no time derivative, and thus these equations need to be used to remove some variables. Also, in the nominal conditions considered here, there are no stall states. The final reduction in the number of variables and equations (and thus order of the nominal system) comes from the fact that the extensional and shear rigidities are very high and thus the corresponding strains are very low. This approximation could be used to further reduce the number of structural equations in half. The final count of variables lead to the order of the system around $12 \times n$ (n is the number of beam elements used), where the variables are three rotational variable and their time derivatives and six inflow states per element.

Table 5.9: SOF performance for various sensor configurations

Sensors config.	Control cost	% increment in cont. rms w.r.t. LQR	c.l.eig.val. real part	c.l.eig.val. imag part
System	0	–	1.0323	21.1978
LQR	586.90	0	-1.0323	21.1978
SOF 1α	628.56	3.49%	-0.9190	21.2219
SOF 2α	626.29	3.30%	-0.9118	21.2646
SOF 3α	625.13	3.21%	-0.9167	21.2528
SOF $1h$	Unstable	–	–	–
SOF $1\alpha 1h$	622.33	2.97%	-0.9598	21.2242

5.5.2 Flutter suppression

The primary aim of the following exercise is to check the effectiveness of the present formulation in providing the necessary state-space model for control design. Some control design parametric studies were conducted and the control designs were checked by time marching.

Table 5.9 shows the results for control cost and closed loop damping due to various static output feedback (SOF) controllers. The system under consideration is the HALE wing at 35 m/s (slightly above flutter speed of 32.21 m/s). The system matrices A, B, C are obtained by transforming the jacobian matrix as described in Section 5.5.1. The controller is optimized for minimum control rms. Thus, the state is not penalized ($Q = 0$) and the control coefficient is assumed unity ($R = 1$). The control mechanism is the wing tip flap. The process noise is assumed to affect all the structural equations of motion equally. The SOF results are compared to results obtained using linear quadratic regulator (LQR) controller. The LQR design is a good baseline comparison because LQR gives the best performance measure. But LQR cannot be practically implemented because all the states are not known and thus, it must include an estimator like the Kalman filter. Once an estimator is added the re-

sultant dynamic controller increases the controller complexity considerably. But LQR gives a best achievable performance and is thus a good indication of the optimality of the SOF controller.

The SOF controllers are denoted by the sensors used. Thus, 1α denotes a root twist and root twist rate sensor, 2α denotes a twist and twist rate sensors at the root and the mid-span, 3α denotes twist and twist rate sensors at the root, one-third spanwise position and two-third spanwise position. $1h$ denotes the curvature and curvature rate sensors at the root. As can be seen, the SOF controller using just one strain and strain rate feedback can give very good performance. For example, if one uses just a root twist and root twist rate feedback one stabilizes the system with just around 7% more cost, which in turn means around 3.5% increase in control root mean square (rms) value. Also the closed loop damping of the flutter mode is quite close to that provided by LQR. As the number of sensors is increased, the performance and the stability improves. Another point to note is that using only the root curvature and root curvature rate sensor feedback cannot stabilize the system. This is because the aeroelastic energy transfer is dominated by the torsional instability which in turn transfers some energy to the bending mode. Thus, the knowledge of torsional variables is more important for a stabilizing controller design. This suggests that a optimal placement of sensors is required for good performance which may lead to approximate recovery of LQR performance.

The SOF gives a good controller in terms of stabilizing the system. The performance comparisons with LQR were also quite favorable. However, it should be pointed out that SOF gives the optimal performance for the given disturbance, whereas LQR gives the best performance for any disturbance (since solution is independant of D). Thus, if the disturbance were such that the aerodynamic equations were more affected, or that the structural equations were affected in a different mode

then that assumed, then one would not get the best possible SOF performance for the new disturbance but the LQR performance is still the best, and consequently the comparison of SOF with LQR would not be as close.

To test the controller effectiveness, the system is simulated with and without the controller. Fig. 5.43 shows the controlled and uncontrolled time history of the wing at 35 m/s with an initial disturbance of 0.1m at the tip. The controller with root twist and root twist rate feedback is used. The flutter is effectively suppressed. Fig. 5.44 shows the time history of the tip displacement if the controller is activated after the first five seconds into flutter. With an initial tip disturbance of 0.1m, the system reaches high deformations within 5s. Thus, the control actuation required is also quite high. In reality a single flap may not be able to provide the required high control authority. But high authority control is possible if more flaps are distributed through out the wing span.

Due to the simplicity of the SOF controller, it can be easily combined with gain scheduling to obtain a nonlinear controller. To demonstrate the ease of designing a nonlinear controller, a simple nonlinear controller is designed to control the nonlinear phenomena of limit cycle oscillations (LCO). It should be noted here that it is mainly due to the insight into the nonlinear physical mechanisms responsible for the LCO that leads to a design of a simple nonlinear controller.

Before the design of the nonlinear controller is explained, there is a need to go back to the nonlinear limit cycle oscillation results explained earlier. It is seen that there is a drastic decrease in stability with wing bending. Thus, a wing when curved behaves completely different. In fact it leads to instability at much lower speeds. The dominant nonlinearity seems to be the one due to wing bending, as it is exhibited in tip displacement. Thus, the tip displacement seems to be a good parameter on which to base a nonlinear controller. A simple nonlinear controller is designed using dynamic

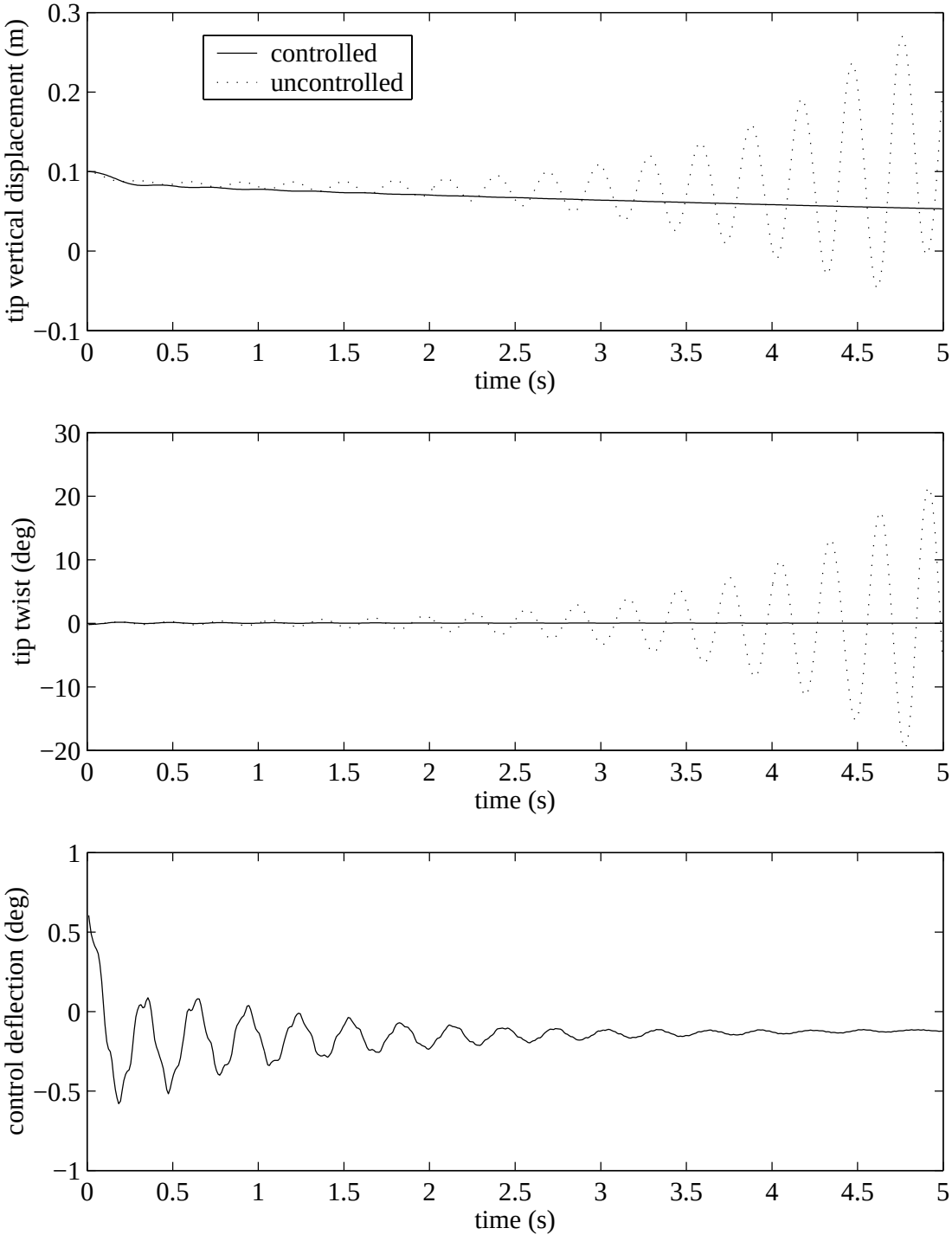

Figure 5.43: SOF applied for flutter suppression at flight speed of 35 m/s

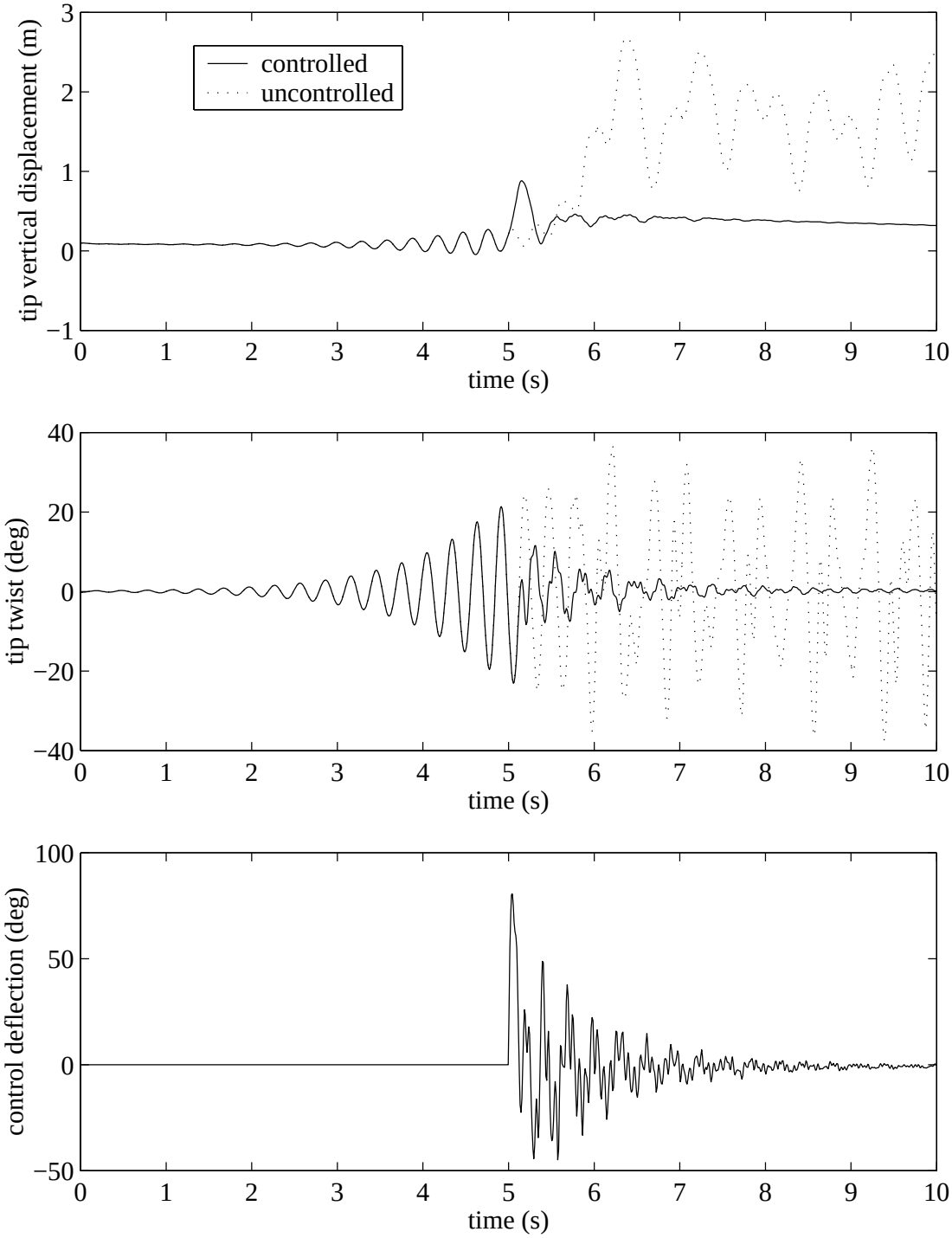

Figure 5.44: Flutter suppression at speed of 35 m/s with SOF controller activated after the first five second

gain scheduling based on the tip displacement. The case used is the HALE wing at 30 m/s, which is stable if linear analysis is used. There is a decrease in stability margin with curving of beam and at a tip displacement of around 0.6m it becomes unstable. A series of SOF controllers with root strain and root strain rate feedback are designed at intervals of tip displacement. The controller is linearly interpolated at in-between tip displacements.

Fig. 5.45 shows the effect of such a nonlinear controller on the aeroelastic behavior of the HALE wing at 30 m/s when disturbed by a tip displacement of 2m. The uncontrolled case gets attracted to a limit cycle oscillation but the controlled wing approaches the undeformed state. If the damping of various modes is evaluated, one finds that even without control the first bending mode is damped. But as the wing moves from the deformed state, it excites the torsional mode which gains energy from the flow and then transfers it back to the bending modes. The controller does not let the torsional energy increase, and since the bending mode is highly damped it goes to an equilibrium. The nonlinear SOF controller effectively suppresses the torsional mode and thus avoids LCOs.

Before ending this section on flutter suppression the SOF controllers are compared to a LQR controller in series with a Kalman estimator, *i.e.*, a linear quadratic gaussian (LQG) controller. LQG controller will give the optimal output feedback law, but the controller is very complex as compared to simple constant output feedback. Also, to adapt the LQG controller to a nonlinear system would be very difficult. Since the SOF controllers are designed under the assumption of zero sensor noise, the LQG controllers are also designed by using small sensor noise (the sensor noise matrix is reduced till the cost converges to a value).

Table. 5.10 shows the results for a LQG controller. As seen in the table, the LQG controller performance is not as good as LQR (which is not possible to implement)

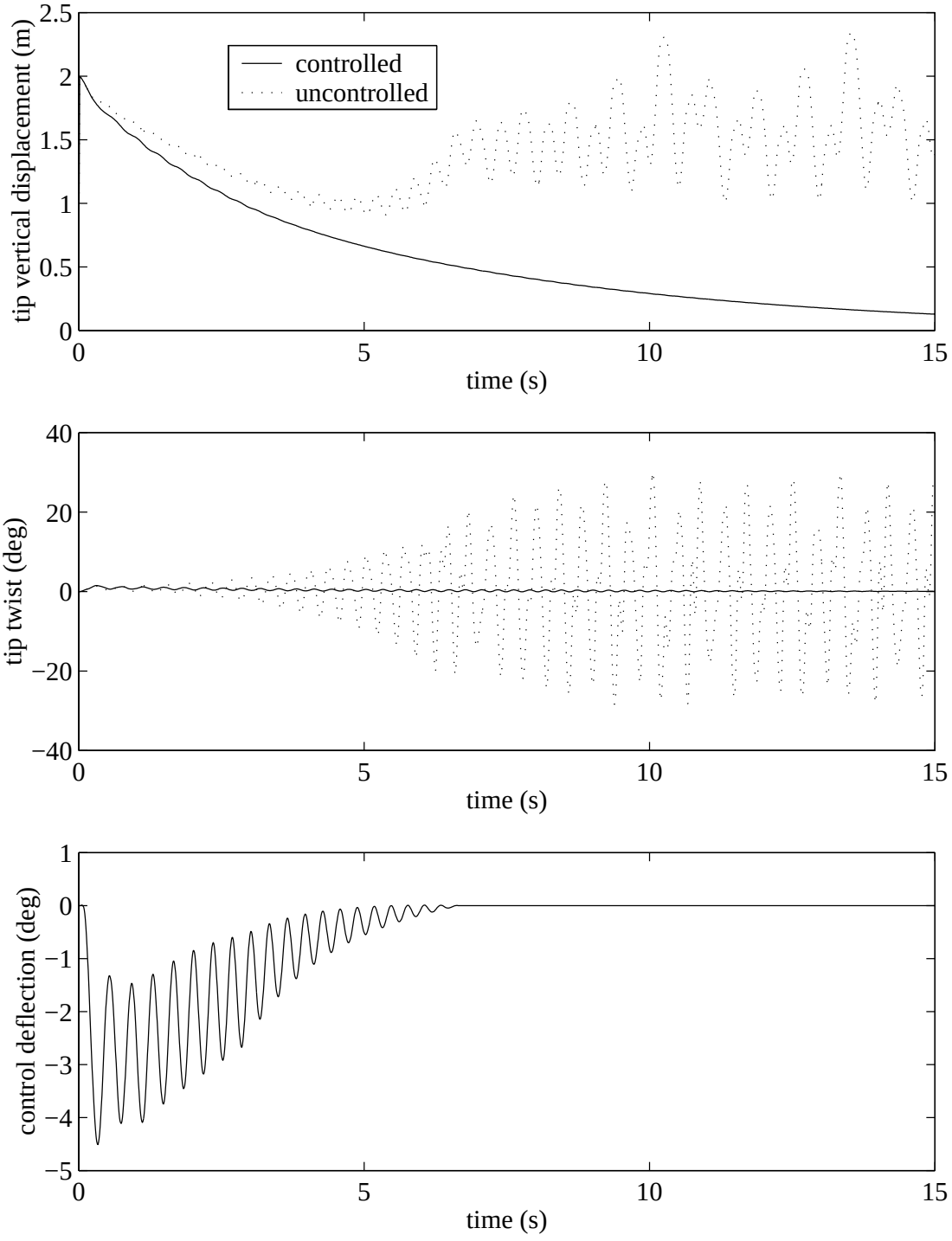

Figure 5.45: Nonlinear SOF controller applied to LCO control at 30 m/s

Table 5.10: SOF/LPF performance

Sensors config.	Control cost	% increment in cont rms w.r.t. LQR	w.r.t. LQG	c.l.eig.val. real part	c.l.eig.val. imag part
System	0	–	–	1.0323	21.1978
LQR	586.90	0	–	-1.0323	21.1978
LQG 1α	607.46	1.74%	0%	-1.0323	21.1978
SOF 1α	626.29	3.49%	1.72%	-0.9190	21.2219
SOF 1α + LPF	796.13	16.47%	14.48%	-0.6438	22.0321
Reoptimized	623.72	3.09%	1.33%	-0.9396	21.2038

but is only slightly better than a SOF. Thus, LQG cannot be preferred over SOF just for performance. There are some other characteristics of LQG controllers which make it a better choice as compared to SOF. One of which is the high-frequency roll off. High-frequency roll off would mean that the high-frequency unmodeled dynamics of the system are not as much affected by the controller and thus lessening the risk of the controller destabilizing the system. One can introduce high-frequency roll off in SOF by utilizing a low-pass filter (LPF) in series with the SOF controller. Such characteristics have been shown earlier for a second order acceleration feedback controllers [76].

In this example a fixed low-pass filter of frequency cutoff of 100 rad/s and damping factor of 1.0 is used. As can be expected, such a low-pass filter will change the magnitude and phase characteristics of the effective controller thus leading to decrease in the controller performance. But, the SOF controller could be reoptimized by assuming it to be attached to a low-pass filter. The reoptimized combination of the low-pass filter and SOF leads to a simple yet very effective controller. The control rms is only 1.33% higher for the low-pass filter plus SOF combination as compared to a LQG, with a better roll-off characteristics, and a simple implementation.

Finally, one of the most important properties of a controller is its robustness.

Table 5.11: Comparison of the stability margins

Sensors config	gain margins		phase margins	
LQR	-6.02 db	$+\infty$ db	$-60°$	$+60°$
LQG 1α	-5.84 db	$+12.03$ db	$-58.70°$	$+56.15°$
SOF 1α	-5.44 db	$+9.66$ db	$-58.98°$	$+54.87°$
SOF 1α + LPF	-4.30 db	$+9.50$ db	$-80.29°$	$+28.36°$
SOF 1α + LPF (reopt.)	-5.69 db	$+9.81$ db	$-59.28°$	$+56.29°$

Stability margins are a good indication of the controller robustness to gain and phase shifts. Table 5.11 shows the stability margin predictions for the various controllers under investigation. As expected, LQR controller has a gain margin of -6.02 db and $+\infty$ db and phase margin of $\pm 60°$. The LQG controller has similar lower gain margin and phase margins. There is a degradation in the upper gain margin to around $+12$ db (ensuring stability at controller gains up to only four times the nominal). As to the SOF controller, it shows gain and phase margins similar to the LQG design. Thus, SOF controller can be expected to have equivalent robustness properties. By adding a LPF to the SOF controller there is a shift in the phase margin. The phase shift is introduced because the LPF itself has a phase shift of around $25°$ at the unstable frequency. This phase shift is overcome by reoptimizing the SOF controller with LPF. Such a reoptimized controller regains the characteristics of the stand-alone SOF. Thus, a reoptimized SOF+LPF controller has performance, high-frequency roll off and stability margins very close to LQG controller without the associated complexity.

To summarize, a SOF controller could be designed for optimal performance which is very close to LQR with proper choice of sensors. It may be possible to modify such a simple SOF controller for control of nonlinear system response like LCOs. High-frequency roll off could be achieved by combining such a controller with a low-pass filter. The SOF controllers also have gain and phase margins equivalent to LQG

controllers.

5.5.3 Gust load alleviation

Gust load alleviation problem is very important to keep the disturbance response of the wing low. Low disturbance response would extend the fatigue life of the structure. To solve a gust response problem one need to define a gust model. For the results presented here the gust model is based on the continuous atmospheric turbulence model given in Bisplinghoff *et al.* [61]. Using this model, the power spectrum of atmospheric turbulence in terms of space frequency can be represented as,

$$\Phi\left(\frac{\omega}{\bar{U}}\right)\left[\frac{(ft/s)^2}{rad/ft}\right] = \frac{0.060}{0.000004+\left(\frac{\omega}{\bar{U}}\right)^2} \tag{5.1}$$

For a given speed ($\bar{U}$), one could write the power frequency spectrum of atmospheric turbulence in MKS units as,

$$\Phi\left(\omega\right)\left[\frac{(m/s)^2}{rad/s}\right] = \frac{0.078\bar{U}}{0.000043U^2+\omega^2} \tag{5.2}$$

The above equation for a given flight speed has the form of the power spectrum of a first order dynamic system excited by a white noise. Thus, the atmospheric turbulence model can be easily represented in terms of a single state-space equation. This equation was added to the system equations. The output of the gust equation to white noise was given as the disturbance to the original system. The model is the HALE wing at flight speed of 25 m/s. The state cost is defined in terms of the structural energy [77] as $J_s = x_s^T[K]x_s + \dot{x}_s^T[M]\dot{x}_s$, where x_s are the structural states.

Table 5.12 shows the state and control cost associated with SOF controllers using various sensors. The results are very different from those obtained for flutter suppression. For flutter suppression, twist sensing was most important since the unstable

Table 5.12: SOF performance for gust alleviation at 25 m/s

Sensors config.	Performance measure	State cost	Control cost
SOF 1α	74.614	74.215	0.399
SOF $1h$	62.788	53.342	9.446
SOF $2h$	62.598	53.016	9.582
SOF $3h$	62.580	52.985	9.595
SOF $1\alpha 1h$	62.605	53.033	9.572

mode was dominant in twist. In gust alleviation the curvature (bending) sensing seems to lead to best performance. The reason stems from the fact that the gust spectrum is very high at low frequencies and drops drastically with increase in frequencies. The bending frequencies are thus the modes which are most excited by the gust. Curvature sensing is thus most important for gust load alleviation since it senses the modes that are most disturbed and thus these modes could be easily controlled.

Fig. 5.46 shows the plot of state cost versus control cost for optimal SOF controller using only the root curvature and root curvature rate sensing. At flight speed of 25 m/s the system is stable and thus the uncontrolled state cost is finite. With slight increase in control cost there is drastic reduction in the state cost. But the decrease in state cost is limited due to the use of only two sensors. Furthermore the edgewise bending modes are neither observed nor can these modes be controlled thus leading to a finite minimum state cost. Using the plot a designer could choose the controller design based on the available control authority and expected amplitude of disturbance.

Before comparing the results presented in Table 5.12 with LQR designs, the various LQR controllers are discussed below. The way to represent a LQR controller for a

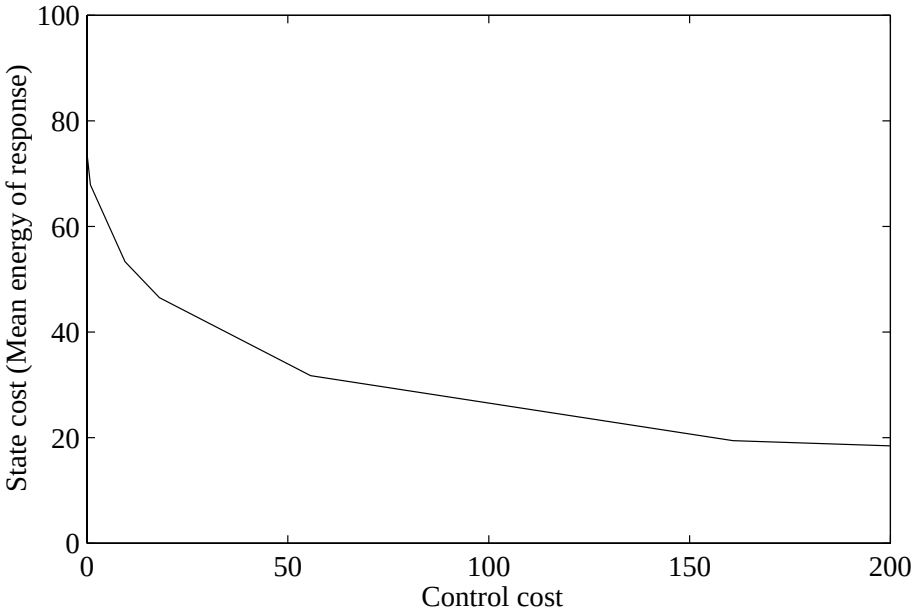

Figure 5.46: State versus Control cost plot for gust alleviation using SOF

Table 5.13: Comparison of SOF performance with LQR

Sensors config.	Performance measure	State cost	Control cost
SOF $1h$	62.788	53.342	9.446
LQR (white noise)	75.015	75.014	0.00025
LQR (gust model)	48.584	38.968	9.616
SOF (all states)	62.552	52.938	9.614

system with a gust state is unclear. The reason is that, even though the gust state is part of the mathematical system which is used for design, it is not a part of the actual system. Thus, whether to include the gust state feedback is unclear. There are three LQR-like controllers designs possible. First one denoted as LQR (white noise) is based on the assumption of a white noise disturbance to the system, *i.e.*, no gust state equation. The second, LQR (including gust model) is the LQR design based on the model which includes the gust state. This model assumes the knowledge of the gust state, which actually is not known. The third controller denoted by SOF (all states) is a full state feedback of only the original model states but the gust state is not used for feedback.

Table. 5.13 gives the performance results for various LQR designs and compares with SOF. If LQR controller is designed without considering the actual gust spectrum, *i.e.*, assuming a white noise, then the design is not useful in controlling the response of an actual gust. This is because though LQR is by design an optimal controller for any disturbance spatial mode it assumes that the disturbance is a white noise process affecting all the modes. But the actual gust spectrum is such that it affects the first couple mode much more than the higher modes. Consequently even if the higher frequency modes have a lower stability margin these modes are not as affected due to the lower excitation power and thus need not be given priority over the lower modes. Thus, the results obtained using a LQR (white noise) controller are not good. Now, if the gust model is included and a LQR controller is designed assuming gust state feedback, it gives the best achievable results. But LQR (gust model) is inconsistent in assuming knowledge of the gust state which by definition is quite random. Though unachievable, it is a good baseline result for comparison. Now if a full original model state feedback is designed, the performance gives the best achievable results of constant gain output feedback. It is seen that this result is quite

close to that obtained by using only a root curvature and root curvature rate feedback. Thus, using just a pair of sensors, *i.e.*, root curvature and root curvature rate, a SOF controller could be designed to give performance with 1% of the performance one would achieve by feeding back all the 96 states. This again points out that effective SOF controllers could be designed by choosing the right sensors.

In summary, SOF controllers can be effective in gust alleviation with proper choice of sensor. Inclusion of a proper gust model is also necessary for optimal performance. LQR performance using white noise disturbance assumptions do not lead to effective controllers.

Chapter 6

CONCLUSIONS

The present work had the goal of developing a low-order, high-fidelity aeroelastic model for preliminary design and control synthesis of a high-aspect-ratio wing aircraft. The following modeling and analysis capabilities have been achieved:

- Geometrically nonlinear modeling of the wing structures as beams
- Cross-sectional analysis of arbitrary, anisotropic cross sections
- Finite-state unsteady induced flow modeling
- ONERA stall model
- Rigid body modes in the analysis
- Control surface aerodynamics
- Static Output Feedback control design for gust load alleviation and flutter suppression.

With such a modeling capability various problems have been investigated, and insights into higher-order effects gained. They include:

- Parametric studies of composite wings

- Aeroelastic instabilities (and the damping of various modes)
- Effect of steady-state lift on aeroelastic characteristics
- Limit cycle oscillations
- Flight dynamics of a flexible aircraft
- Control system design and evaluation

Aeroelastic tailoring results indicate the enormous effect that coupling has on the aeroelastic characteristics of the wing. Also the studies indicate the necessity of using correct cross-sectional analysis because the aeroelastic results are very sensitive to the cross-sectional stiffness parameters. Divergence is drastically affected by flatwise bending-torsion coupling. Flutter is also affected by coupling, but the effect is not as clearly observed. There are a number of flutter modes and these flutter modes are affected in different ways.

The nonlinear aeroelastic results are interesting to say the least, and complex at most. The results give deeper insight into effects on nonlinearities on aeroelastic stability. For the metallic wing structural nonlinearities were stiffening. Stall nonlinearities decreased the flutter speed drastically due to coupling between the low frequency stall dynamics and structural modes. Limit cycle oscillations were observed, but the amplitude was very high which might lead to failure in an actual wing. A very interesting nonlinear effect was that of finite disturbances. It has been shown that even for speeds lower than the predicted linearized instability speed, instabilities could be induced due to finite disturbances.

A nonlinear aeroelastic analysis has also been conducted on a complete aircraft model representative of the current High-Altitude Long-Endurance (HALE) aircraft.

Due to the large aspect ratio of the wing, the corresponding large deflections under aerodynamic loads, and the changes in the aerodynamic loads due to the large deflections, there can be significant changes in the aeroelastic behavior of the wing. In particular, significant changes can occur in the natural frequencies of the wing as a function of its tip displacement which very closely track the changes in the flutter speed. This behavior can be accounted for only by using a rigorous nonlinear aeroelastic analysis.

Limit cycle oscillations were also observed in the HALE wing. As expected, the results show that stall limits the amplitude of post-flutter unstable oscillations. Geometrical nonlinearities are responsible for the low nonlinear flutter speed. Thus, even at speeds below the linear flutter speed, LCO can be observed if the stable steady state is disturbed by a finite-amplitude disturbance. A critical disturbance magnitude is required at a given speed or a critical speed is required at a given disturbance magnitude to initiate LCO.

The overall flight dynamic characteristics of the aircraft also change due to wing flexibility. In particular, the trim solution, as well as the short-period and phugoid modes, are affected by wing flexibility. Neglecting the nonlinear trim solution and the flight dynamic frequencies, one may find the predicted aeroelastic behavior of the complete aircraft very different from the actual one.

Controllers based on optimal static output feedback theory were designed and compared with linear quadratic regulator and linear quadratic gaussian designs. Static output feedback controllers seem to give a comparable performance at a much lower complexity. Due to its simplicity, static output feedback can be easily coupled with other controllers or can be used with gain scheduling for a nonlinear controller. Optimal sensor position is critical to get good performance from static output feedback.

Future Work

There are various areas of research which could be pursued with the help of the present analysis.

Aeroelastic tailoring of composite wings is a promising field. But there are no consistent ways of conducting parametric studies. Just changing the ply lay-up is not right. The aeroelastic tailoring results need to satisfy some strength and frequency constraints. Without some research into this aspect, the aeroelastic tailoring results would be academic. However, realism gained through proper design constraints would lead to realistic improvements in overall aeroelastic response. Nonlinear aeroelastic and structural tailoring is another important area in which further work is needed. As was seen in the results, it is possible to avoid the deleterious effects of nonlinear deformation by structural coupling or pre-curving of the wing. Such effects need to be exploited to the fullest extent so as to maintain wing stability at large deformation.

The nonlinear aeroelastic effects are strong function of the wing aspect ratio. A parametric study can be conducted to study the effects of various nonlinearities on the aeroelastic behavior. It is expected that stall nonlinearities are dominant at low aspect ratios, while geometrical nonlinearities are more important at high aspect ratios. Also, some results indicated that the nonlinearity is related to the edgewise stiffness and the corresponding frequency. Investigating the effect of frequency distribution of various modes would lead to rules of thumb as to when the nonlinearities are critical. The nonlinearities are also affected by other structural parameters like taper and sweep. Wing taper has an important effect on the frequencies of a straight wing and can be assumed to affect the variation of frequencies with large deformation. Such effect may lead to different nonlinear aeroelastic characteristics. Research in these areas would study the importance of various structural planform parameters in nonlinear

behavior and would bring out any new critical nonlinear features.

Before practical use, the analysis should be evaluated using more rigorous tools. A combination of FEM for structural analysis and CFD for aerodynamic analysis would give good baseline comparison results. There is also a possibility of modifying the finite-state aerodynamic model to incorporate corrections from a CFD model. Such correction would make the analysis more accurate and a control design based on such model likely to be successful. Also, the nonlinear structural analysis could be coupled with a CFD code to give a good model to evaluate control designs. There is also a need to investigate the stresses in the wing when it is undergoing large deformation. These stresses could then be used to evaluate a failure criterion. By knowing the failure limit one could then investigate the cases in which nonlinear effects really happen before failure. For example, one could study whether the wing fails before settling into a LCO.

One of the most important extension to this work would be the design and evaluation of robust controllers based on this model. Before attempting to design controllers it would be necessary to develop an uncertainty model. Developing an uncertainty model which is an accurate representation of the expected uncertainty would help design controllers with less conservatism and thus better performance.

The nonlinear interaction between flight dynamics and wing elastic deformation is of importance in HALE aircraft. Further research is necessary to get physical insight into this important interaction. By doing a parametric study with wing flexibility and aircraft weight one can expect to get qualitative indicators as to when these interactions become important.

Bibliography

[1] Housner, J. M. and Stein, Manuel, "Flutter Analysis of Swept-Wing Subsonic Aircraft with Parametric Studies of Composite Wings," Technical report, NASA-TN-D-7539, Sept. 1974.

[2] Hollowell, Steven J. and Dugundji, John, "Aeroelastic Flutter and Divergence of Stiffness Coupled, Graphite/Epoxy Cantilevered Plates," *Journal of Aircraft*, Vol. 21, No. 1, Jan. 1984, pp. 69 – 76.

[3] Lottati, I., "Flutter and Divergence Aeroelastic Characteristics for Composite Forward Swept Cantilevered Wing," *Journal of Aircraft*, Vol. 22, No. 11, Nov. 1985, pp. 1001 – 1007.

[4] Green, J. A., "Aeroelastic Tailoring of Aft-Swept High-Aspect-Ratio Composite Wings," *Journal of Aircraft*, Vol. 24, No. 11, 1987, pp. 812 – 819.

[5] Shirk, M. H., Hertz, T. J., and Weisshaar, T. A., "Aeroelastic Tailoring – Theory, Practice, and Promise," *Journal of Aircraft*, Vol. 23, No. 1, Jan. 1986, pp. 6 – 18.

[6] Weisshaar, T. A., "Aeroelastic Tailoring of Forward Swept Composite Wings," *Journal of Aircraft*, Vol. 18, No. 8, Aug. 1981, pp. 669 – 676.

[7] Librescu, L. and Song, O., "On the Static Aeroelastic Tailoring of Composite Aircraft Swept Wings Modelled as Thin-Walled Beam Structures," *Composites Engineering*, Vol. 2, No. 5-7, 1992, pp. 497 – 512.

[8] Librescu, L., Meirovitch, L., and Song, O., "Refined Structural Modeling for Enhancing Vibrational and Aeroelastic Characteristics of Composite Aircraft Wing," *Recherche Aerospatiale*, 1996, pp. 23 – 35.

[9] Butler, R. and Banerjee, J. R., "Optimum Design of Bending-Torsion Coupled Beams with Frequency or Aeroelastic Constraints," *Computers & Structures*, Vol. 60, No. 5, 1996, pp. 715 – 724.

[10] Lillico, M., Butler, R., Guo, S., and Banerjee, J. R., "Aeroelastic Optimization of Composite Wings Using the Dynamic Stiffness Method," *Aeronautical Journal*, Vol. 101, 1997, pp. 77 –86.

[11] Chattopadhyay, A., Zhang, S, and Jha, R., "Structural and Aeroelastic Analysis of Composite Wing Box Sections Using Higher-Order Laminate Theory," In *Proceedings of the 37th Structures, Structural Dynamics, and Materials Conference*, Salt Lake City, Utah, April 1996.

[12] Cesnik, C. E. S., Hodges, D. H., and Patil, M. J., "Aeroelastic Analysis of Composite Wings," In *Proceedings of the 37th Structures, Structural Dynamics, and Materials Conference*, Salt Lake City, Utah, April 18 – 19, 1996, pp. 1113 – 1123.

[13] Patil, M. J., "Aeroelastic Tailoring of Composite Box Beams," In *Proceedings of the 35th Aerospace Sciences Meeting and Exhibit*, Reno, Nevada, Jan. 1997.

[14] Boyd, N., *Effect of Chordwise Deformation and Steady-State Lift on Flutter of a Cantilevered Wing*, Ph.D. Thesis, Stanford U., California, 1977.

[15] Chen, G-S and Dugundji, J., "Experimental Aeroelastic Behavior of Forward-Swept Graphite / Epoxy Wings with Rigid-Body Freedom," *Journal of Aircraft*, Vol. 24, No. 7, July 1987, pp. 454 – 462.

[16] Dunn, P. and Dugundji, J., "Nonlinear Stall Flutter and Divergence Analysis of Cantilevered Graphite/Epoxy Wings," *AIAA Journal*, Vol. 30, No. 1, Jan. 1992, pp. 153 – 162.

[17] Dugundji, J., "Nonlinear Problems of Aeroelasticity," In Atluri, S. N., editor, *Computational Nonlinear Mechanics in Aerospace Engineering*, chapter 3. AIAA, Washington, DC, 1992.

[18] Tang, D., Conner, M. D., and Dowell, E. H., "Reduced-Order Aerodynamic Model and Its Application to a Nonlinear Aeroelastic System," *Journal of Aircraft*, Vol. 35, No. 2, Mar – Apr 1998, pp. 332 – 338.

[19] Tang, D. M. and Dowell, E. H., "Experimental and Theoretical Study for Nonlinear Aeroelastic Behavior of a Flexible Rotor Blade," *AIAA Journal*, Vol. 31, No. 6, June 1993, pp. 1133 – 1142.

[20] Patil, Mayuresh J. and Hodges, Dewey H., "Nonlinear Aeroelasticity and Flight Dynamics of Aircraft in Subsonic Flow," In *Proceedings of the 21st Congress of International Council of the Aeronautical Sciences, Australia*, Sept. 13 P 18, 1998, AIAA Paper A98-31713.

[21] Lind, R., Snyder, K., and Brenner, M., "Investigating Transient and Limit Cycle Behaviors of a Nonlinear Structure by Wavelet Transforms," In *Proceedings of the 39th Structures, Structural Dynamics, and Materials Conference*, Long Beach, California, April 1998, pp. 942 – 952.

[22] O'Neil, T. and Strganac, T. W., "Nonlinear Aeroelastic Response - Analyses and Experiments," In *Proceedings of the 34th Aerospace Sciences Meeting and Exhibit*, Reno, Nevada, Jan 1996, AIAA-96-0014.

[23] Gilliatt, H. C., Strganac, T. W., and Kurdila, A. J., "On the Presence of Internal Resonances in Aeroelastic Systems," In *Proceedings of the 39th Structures, Structural Dynamics, and Materials Conference*, Long Beach, California, April 1998, pp. 2045 – 2055.

[24] VanSchoor, Marthinus C. and VonFlotow, Andreas H., "Aeroelastic Characteristics of a Highly Flexible Aircraft," *Journal of Aircraft*, Vol. 27, No. 10, October 1990, pp. 901 – 908.

[25] Waszak, M. R. and Schmidt, D. K., "Flight Dynamics of Aeroelastic Vehicles," *Journal of Aircraft*, Vol. 25, No. 6, June 1988, pp. 563 – 571.

[26] Newman, B. and Schmidt, D. K., "Numerical and Literal Aeroelastic-Vehicle-Model Reduction for Feedback Control Synthesis," *Journal of Guidance, Control and Dynamics*, Vol. 14, No. 5, Sep.-Oct. 1991, pp. 943 – 953.

[27] Pendaries, C., "From the HALE Gnopter to the Ornithopter - or how to take Advantage of Aircraft Flexibility," In *Proceedings of the 21st Congress of the International Council of the Aeronautical Sciences*, Melbourne, Australia, Sept. 13 – 18, 1998, A98 - 31715.

[28] Drela, M., "Integrated Simulation Model for Preliminary Aerodynamic, Structural, and Control-Law Design of Aircraft," In *Proceedings of the 40th Structures, Structural Dynamics and Materials Conference, Saint Louis, Missouri*, April 12 – 15, 1999, pp. 1644 – 1656.

[29] Noll, T. E., "Aeroservoelasticity," In *Proceedings of the 31th Structures, Structural Dynamics, and Materials Conference*, Long Beach, California, April 1990, pp. 1560 – 1570.

[30] Noll, T. E., Eastep, F. E., and Calico, R. A., "Prevention of Forward Swept Wing Aeroelastic Instabilities with Active Controls," In *Proceedings of the 14th Congress of the International Council of the Aeronautical Sciences*, Toulouse, France, 1984, pp. 439 – 448.

[31] Trame, L. W., Williams, L. E., and Yurkovich, R. N., "Active Aeroelastic Oscillation Control on the F/A-18 Aircraft," In *Proceedings of the AIAA Guidance, Navigation and Control Conference*, Snowmass, Connecticut, 1985, pp. 94 – 104.

[32] Newsom, J. R., Pototzky, A. S., and Abel, I., "Design of a Flutter Suppression System for an Experimental Drone Aircraft," *Journal of Aircraft*, Vol. 22, No. 5, May 1985, pp. 380 – 386.

[33] Newsom, J. R. and Mukhopadhyay, V., "Multiloop Robust Controller Design Study using Singular Value Gradients," *Journal of Guidance Control Dynamics*, Vol. 8, No. 4, Jul.-Aug. 1985, pp. 514 – 519.

[34] Mukhopadhyay, V., "Stability Robustness Improvement using Constrained Optimization Techniques," *Journal of Guidance, Control and Dynamics*, Vol. 10, No. 2, Mar.-Apr. 1987, pp. 172 – 177.

[35] Mukhopadhyay, V., "Digital Robust Control Law Synthesis using Constrained Optimization," *Journal of Guidance, Control and Dynamics*, Vol. 12, No. 2, Mar.-Apr. 1989, pp. 175 – 181.

[36] Rimer, M., Chipman, R., and Muniz, B., "Control of a Forward-Swept-Wing Configuration Dominated by Flight Dynamics/Aeroelastic Interactions," *Journal of Guidance, Control and Dynamics*, Vol. 9, No. 1, Jan.-Feb. 1986, pp. 72 – 79.

[37] Lin, C. Y. and Crawley, E. F., "Aeroelastic Actuation Using Elastic and Induced Strin Anisotropy," *Journal of Aircraft*, Vol. 32, No. 5, Sep. – Oct. 1995, pp. 1130 – 1137.

[38] Lin, C. Y., Crawley, E. F., and Heeg, J., "Open- and Closed-Loop Results of a Strain-Actuated Active Aeroelastic Wing," *Journal of Aircraft*, Vol. 33, No. 5, Sep. – Oct. 1996, pp. 987 – 994.

[39] Levine, William S. and Athans, Michael, "On the Determination of the Optimal Constant Output Feedback Gains for Linear Multivariable Systems," *IEEE Transactions on Automatic Control*, Vol. AC-15, No. 1, Feb. 1970, pp. 44 – 48.

[40] Syrmos, V. L., Abdallah, C. T., Dorato, P., and Grigoriadis, K., "Static Output Feedback – A Survey," *Automatica*, Vol. 33, No. 2, 1997, pp. 125 – 137.

[41] Guruswamy, G. P. and Byun, C., "Fluid-Structural Interactions Using Navier-Stokes Flow Equations Coupled With Shell Finite Element Structures," In *Proceedings of the AIAA 24th Fluid Dynamics Conference, Orlando, Florida*, July 6 – 9, 1993, AIAA-93-3087.

[42] Byun, C. and Guruswamy, G. P., "Wing-Body Aeroelasticity on Parallel Computers," *Journal of Aircraft*, Vol. 33, No. 2, Mar.-Apr. 1996, pp. 421 – 428.

[43] Guruswamy, G. P. and Byun, C., "Direct Coupling of Euler Flow Equations with Plate Finite Element Structures," *AIAA Journal*, Vol. 33, No. 2, Feb. 1995, pp. 375 – 377.

[44] Cunningham, H. J., Batina, J. T., and Bennett, R. M., "Modern Wing Flutter Analysis by Computational Fluid Dynamics Method," *Journal of Aircraft*, Vol. 25, No. 10, Oct 1988, pp. 962 –968.

[45] Bennett, R. M., Batina, J. T., and Cunningham, H. J., "Wing-Flutter Calculations with the CAP-TSD Unsteady Transonic Small-Disturbance Program," *Journal of Aircraft*, Vol. 26, No. 9, Sept. 1989, pp. 876 – 882.

[46] Schuster, D. M., *Application of an Aeroelastic Analysis Method for Aerodynamic Improvement of Fighter Wings at Maneuver Flight Conditions*, Ph.D. Thesis, Georgia Institute of Technology, Atlanta, Georgia, 1992.

[47] Anon., , "Flight Loads Prediction Methods for Aircraft, Volume I: Euler/Navier-Stokes Aeroelastic Method (ENS3DAE) Technical Development Summary," Technical Report WRDC-TR-3104, Wright Research and Development Center, Wright Patterson Air Force Base, Ohio, 1989.

[48] Fulton, M. V., *Stability of Elastically Tailored Rotor Blades*, Ph.D. Thesis, Georgia Institute of Technology, Atlanta, Georgia, May 1992.

[49] Shang, X., *Aeroelastic Stability of Composite Hingeless Rotors with Finite-State Unsteady Aerodynamics*, Ph.D. Thesis, Georgia Institute of Technology, Atlanta, Georgia, August 1995.

[50] Fulton, Mark V. and Hodges, Dewey H., "Aeroelastic Stability of Composite Hingeless Rotor Blades in Hover – Part I: Theory," *Mathematical and Computer Modelling*, Vol. 18, No. 3/4, 1993, pp. 1 – 18.

[51] Hodges, D. H., "A Mixed Variational Formulation Based on Exact Intrinsic Equations for Dynamics of Moving Beams," *International Journal of Solids and Structures*, Vol. 26, No. 11, 1990, pp. 1253 – 1273.

[52] Shang, X. and Hodges, D. H., "Aeroelastic Stability of Composite Hingeless Rotors with Advanced Configurations," In *Proceedings of the 37th Structures, Structural Dynamics and Materials Conference*, Salt Lake City, Utah, April 15 – 17, 1996, pp. 1991 – 2001, AIAA Paper 96-1548.

[53] Peters, David A. and He, Cheng Jian, "Comparison of Measured induced velocities with results from a closed-form finite state wake model in forward flight," In *Proceedings of the 45th Annual National Forum of the American Helicopter Society*, Boston, Massachusetts, May 1989.

[54] Hodges, D. H., Atilgan, A. R., Cesnik, C. E. S., and Fulton, M. V., "On a Simplified Strain Energy Function for Geometrically Nonlinear Behaviour of Anisotropic Beams," *Composites Engineering*, Vol. 2, No. 5 – 7, 1992, pp. 513 – 526.

[55] Cesnik, C. E. S. and Hodges, D. H., "VABS: A New Concept for Composite Rotor Blade Cross-Sectional Modeling," *Journal of the American Helicopter Society*, Vol. 42, No. 1, January 1997, pp. 27 – 38.

[56] Rehfield, L. W., Atilgan, A. R., and Hodges, D. H., "Nonclassical Behavior of Thin-Walled Composite Beams with Closed Cross Sections," *Journal of the American Helicopter Society*, Vol. 35, No. 2, April 1990, pp. 42 – 50.

[57] Berdichevsky, V. L., Armanios, E. A., and Badir, A. M., "Theory of Anisotropic Thin-Walled Closed-Section Beams," *Composites Engineering*, Vol. 2, No. 5 – 7, 1992, pp. 411 – 432.

[58] Shang, X. and Hodges, D. H., "Aeroelastic Stability of Composite Rotor Blades in Hover," In *Proceedings of the 36th Structures, Structural Dynamics and Materials Conference*, New Orleans, Louisiana, April 10 – 12, 1995, pp. 2602 – 2610, AIAA Paper 95-1453.

[59] Peters, D. A. and Johnson, M. J., "Finite-State Airloads for Deformable Airfoils on Fixed and Rotating Wings," In *Symposium on Aeroelasticity and Fluid/Structure Interaction, Proceedings of the Winter Annual Meeting*. ASME, November 6 – 11, 1994.

[60] Peters, D. A., Boyd, D. D., and He, C.-J., "Finite-State Induced-Flow Model for Rotors in Hover and Forward Flight," *Journal of The American Helicopter Society*, Oct. 1989, pp. 5 – 17.

[61] Bisplinghoff, R. L., Ashley, H., and Halfman, R. L., *Aeroelasticity*, Addison-Wesley Publishing Co., Reading, Massachusetts, 1955.

[62] Greenberg, J. Mayo, "Airfoil in Sinusoidal Motion in a Pulsating Stream," Technical Note 1326, National Advisory Committee for Aeronautics, Washington, DC., June 1947.

[63] Peters, D. A., Barwey, D., and Johnson, M. J., "Finite-State Airloads Modeling with Compressibility and Unsteady Free-Stream," In *Proceedings of the Sixth International Workshop on Dynamics and Aeroelastic Stability Modeling of Rotorcraft Systems*, November 8 – 10, 1995.

[64] Peters, D. A., Karunamoorthy, S., and Cao, W.-M., "Finite State Induced Flow Models; Part I: Two-Dimensional Thin Airfoil," *Journal of Aircraft*, Vol. 32, No. 2, Mar.-Apr. 1995, pp. 313 – 322.

[65] Tran, C. T. and Petot, D., "Semi-Empirical Model for the Dynamic Stall of Airfoils in View of the Application to the Calculation of Responses of a Helicopter Blade in Forward Flight," *Vertica*, Vol. 5, 1981, pp. 35 – 53.

[66] Hodges, D. H., Shang, X., and Cesnik, C. E. S., "Finite Element Solution of Nonlinear Intrinsic Equations for Curved Composite Beams," *Journal of the American Helicopter Society*, Vol. 41, No. 4, Oct. 1996, pp. 313 – 321.

[67] Atilgan, A R., Hodges, D. H., Ozbek, A. M., and Zhou, W., "Space-Time Mixed Finite Elements for Rods," *Journal of Sound and Vibration*, Vol. 192, No. 3, May 9 1996, pp. 731 – 739.

[68] Makila, Pertti M. and Toivonen, Hannu T., "Computational Methods for Parametric LQ Problems – A Survey," *IEEE Transactions on Automatic Control*, Vol. AC-32, No. 8, August 1987, pp. 658 – 671.

[69] Shanno, D. F. and Phua, K. H., "Numerical Comparison of Several Variable-Metric Algorithms," *Journal of Optimization Theoryand Applications*, Vol. 25, 1978, pp. 507 – 518.

[70] Moerder, Daniel D. and Calise, Anthony J., "Convergence of a Numerical Algorithm for Calculating Optimal Output Feedback Gains," *IEEE Transactions on Automatic Control*, Vol. AC-30, No. 9, September 1985, pp. 900 – 903.

[71] Patil, M. J., Hodges, D. H., and Cesnik, C. E. S., "Nonlinear Aeroelastic Analysis of Aircraft with High-Aspect-Ratio Wings," In *Proceedings of the 39th Structures, Structural Dynamics, and Materials Conference*, Long Beach, California, April 20 – 23, 1998, pp. 2056 – 2068.

[72] Goland, M., "The Flutter of a Uniform Cantilever Wing," *Journal of Applied Mechanics*, Vol. 12, No. 4, December 1945, pp. A197 – A208.

[73] Cesnik, C. E. S., Hodges, D. H., and Sutyrin, V. G., "Cross-Sectional Analysis of Composite Beams Including Large Initial Twist and Curvature Effects," *AIAA Journal*, Vol. 34, No. 9, Sept. 1996, pp. 1913 – 1920.

[74] Nayfeh, A. H. and Mook, D. T., *Nonlinear Oscillations*, John Wiley and Sons, New York, 1979.

[75] Roskam, J., *Airplane Flight Dynamics and Automatic Flight Controls*, Roskam Aviation and Engineering Corporation, Ottawa, Kansas, 1979.

[76] Bayon De Noyer, M. and Hanagud, S., "A Comparison of H_2 Optimized Design and Cross-Over Point Design for Acceleration Feedback Control," In *Proceedings of the 39th Structures, Structural Dynamics, and Materials Conference*, Long Beach, California, April 20 – 23, 1998, pp. 3250 – 3258, AIAA-98-2091.

[77] Belvin, W. K. and Park, K. C., "Structural Tailoring and Feedback Control Synthesis: An Interdisciplinary Approach," *Journal of Guidance, Control, and Dynamics*, Vol. 13, No. 3, May – Jun. 1990, pp. 424 – 429.

Vita

Mayuresh Patil was born in Bombay, India, in July 1973. After completing his high school, he joined the Indian Institute of Technology at Bombay for his undergraduate education. There he recieved his Bachelor's degree in Aerospace Engineering in May 1994. He also received a silver medal for standing first in terms of academic performance. He continued his education in the School of Aerospace engineering at Georgia Institute of Technology. He started as a graduate student and research assistant in September 1994 and received his Master's degree in June 1996. He stayed on to complete his PhD in May 1999.